UNIVERSITÀ DEGLI STUDI DI PADOVA

Università degli Studi di Padova

Dipartimento di Biologia

SCUOLA DI DOTTORATO DI RICERCA IN : BIOSCIENZE E BIOTECNOLOGIE

INDIRIZZO: BIOLOGIA CELLULARE

CICLO XXVI

The multifunctional mitochondrial inner membrane protein Optic Atrophy 1 controls cellular damage in vivo

Direttore della Scuola : Ch.mo Prof. Giuseppe Zanotti

Coordinatore d'indirizzo: Ch.mo Prof. Paolo Bernardi

Supervisore :Ch.mo Prof. Paolo Bernardi

Dottoranda : Varanita Tatiana

31 Gennaio **2014**

Table of Contents

1 Riassunto dell'attività svolta

L'obbiettivo della tesi è stato rivolto all' analisi del ruolo di OPA1 nella morte cellulare in vivo attraverso la caratterizzazione di un modello murino over-esprimente OPA1 (*Opa1*^{tg}) generato nel nostro laboratorio; in tale modello il transgene Opa1 è stato inserito in una specifica posizione del cromosoma X e sotto il controllo del promotore debole ed ubiquitario per la beta-actina umana. Attraverso l'incrocio dei topi in due diversi background genetici C57/BL6 e SV129, abbiamo ottenuto linee murine in cui OPA1 è debolmente espressa in diversi tessuti. Il lieve incremento dei livelli di OPA1 non altera le altre proteine coinvolte nella dinamica mitocondriale e non ha alcun effetto sullo sviluppo, la longevità e la fertilità degli animali. Abbiamo osservato che la longevità dei topi *Opa1*^{tg} C57/Bl6 non mostrava variazioni rispetto ai wild type (WT), mentre era notevolmente ridotta negli *Opa1*^{tg} SV129, prevalentemente a causa di insorgenza di tumori ematologici e solidi. Poiché i topi *Opa1*^{tg} non mostravano alcun evidente fenotipo, abbiamo deciso di effettuare un analisi morfologica ed istologica in ogni organo. I cuori degli animali Opa1tg all'età di 9 mesi erano più grandi. Le analisi istologiche e di immunofluorescenza non rivelavano segni di ipertrofia e la funzionalità cardiaca era invece preservata come dimostrato dalle analisi ecocardiografiche, indicando che l'ipertrofia cardiaca osservata non era patologica e suggerendo altresì che l'atrofia cardiaca associata all'invecchiamento era inibita nei topi *Opa1*^{tg}.

Per verificare se l'over-espressione di Opa1 interferiva in qualche modo con l'atrofia associata al muscolo striato, abbiamo utilizzato un noto modello di atrofia

muscolare indotta tramite recisione del nervo sciatico. L'atrofia muscolare era significativamente ridotta nei topi *Opa1*^{tg}, dove la funzionalità mitocondriale nelle fibre denervate era preservata. Questi risultati suggerivano che OPA1 può interferire con almeno una forma di danno cellulare in vivo e ci ha spinto a verificare se ciò potesse interferire anche in altri modelli conosciuti di morte cellulare quali necrosi ed apoptosi.

In un modello di ischemia riperfusione di cuore isolato, i cuori *Opa1*^{tg} erano meno suscettibili al danno ischemico e l'area d'infarto era significativamente ridotta nei topi *Opa1*^{tg} dopo il danno da ischemia cerebrale indotto tramite l'Occlusione dell'arteria Cerebrale Mediale (MCAo).

In fine, l'apoptosi epatocellulare in vivo indotta da Fas era drasticamente ridotta in topi *Opa1*^{tg} , dove il danno epatico era diminuito. Meccanisticamente, i mitocondri da muscolo e fagato dei *Opa1*^{tg} topi sono risultati resistenti al rimodellamento delle cristae ed al rilascio di citocromo *c* indotto dalla proteina proapoptotica cBID; mostrano inoltre una aumentata efficienza nella respirazione mediata dal complesso I, mentre glia altri parametri di morte cellulare mediata dai mitocondri non sono risultati alterati. L'aumento della respirazione dipendente da complesso I correla con un aumento dei Supercomplessi della Catena Respiratoria (RCS) che, come da noi dimostrato, è una conseguenza della stabilizzazione delle cristae dipendente da OPA1.

I nostri dati dimostrano un ruolo della struttura delle cristae in diversi modelli di morte cellulare in vivo e comprovano un ruolo cruciale del rimodellamento

dell'ultrastruttura mitocondriale in risposta a diverse condizioni patologiche, che vanno dall'ischemia-riperfusione all'atrofia muscolare. Possiamo concludere che OPA1, la biogenesi ed il rimodellamento delle cristae sono processi fondamentali di danno reversibile ed irreversibile e di morte cellulare in vivo.

2 Summary

Mitochondria are crucial organelles for cell life and death. They represent the site of oxidative phosphorylation which provides energy for cellular processes, and play key roles in Ca^{2+} signaling and integration and amplification of apoptotic signals. Mitochondria are double membrane organelles: they possess an outer mitochondrial membrane (OMM), and an inner mitochondrial membrane (IMM) that can be further subdivided in an inner ''boundary membrane'' and in the cristae which are compartments separated from the inner boundary membrane by narrow tubular junctions. In addition mitochondria are highly dynamic and heterogeneous. Mitochondrial morphology and distribution are actively controlled to respond to the functional needs of the cell. This functional versatility is controlled by a growing family of ,,mitochondria-shaping'' proteins that regulate fusion and fission events. In mammals mitochondrial fission depends on the cytoplasmic GTPase, dynamin related 1 (DRP1), and its adaptors on the outer mitochondrial membrane (OMM). Mitochondrial fusion is regulated by two OM proteins mitofusin 1and 2 (MFN1and MFN2), and Optic Atrophy 1 (OPA1) in the inner membrane (IM). OPA1 promotes mitochondrial fusion depending on MFN1 and has an antiapoptotic function genetically distinguishable from its role in fission. OPA1 controls apoptotic cristae remodeling, a process required for the complete release of cytochrome *c*, the only soluble component of the respiratory chain. OPA1 oligomerizes in high molecular weight complexes, required for the maintenance of the cristae junction tight, thus preventing cytochrome *c* mobilization.

In vitro, disruption of these complexes by BH3 only proteins correlates with the widening of the narrow tubular junction and with the fusion of the individual cristae. Recently we identified a new role for OPA1 in the control of stability and assembly of the respiratory chain supercomplexes, mitochondrial respiratory efficiency and respiratory growth. However, very little is known about the role of OPA1 and of OPA1-dependent cristae changes in vivo.

The aim of this thesis was to explore the role of OPA1 in cell death in vivo, by characterizing an OPA1 overexpressing (*Opa1*^{tg}) mice generated in our laboratory where the Opa1 transgene is targeted to a specific position in the X chromosome and under the control of the weak ubiquitous human beta-actin promoter. By backcrossing mice in the genetic backgrounds C57/ Bl6 and SV129 we obtained inbred lines where OPA1 was mildly overexpressed in a variety of tissues. This slight increase in OPA1 levels did not alter other proteins involved in mitochondrial dynamics, and did not affect the development, life and fertility of the animals. We found that the life span of *Opa1*^{tg} C57/Bl6 was not different from that of wild type (Wt) littermates, while it was significantly decreased in *Opa1*^{tg} SV129, mostly due to the development of hematologic and solid tumors. Since *Opa1*^{tg} mice did not show any overt phenotype, we decided to analyze morphologically and histological every organ. Hearts were bigger in Opa1tg animals 9 months after birth. Histological and immunofluorescence analysis did not reveal signs of hypertrophy and heart functionality was indeed preserved as demonstrated by ecocardiographyc analysis, indicating that the retrieved cardiac hypertrophy was not pathological and suggesting that perhaps aging-associated heart atrophy is

inhibited in *Opa1*^{tg} mice. To test if Opa1 overexpression interfered with the program of striated muscle atrophy, we turned to a well-established model of skeletal muscle atrophy, induced by sciatic nerve resection. Muscle atrophy was significantly reduced in *Opa1*^{tg} mice, where mitochondrial function was preserved in the denervated fibers. This result suggested that Opa1 can interfere with at least one form of cell damage in vivo and prompted us to verify if it could interfere with other well established models of necrotic and apoptotic cell death. In a model of isolated perfused heart ischemia reperfusion, *Opa1*^{tg} hearts were less susceptible to ischemic damage, and the size of the infarcted area was significantly reduces in *Opa1*^{tg} mice following brain ischemic damage induced by Middle Cerebral Occlusion (MCAo). Finally, Fas induced hepatocellular apoptosis in vivo was drastically reduced in *Opa1*^{tg} mice where hepatic damage was accordingly blunted. Mechanistically, muscle and liver mitochondria from *Opa1*^{tg} mice were resistant to cristae remodeling and cytochrome *c* release induced by the pro-apoptotic BH3-only protein cBID and displayed increased efficiency of complex I dependent respiration, while other parameters of mitochondrial involvement in cell death were not affected. This increase in complex I dependent respiration correlated with an increase in Respiratory Chain Supercomplexes (RCS) that we demonstrated to be a consequence of OPA1-dependent cristae stabilization.

Our data elucidate a role for cristae shape in different modes of cell death in vivo and point out a crucial role for mitochondrial ultrastructural remodeling in response to widespread pathological conditions, ranging from ischemia reperfusion to muscular atrophy.

We can conclude that Opa1, cristae biogenesis and remodeling are central players of reversible and irreversible cell damage and death in vivo.

3 Mitochondria

Mitochondria are key organelles present in every cell type, crucial for life and death of the cell. The main function of mitochondria is provide energy for cellular processes. mitochondria are the site of oxydative phosphorylation that ensure the most ATP. They are also involved in TCA cycle, fatty acid metabolism, hemesynthesis, and gluconeogenesis (Corrado et al., 2012). Mitochondria are involved in several catabolic and anabolic pathways and control Ca^{2+} and red-ox homeostasis. They are the main generators of reactive oxygen species (ROS) that act as second messengers. Mitochondria are implicated in main cellular pathways that control cell fate, during apoptosis mitochondria release proapoptotic proteins that trigger the activation in the cytosol of effectors caspases, after mitochondrial membrane permeabilization and cristae remodeling (Rizzuto et al., 2000; Wasilewski and Scorrano, 2009; Apostolova et al., 2011). According to the endosymbiotic theory, developed in 1971 by Margulis, mitochondria have an ancestral extracellular origin, deriving from primordial rickettsia-like intracellular bacteria that colonized the eukaryotic cell and become essential for its life (Margulis, 1971)**.** Mitochondria are the only organelles (other than the nucleus) that have its own DNA, mitochondrial DNA (mtDNA) that is independent of the cell's chromosomal DNA. Human mtDNA is circular double stranded DNA of about 16,569 bp in length. Human mtDNA is maternally inherited (Sato and Sato, 2011; Al Rawi et al., 2011) contains 37 genes encoding 13 proteins, that are subunits of electron transport chain(ETC) complexes I, III, IV and V, (Attardi and Schatz, 1988) as well as the 22 tRNA and 2 ribosomal RNA genes required for their translation.

Mutations in these genes result in severe diseases, mostly because of impaired energy production. According to the chemiosmotyc theory proposed by Mitchell, respiratory chain complexes pump protons across the inner mitochondrial membrane generating an electrochemical gradient, that in turn is used by ATP synthase to generate ATP from ADP and phosphate ions, thus coupling respiration to ATP production. Abnormality in this processes are termed mitochondrial dysfunction. This latter is associated with inherited disorders and implicated in common diseases such as cardiomyopaties, neurodegenerative disorders, metabolic syndrome, cancer, obesity and aging.

3.1 Mitochondrial ultrastructure

In the 1950s, with the developments in electron microscopy, mitochondrial research became focused on ultrastructural analysis. By studying electron micrographs Palade and Sjostrand independently revealed that mitochondria possess two membranes– an outer mitochondrial membrane (OMM) and a highly convoluted the inner membrane (IMM), folded in a series of ridges that were named cristae (Palade, 1952; Sjostrand, 1953). From these pioneering works on structural details, at least two models of mitochondrial structure have been proposed: the baffle and the septa model. According to the model described by Palade, also known as the “baffle model”, **(Fig. 1 A)** cristae are invaginations of the IMM with broad openings to the intermembrane space (IMS), where occurs the ATP production through the oxidative phosphorylation.

Sjostrand proposed the septa model, that differs from Palade's model in the interpretation of the inner membrane structure, which consists of distinct compartments forming septa spanning through the matrix. Technical improvements of electronic microscopy allowed researchers to better inspect mitochondrial ultrastructure. Mitochondria are complicated organelles composed of compartments that carry out specialized functions. These compartments include OMM, IMS, IMM, cristae and matrix. The two membranes, composed of a phospholipid bilayer, are distinct in appearance and in physico-chemical properties.

The OMM is topologically simple, varying in shape depending on whether the mitochondrion is shaped. Usually it is tubular in a cell when attached to the cytoskeleton, but sometimes it is reticulated or isolated in suspension ellipsoidal or spherical. The OMM is freely permeable to ions and small molecules, it has a composition similar to other eukaryotic membranes and contains voltage dependent anion channels (VDAC), responsible for metabolite flux in and out of mitochondria (Colombini and Mannella, 2012). The OMM is enriched by proteins of the import machinery such as the mitochondrial protein translocase of the outer membrane (TOM) complex that functions as the gateway through which nuclear-encoded polypeptides can be imported into a mitochondrion (Ahting et al., 1999).

The IMM is freely permeable only to oxygen, carbon dioxide, and water. Its structure is highly complex, including all of the complexes of the electron transport

system, the ATP synthase complex, and transport proteins. Almost all ions and molecules require special membrane transporters to enter or exit the matrix.

Proteins are transported into the matrix via the translocase of the inner membrane (TIM) complex or via Oxa1 (Herrmann and Neupert, 2000). Mitochondrial tubular cristae represent specific compartments connected to the IMM by narrow tubular junction, called cristae junctions (Perkins et al., 1997; Mannella et al., 1997). Electron tomography revealed that the diameter of cristae junctions is about 28 nm and the average distance across the OMM and IMM is 20 nm **(Fig. 1 B)**. Cristae compartment represents the site of oxidative phosphorylation where the respiratory chain is located, and cytochrome *c* is separated from the IMS by narrow cristae junctions. The ratio of cristae/ mitochondrion surface area can be viewed as the ATP synthesizing capacity of the mitochondrion (Gilkerson et al., 2003; Vogel et al., 2006; Perotti et al., 1983). The cristae shape is dynamic: upon activation of mitochondrial respiration, ‘‘orthodox’’ mitochondria become ‘‘condensed,’’ with an expanded cristae space (Hackenbrock et al., 1980). As we will see below, the changes in cristae shape are important determinants of apoptosis and mitochondrial respiratory efficiency.

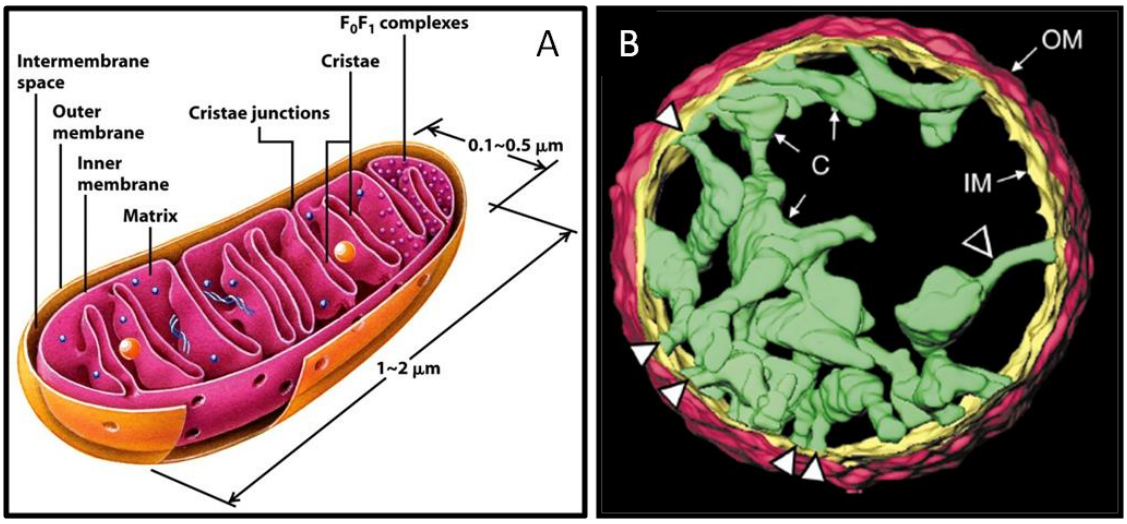

Figure 1 – Mitochondrial ultrastructure. (A) A text book-like representation of the baffle model adapted from **(B)** Three-dimensional reconstructions of isolated rat liver mitochondria obtained by highvoltage electron tomography. OM: outer membrane, IM: inner membrane, C: selected cristae; arrowheads point to narrow tubular regions that connect cristae to periphery and to each other. Bar, 0.4 µm. Adapted from (Frey and Mannella, 2000).

3.1.1 Mitochondria respiratory chain complexes (OXPHOS)

Mitochondria are central players in energy metabolism. They provide most of the ATP by oxidative phosphorylation (OXPHOS). In the tricarboxylic acid cycle (TCA) the acetyl-CoA produced by catabolic pathways such as glycolysis and fatty acid oxidation, is oxidized and the energy, released in form of reduced form of nicotinamide–adeninedinucleotide (NADH) and reduced form of flavin–adenine dinucleotide ($FADH_2$), fuels the electron transport chain (ETC) (Fig. 2). The components of ETC are located in the IMM and include four complexes (CI, CII, CIII and IV) and mobile carriers coenzyme Q (CQ) and cytochrome *c*. While the electrons pass along the ETC the energy released is used to expel protons from

matrix to the IMS and to build up the proton motive force. Only three of the four complexes act as proton pumps; Complex II is not able to pump protons. The proton motive is then utilized by ATPase to generate ATP from ADP and phosphate Pi, allowing the protons to re-enter the mitochondrial matrix, thus coupling electron transport and proton pump to ATP synthesis.

The coupling of electron transport to ATP synthesis is the main postulate of the chemiosmotic theory, for which in 1978 Peter Mitchell was awarded by a Nobel Prize in chemistry.

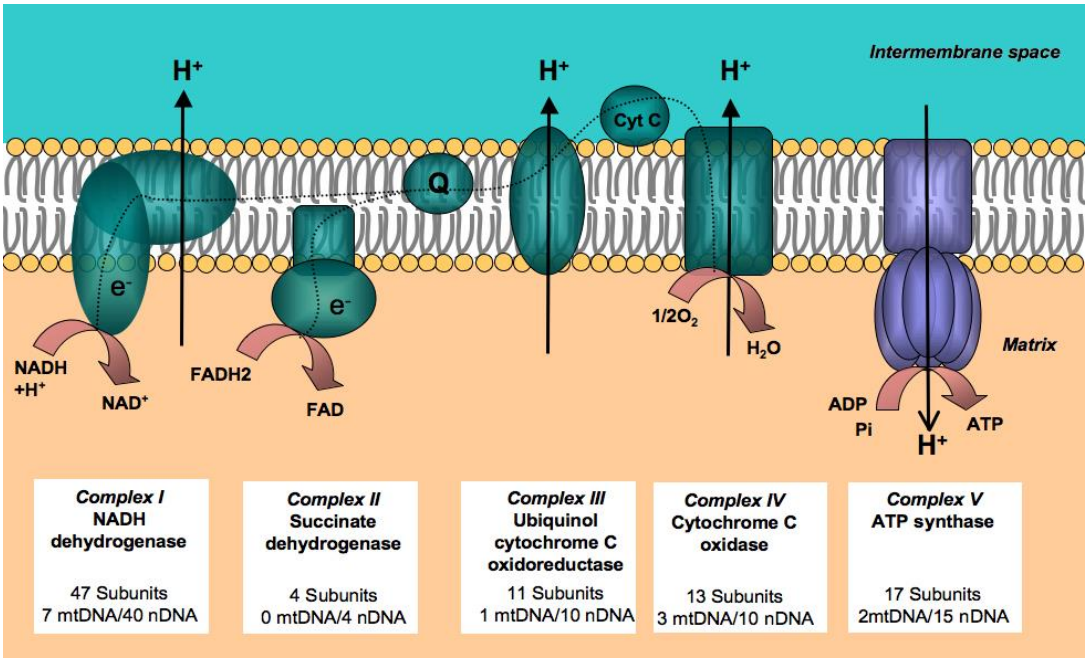

Figure 2- Mitochondrial respiratory chain. For mammals, the respiratory chain consists of four enzyme complexes (complexes I - IV) and two intermediary substrates (coenzyme Q and cytochrome c). The $NADH+H^+$ and $FADH_2$ produced by the intermediate metabolism are oxidized further by the mitochondrial respiratory chain to establish an electrochemical gradient of protons, which is finally used by the F1F0-ATP synthase (complex V) to produce ATP, the only form of energy used by the cell. In this simple representation of the respiratory chain, the supramolecular organization (supercomplexes, dimers) is not shown. (From:Bellance Nadege et al., Mitochondria: from bioenergetics to the metabolic regulation of carcinogenesis Frontiers in Bioscience 14, 4015-4034, January 1, 2009)

3.1.2 OXPHOS components

Complex I

Complex I or NADH dehydrogenase is the largest enzyme of the respiratory chain (almost 1MDa in size) and the entry point of the ETC. It couples electron transport from NADH to ubiquinone via flavin mononucleotide (FMN). Complex I consists of 45 subunits, encoded by both mtDNA and nuclear DNA, whose mutations lead to the most common mitochondrial diseases. The enzyme is the main site of ROS production which can lead to mtDNA damages and is involved in Parkinson's disease and aging. The enzyme has an "L" shape structure, as shown by a very recent crystal structure of the entire, intact complex I (from *T. thermophilus*) at 3.3 Å resolution (Baradaran et al., 2013)

Complex II

Complex II or succinate deydrogenase (SDH) is the second entry point of electrons to the ETC. It directly extracts electrons from succinate, an intermediate of the TCA cycle, using flavin adenine dinucleotide (FAD) as coenzyme, three iron–sulfur clusters and cytochrome b5. Complex II consists of four nuclear encoded proteins. Mutations in complex II are extremely rare. The 70 kDa flavoprotein (SDHA) and complex II assembly factor (SDHAF1) are responsible for mitochondrial respiratory chain diseases. Mutations in the other three subunits (SDHB, SDHC, SDHD) and the second assembly factor (SDHAF2) have so far only been associated with hereditary paragangliomas and phaeochromocytomas (Jackson et al., 2013).

Complex III

Complex III or cytochome *c* oxidoreductase, catalyzes electron transfer from reduced CoQ to cytochrome *c* and pumps two protons from matrix to the IMS. Complex III is composed by 10 subunits encoded by nuclear DNA and 1 by mtDNA. Mutations in complex III subunit genes are involved in debilitating and often fatal disorders (Tucker et al., 2013).

Complex IV

Complex IV or cytochrome *c* oxidase (COX) is the terminal enzyme of the respiratory chain. It transports electrons from cytochrome *c* and delivers them to oxygen to generate two water molecules. In this reaction four protons are pumped to the IMS. This complex consists of 14 subunits, three codified by mtDNA, that form the catalytic core of the enzyme, and 11 by nuclear DNA (Balsa et al., 2012). Genetic mutations affecting COX result in severe, often fatal, metabolic disorders. Such disorders usually manifest in early childhood and affect tissues with high energy demand. Only few COX genetic disorders are caused by mutation in mtDNA. The majority of COX defects are associated with pathogenic mutations in the nuclear encoded subunits. These mutations are located in genes encoding COX-specific assembly proteins including SURF1, SCO1, SCO2, COX10, and COX15. Dysfunctional COX assembly results in the most severe mitochondrial diseases (Pecina et al., 2004). COX15 was identified in yeasts as one of COX assembly factors. It plays a key role in the mitochondrial heme biosynthetic pathway in which protoheme (heme B) is converted to heme A, the prosthetic

heme group in COX. COX deficiency results in an early onset, fatal hypertrophic cardiomyopathy, severe loss of myofibrillar material and greatly increased numbers of mitochondria with abnormal shapes, abnormally arranged cristae, and numerous matrix densities (Antonicka et al., 2003) Mice with a general deletion of COX15 are embryonic lethal. A muscle specific COX15 knock-out (KO) mice display a COX defective mitochondrial myopathy (Viscomi et al., 2011).

ATP synthase

ATP synthase or Complex V is a large protein complex located in the IMM that uses the proton motive force to convert ADP and Pi in ATP. Complex V is composed of two functional domains F0 located in the IMM and F1 in the matrix. F0 acts as a pore transferring protons to the F1 by a rotatory movement. Complex V consists of 16 subunits encoded by both mtDNA and nuclear DNA. Complex V deficiency associates mostly with an early onset in the neonatal period with severe multi organ failures, and high mortality (Li XY et al., 2013).

3.1.3 Respiratory Chain Supercomplexes (RCS)

Mitochondrial respiratory chain is organized in supramolecular units called supercomplexes. The first “fluid model” in which mitochondrial respiratory chain complexes were free-moving entities linked by the mobile carriers coenzyme Q and cytochrome *c*, has been proposed by Hackenbrock (Hackenbrock et al., 1986).

A second “solid model” proposes that a supercomplex formed by complexes I, III and IV is the only functional mitochondrial electron transport chain (Schagger and Pfeiffer, 2000). The first proposed fluid model was challenged by the finding that all respiratory chain complexes, except for complex II, can associate into supercomplexes (Lapuente-Brun et al., 2013).

The best experimental system to investigate RCS is the blue-native polyacrylamide gel electrophoresis (BNGE) introduced by Schagger in 1995, which allows the separation of protein complexes preserving their physiological structure and activity. Using BNGE, Shagger found a variety of RCS of which perhaps the most prominent one is the I+III+IV also called the “respirasome” supercomplex, as well as the other supercomplexes I+III and III+IV (Acin-Perez et al., 2008). Studies in cells derived from patients with OXPHOS deficiencies revealed which are the complexes important for the structure of the supercomplexes. Low levels of supercomplexes are detected in the absence of complex III (Acin-Perez et al., 2004) and complex IV (Diaz et al., 2006). These two complexes have been found to be required for the stability of complex I. On the other hand the lack of complex I prevents supercomplexes formation, but has not been found to affect complex III or IV stability. Functionally, the electrons generated from NADH substrates feed complex I promoting respiration from complex I to complex III and complex IV; while electrons generated from FAD-linked substrates feed complex II until complex III and complex IV. The electron flow from complex II to complex III is independent from the flow that takes place in I to III.

These two pathways use separate CoQ pools to supply electrons from complex I and complex II to complex III. The two CoQ pools compete for the delivery of electrons to complex III. Complex IV receives electrons from either one or the other pathway depending on the supercomplexes. In particular, Cox7a2l that has been renamed supercomplex assembly factor I (SCAFI) has been identified to be required to stabilize the interaction between complexes III and IV and therefore to favor oxidation of NADH linked substrates. Interestingly, C57/BL6 mice lack SCAFI, having a profound impact on their mitochondrial metabolism and the fuel choice.

3.2 Mitochondria and cell death

Cell death is a key physiological process both in the development and in the homeostasis of multicellular organisms. Mitochondria are essential organelles for cell survival, but they also are recognized as central players in cell death. Cell death may be programmed or non-programmed. According to its morphological appearance cell death can be classified in apoptotic, autophagic or necrotic, and mitochondria can actively contribute to all of these cell deaths (Kroemer et al., 2009).

3.2.1 Apoptosis

Apoptosis is a physiological process that occurs in multicellular organisms, also known as programmed cell death (PCD) (Lockshin and Williams, 1965). The term apoptosis was first coined by Currie and co-workers and it is used to describe the

“dropping off” or “falling off” of petals from flowers or leaves from trees, a necessary part of the life cycle (Kerr et al., 1972).

In multicellular organisms, apoptosis contributes to homeostasis through the elimination of surplus or damaged cells. During embryonic development, it is essential for successful organogenesis and crafting of complex multicellular tissues, as elimination of the webbing between digits in humans and mice or the mammary tissue in males. During adulthood, apoptosis guarantees the maintenance of normal cellular homeostasis and immunity regulation. Impairment of apoptosis contributes to the development of several pathological conditions: insufficient apoptosis manifests as cancer or autoimmunity, while accelerated cell death is evident in acute and chronic degenerative diseases (Kerr et al., 1972; Kroemer and Zitvogel, 2007; Meier et al., 2000). Like other forms of cell death, apoptosis can be recognized by a series of morphological and biochemical characteristics. Apoptosis is characterized by loss of cell-cell contact, cellular shrinkage, pyknosis, chromatin condensation, nuclear fragmentation, membrane blebbing, appearance of apoptotic bodies and rapid phagocytosis by neighbouring cells (Kerr et al., 1972).

There are two main apoptotic pathways in mammalian cells, depending on the cell type and on the death stimulus. The extrinsic pathway is triggered by the activation of “death receptors” that after the formation of the protein complex called “death inducing signaling complex” (DISC) leads to the activation of caspase 8 followed by the activation of the effector caspase 3. The intrinsic apoptotic

pathway is triggered by intracellular apoptotic signals and is mediated by mitochondria (Scaffidi et al., 1998; Scaffidi et al., 1999).

The extrinsic apoptotic pathway is initiated at the cell surface via activation of specific death receptors. After the activation of both pathways, mitochondria release in the cytosol cytochrome *c* that form a complex with Apaf-1 to activate caspase 9 which in turn activates the effector caspase 3. The mitochondrial pathway of apoptosis is tightly regulated by the central regulators of cell death BCL-2- proteins, that act upstream of mitochondria and include both anti and pro-apoptotic members (Fig. 3).

BCL-2 family members posses conserved α-helices with sequence conservation clustered in the so called BCL-2 homology (BH) domains. According to their functions and to the homology displayed in the BH domains, BCL-2 family proteins can be subdivided in three principal groups. The anti-apoptotic or prosurvival BCL -2 proteins, such as BCL -2 itself, BCL -xL, BCL -w, BCL -1 and A1 that display a sequence conservation in all four domains (BH1-4). They inhibit cell death through direct interactions with the pro-apoptotic members. The pro-apoptotic molecules display less sequence conservation of the first alpha-helical segment BH4. BH3 is of particular importance for the pro-apoptotic family members that can be further subdivided into ‘‘multidomain’’ and ‘‘BH3-only’’ proteins. Multidomain pro-apoptotic members such as BAX and BAK display sequence conservation in BH1-3 domains and are believed to participate directly in OMM permeabilization. The BH3-only members like Bim, Bid, Bad, Bik, Noxa, Puma, Hrk, Bmf, display sequence conservation only in the amphipathic α-helical BH3 domain and are important to

sense different stress in the cell and to initiate apoptosis (Scorrano and Korsmeyer, 2003). The BH3-only proteins are further classified as sensitizer, for example Noxa, Bfm or Bik exert their pro-apoptotic role by interacting with the pro survival members and antagonizing their function, and as activators, like Bid and Bim, Puma that have the ability to directly activate Bax and Bak (Cheng et al., 2001) (Ren et al., 2010).

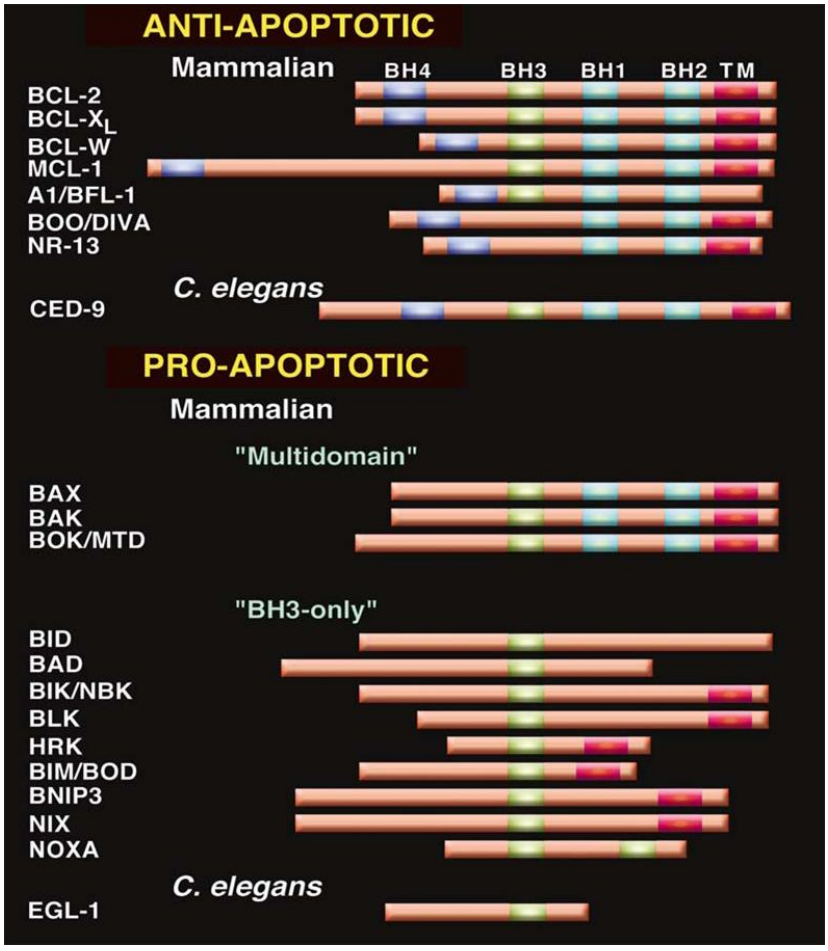

Figure 3- Summary of anti- and proapoptotic BCL-2 family members. BCL-2 homology domains are highlighted. From (L. Scorrano, S.J. Korsmeyer / Biochemical and Biophysical Research Communications 304 (2003) 437–444)

3.2.2 Mitochondria in apoptosis

Mitochondria are key organelles in the modulation of apoptosis, since they release both pro- and anti-apoptotic factors.

When pro-apoptotic signal predominates, OMM loses its integrity resulting in loss mitochondrial membrane potential, decrease ATP synthesis and release of apoptotic regulators from IMS to the cytosol. Among them cytochrome *c*, SMAC/DIABLO, OMI/HTRA2 , apoptosis–inducing factor (AIF) and endonuclease G. Once released into the cytosol, these mitochondrial proteins activate both caspase-dependent and independent cell death pathways (Saelens et al., 2004). SMAC/DIABLO and OMI/HTRA2 contribute to the apoptotic cascade by inactivation of proteins that inhibit effector caspases (Du et al., 2000; Verhagen et al., 2000). AIF (Susin et al., 1999) and endonuclease G (Li et al., 2001) have been proposed to mediate nuclear DNA damages in a caspase-independent way. Cytochrome *c* is a crucial factor for caspase activation upon an apoptotic stimulus (Liu et al., 1996). The OMM was shown to be impermeable to cytochrome *c* (Wojtczak et al., 1972), but in most apoptotic conditions it becomes permeable, resulting in release of cytochrome *c* into the cytosol. The release of cytochrome *c* into the cytosol requires a crucial process, mitochondrial outer membrane permeabilization (MOMP), that is mainly controlled by BCL-2 family members (Bender and Martinou, 2013; Bender and Martinou, 2013). After an apoptotic stimulus BH3-only proteins become activated and translocate to the OMM, where they activate multi domain pro-apoptotic. Activation of BAX/BAK by their oligomerization is required for the permeabilization of the OMM (Wei et al., 2000).

Once released into the cytosol, cytochrome *c* forms a caspase-activating complex with Apaf-1 called “apoptosome”, which activates caspase 9 to result in the activation of effector caspases 3 and 7 (Zou et al., 1997).

3.2.3 Fas- hepatocellular apoptosis and mitochondria

Apoptosis is a distinct feature of many liver diseases, since it can occur in response to viral infections and exposure to hepatocarcinogen agents, excessive alcohol consumption or genetic mutations. Liver resident cells, in particular hepatocytes, cholangiocytes, activated stellate cells and Kupffer cells, are susceptible to death receptor mediated apoptosis, due to the ubiquitous expression of these receptors in the organ (Chakraborty et al., 2012; Guicciardi et al., 2013). In the healthy liver, apoptosis is not a frequent mode of hepatic cell demise, but when it occurs morphological and biochemical characteristics do not differ from that observed in other cells (Feldmann, 2006). Liver death receptors belong to the tumor necrosis factor receptor (TNFR) superfamily, that includes TNFR1, Fas (CD95, Apo-1), the TNF-related apoptosis-inducing ligand (TRAIL), receptor activator of NF-kB ligand (RANKL), CD40 ligand (CD40L) another members of TNF family of cytokines. The members of this family are type-I transmembrane proteins with a C-terminal intracellular tail, a membrane-spanning region, and an extracellular ligand-binding N-terminal domain. Death receptors are characterized by a cytoplasmic sequence known as the death domain (DD), that enables the receptor to trigger cytotoxic signals when bind by their respective ligands. The DD domain is crucial for the induction of apoptosis.

Ligands that activate death receptor are cytokines that belongs to the TNF protein family. These proteins are also known as death ligands and they are mainly expressed as type-II transmembrane proteins containing an intracellular N-terminal domain, a transmembrane region, and a C-terminal extracellular tail (Guicciardi and Gores, 2009). The most studied death receptors are Fas, TNF-α and TRAIL and they are abundantly expressed in the liver and their activation is associated with hepatocyte apoptosis in a wide variety of liver diseases (Faubion and Gores, 1999). The Fas antigen, coded by the structural gene for mouse lymphoproliferation mutation (lpr), is a cell surface protein belonging to the TNF/nerve growth factor (NGF) receptor family, and mediates apoptosis. The Fas antigen messenger RNA is expressed in the thymus, liver, heart, lung and ovary. In particular Fas is constitutively expressed by every cell type in the liver. Ligation of death receptor Fas by its natural ligand, FasL, or by agonistic antibodies has dramatic consequences *in vivo*, resulting in lethal fulminate apoptotic liver destruction (Adachi et al., 1995; Ogasawara et al., 1993). Upon ligation by its cognate ligand FasL, the adaptor molecule Fas-associated death domain (FADD) is recruited to the receptor leading to the formation of the death inducing signaling complex (DISC) responsible for the activation of the initiator caspase 8 (Kischkel et al., 1995). Activation of caspase 8 at the DISC can trigger the apoptotic signaling cascade. Two signaling pathways of Fas-mediated apoptosis has been established, depending on the amount of DISC formation and active caspase 8. Based on this cells expressing Fas are classified in two types (Scaffidi et al., 1998).

In type I cells high levels of CD95 DISC formation and high amounts of active caspase 8 directly leads to the activation of downstream effector caspases 3 and 7.

In type II cell, levels of DISC are lower and only a small amount of active caspase 8 is produced. This cell type requires contribution of mitochondrial involvement to the amplification of caspase cascade. Caspase 8 in type II cells cleaves and activates pro-apoptotic BCL-2 family member BID, which translocates to mitochondria where it activates proapoptotic effectors of BCL-2 family, BAX and BAK and finely results in cytochrome *c* release (Lavrik et al., 2005).

More recently Jost have shown that levels of X-linked inhibitor of apoptosis protein (XIAP) determine whether a cell will undergo type I or type II Fas-mediated apoptosis (Fig. 4). Accordingly, in type II cells, sufficient amounts of XIAP can bind and block the activation of executioner caspases. Apoptosis in these cells occurs after OMM permeabilization by BAX and BAK, that allows release of proteins such as Smac, Omi that antagonize XIAP (Jost et al., 2009; Parsons and Green, 2011) Hepatocytes have been classified as type II cells based on observations that Fas-induced hepatocellular apoptosis is critically dependent on mitochondrial activation. Mice lacking BID, BAX/BAK double knockout mice, BCL-2 transgenic mice were protected from hepatocellular apoptosis following injection with agonistic anti Fas antibody, indicating that mitochondrial amplification loop is essential for the apoptosis in hepatocytes (Lacronique et al., 1996; Rodriguez et al., 1996; Yin et al., 1999; Wei et al., 2001).

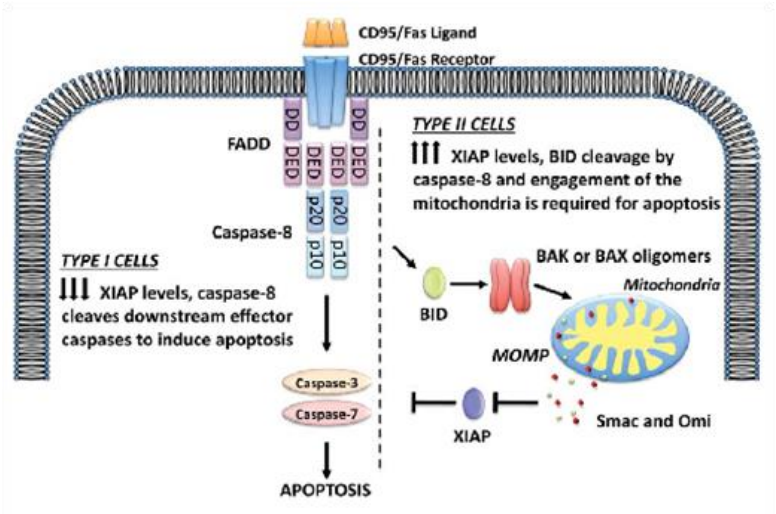

Fig. 4. Type I versus Type II death receptor signaling. Ligation of CD95 induces the recruitment of an adaptor protein FADD via homotypic death domain (DD). FADD then recruits caspase-8 via death effector domain (DED) interactions. Depending on the levels of the executioner-inhibitor protein XIAP, apoptosis will then proceed via one of two ways. In Type I cells, XIAP levels are low, and caspase-8–mediated cleavage and activation of the executioner caspases, caspase-3 and caspase-7, is sufficient to drive apoptosis. In Type II cells, XIAP is present in sufficient amounts to bind to and block the activation of the executioner caspases, preventing apoptosis. Thus, in Type II cells, caspase-8–mediated cleavage of BID, subsequent activation of BAX and BAK, and release of the XIAP inhibitors Smac and Omi from mitochondria during mitochondrial outer membrane permeabilization (MOMP) are required for efficient executioner caspase activation and apoptosis to proceed. From (Jost et al., 2009)

3.2.4 Mitochondria in Skeletal Muscle Atrophy

Muscle is the major consumer of fuels and ATP in the body. Based on functional and structural characteristics, muscle tissue can be divided into three groups: skeletal, cardiac and smooth. Cardiac and skeletal muscles are striated muscles, tissues with high energy demand. Skeletal muscle is a major site of metabolic activity and the largest organ system in all mammals, the most abundant tissue in the human body, accounting for almost 40% of the total body mass (Romanello and Sandri, 2010).

Skeletal muscle is a plastic tissue that responds and adapts its mass in response to physical activity, metabolism and hormones, by affecting pathways that regulate protein and cellular turnover. Skeletal and cardiac muscles are also tissues with limited proliferative capacity. Thus, their cell size is determined by the balance between synthesis of new proteins and the degradation of existing ones, both process with a high ATP demand. Muscle energy level is one of the cellular checkpoints that decide either to promote growth and hypertrophy or activate protein breakdown and atrophy (Sandri, 2008). Adult muscle growth occurs mainly by protein synthesis and decreases in protein degradation, while muscle atrophy occurs when protein degradation rates exceed protein synthesis resulting in gross reduction in fiber size, and may be induced in adult skeletal muscle in a variety of conditions, including starvation, denervation, cancer cachexia, heart failure and aging (Schiaffino et al., 2013).

Muscle protein degradation occurs mainly through two ATP-dependent proteolytic systems. Calpain, caspase-3, ubiquitin-proteasome, and autophagy are the proteolytic systems involved in protein breakdown during disuse muscle atrophy (Powers et al., 2007; Sandri, 2008). Functionally, skeletal muscle is a complex tissue composed of two major types of fibers: slow-twitch oxidative (type I) fibers designed for low-intensity long-lasting contractions, and fast-twitch glycolytic (type II) fibers designed for high-intensity short-duration contractions. The main factor that varies substantially across fiber types is mitochondrial density, slow twitch type I fibers typically displaying a two- to three-fold higher mitochondrial density and substantially lower non oxidative ATP synthesis capacity compared to

fast twitch type II fiber (Picard et al., 2012). The different fiber types display also diverse susceptibility to atrophy. Oxidative fibers are more resistant, while glycolytic fibers are more prone to loose proteins and organelles(Sandri, 2008). Skeletal and cardiac muscle possess two distinct populations of mitochondria that differ not only in their cellular location, but also in certain biochemical properties. Subsarcolemal mitochondria (SS) are located beneath the sarcolemma, and interfibrilar mitochondria (IMF) are situated between the myofibrils (Palmer et al., 1985). These two mitochondrial populations are characterized by differences in the cristae morphology. Lamelliform cristae are predominant in the SS, while tubular cristae are mostly present in IMF (Riva et al., 2006). IMF mitochondria are more abundant, representing about 80% of total mitochondria in muscle fibers (Hoppeler, 1986).

In addition to their structural and biochemical characteristics, the two populations of mitochondria display different bioenergetic capacities and possess distinct antioxidant defenses (Servais et al., 2003). For example IMF display higher OXPHOS activity compared to SS mitochondria (Padrao et al., 2011). Other studies revealed that during atrophy induced by denervation SS mitochondria are less susceptible to apoptotic stimuli and produce higher level of ROS with respect to IMF (Adhihetty et al., 2007). Playing a central role in energy production and in the regulation of cell life and death, alterations in mitochondrial function are primarily involved in myocyte atrophy during aging and disuse muscle wasting (Calvani et al., 2013).

Disuse muscle atrophy has been associated with loss of mitochondria, changes in mitochondrial morphology, increased ROS production, and impaired mitochondrial function. Regarding mitochondrial loss, it involves mitochondrial elimination and changes in mitochondrial biogenesis. Biogenesis is regulated by a family of transcriptional co-activators: the peroxisome proliferator-activated receptor gamma (PGC), including peroxisome proliferator-activated receptor-γ coactivator-1α and β (PGC-1a and PGC-1b). In particular PGC-1α interact and activates several transcription factors including PPARs, nuclear respiratory factors (NRFs), myocyte enhancing factors (MEFs), estrogen-related receptor (ERR), forkhead box (FOX)O1 and yin-yang (YY) (Olesen et al., 2010). PGC-1α can induce mitochondrial biogenesis and respiration by connecting the nuclear regulatory events with mitochondrial transcriptional machinery. PGC-1α binds and activates (NRF2/GABPA) and co-activates NRF1, PPARs and ERRs, increasing their transcriptional activity (Baldelli et al., 2013) NFRs activate the mitochondrial transcription factor A (TFAM) which binds mtDNA and regulates both mitochondrial transcription initiation and mtDNA copy number (Campbell et al., 2012).

Thus PGC-1α can be considered a master regulator of mitochondrial biogenesis widely expressed in tissues with high energy demand like brown adipose tissue, brain, heart and kidney as well as in skeletal muscle (Tritos et al., 2003). In skeletal muscle PGC-1α is primarily involved in the regulation of multiple pathways. Increased levels of PGC-1α through transgenic expression reduce muscle atrophy during denervation or fasting.

Therefore the levels of PGC-1α dramatically decrease after denervation and other types of muscle wasting (Sandri et al., 2006). PGC-1α levels decrease with aging and a slightly increased expression of PGC-1α during aging preserves mitochondrial function and prevent muscle wasting, by reducing apoptosis, autophagy and proteasome degradation (Wenz, 2009).

3.2.5 Mitochondria in Ischemia and Reperfusion Injury

Mitochondria play a central role in ischemic damage. Mitochondrial dysfunction is considered to be one of the main mechanisms involved in ischemic injury in heart, brain, liver, kidney, and other organs and tissues (Borutaite et al., 2013). Mitochondria functionality is affected during ischemia as a consequence of oxygen deprivation that further influence cell viability, through a wide set of events. Loss of mitochondrial function results in reduced ATP synthesis and increase in ATP hydrolysis, impairment in ionic homeostasis, formation of reactive oxygen species (ROS) and release of proapoptotic proteins. This biochemical dysfunctions are recognized as key factors in the generation of irreversible damage (Di Lisa and Bernardi, 2006; Duchen, 2000; Lesnefsky et al., 2001; Crow et al., 2004). The accumulation of lactic acid during ischemia results in a drop of pH that inhibits ATP production from glycolysis. pH normalization results in increased intracellular sodium ions that compete with calcium for extrusion; this in turn leads to an increase in the intracellular calcium.

Mitochondria act as buffering system, removing intracellular calcium that ultimately results in mitochondrial calcium overload. Reintroduction of the blood flow during the reperfusion is of primary importance to recovery the tissue, however the reperfusion phase is also the period where most of the cells die. During reperfusion calcium entry in mitochondria through the mitochondrial calcium uniporter (MCU) (De Stefani et al., 2011; Chen et al., 2003b). Mitochondrial calcium overload is a major feature of cell injury (Crompton, 1999; Carreira et al., 2011). Reperfusion can potentially kill the cell trough increase in reactive oxygen species (ROS) generation. Mitochondria are the key players in ROS production. The major sources of ROS are represented by uncoupling of the electron transport chain (ETC) complexes I and III, monoamine oxidase (MAO) and $p66^{Shc}$ activity (Tompkins et al., 2006; Chen et al., 2003b; Di et al., 2009). In cells acutely exposed to hypoxia mitochondria respond with increased ROS production. The ROS released during hypoxia leads to the stabilization of the transcription factor hypoxia-inducible factor (HIF), the principal regulator of transcriptional responses to hypoxia. HIF members have the ability to regulate several number of genes (Guzy and Schumacker, 2006). For example in response to hypoxia, HIF-1 strongly upregulates Bnip3 expression (Bcl-2 and adenovirus E1B 19 kDa-interacting protein 3), which induces oxidative stress (Guzy and Schumacker, 2006; Kubli et al., 2008). Activation of Bnip3 by its homodimerization promotes mitochondrial swelling and cytochrome *c* release, via disruption of Opa1 oligomers and release of Opa1 in the cytosol, interfering with fusion fission processes, important for normal function of mitochondria (Lee et al., 2009).

Alteration in mitochondrial dynamics have been implicated in I/R injury. Ischemia induces a Drp1 dependent fission, moreover pharmacological inhibition of mitochondrial fission decreases opening of mitochondrial permeability pore and reduces infarct size in a mouse model of myocardial I/R injury(Ong and Gustafsson, 2012). Other studies showed that Mfn-2 knockout hearts were able to develop higher pressures during post-ischemic reperfusion and exhibited diminished cell death following in vivo regional ischemia and reperfusion injury, indicating that Mfn-2 not only serves to maintain mitochondrial morphology in cardiac myocytes but also promotes MPTP opening in the heart under conditions of stress (Papanicolaou et al., 2011). Ischemia induces loss of Opa1 in H9c2 cell line and overexpression of Opa1 keep mitochondrial morphology during ischemia. Coronary ligation in adult rat results in reduced Opa1 levels with increased mitochondrial fragmentation (Chen et al., 2009). Altered mitochondrial dynamics toward fission correlate with increased ROS production, impaired function and activation of cell death (Shenouda et al., 2011; Frank et al., 2001; Germain et al., 2005; Gomes et al., 2011; Yu et al., 2006). Exacerbated ROS production and calcium overload trigger mitochondrial membrane permeability that ultimately leads to the opening of the mitochondrial permeability transition pore (MPTP). A voltage-dependent, high-conductance channel located in IMM. MPTP makes IMM permeable to solutes with molecular masses up to about 1.5 kDa, thereby causing collapse of the membrane potential and ATP depletion (Di Lisa and Bernardi, 2006; Zoratti and Szabo, 1995; Bernardi et al., 1999).

Damaged mitochondria can release cytochrome *c* and activate effector caspases culminating with apoptosis. Although the precise mechanisms by which cytochrome c is released from mitochondria during ischemia are not fully understood, at least three pathways have been discussed in the literature (Fig. 5) (Borutaite et al., 2013). First matrix swelling and rupture of OMM caused by MPTP lades to the release of the proteins from IMS, one of that is cytochrome *c* which after binding with Apaf-1 in the cytosol activates caspase 9 triggering apoptotic cascade (Di Lisa and Bernardi, 2006). Another pathway of cytochrome *c* release from mitochondria involves activation of the proapoptotic BH3 only members of BCL-2 family. The BCl-2 proteins have been found to play an important role in I/R. Transgenic mice overexpressing BCL-2 in the heart are more resistant to apoptosis and I/R, moreover they show smaller infarct size and improved postischemic function compared with wild type littermates Similarly Bax ablation in the heart improves myocardial tolerance to I/R injury, showing reduced infarct size(Hochhauser et al., 2003). Finely cytochrome *c* release during ischemia may be related to changes in the phospholipid composition of the OMM, in particular cardiolipin. Oxidative damage to cardiolipin lead to the alteration of the mitochondrial membrane fluidity, ion permeability structure and function of components of the mitochondrial electron transport chain, resulting in reduced mitochondrial oxidative phosphorylation efficiency and apoptosis (Ong et al., 2010). Cytochrome *c* release during ischaemia, caused by OMM permeabilization, is a major determinant of ROS production by mitochondria under pathophysiological conditions (Pasdois et al., 2011).

Cell death during ischemia and reperfusion injury is characterized by typical features of apoptosis, necrosis and autophagy. During ischemia, most cells die via necrosis due to extended oxygen deprivation and ATP depletion. Upon reperfusion, both apoptosis and necrosis are activated, the acute loss of cells during reperfusion is primarily due to necrosis (Ong and Gustafsson, 2012). A key regulator of both necrotic and apoptotic cell death is MPTP. MPTP opening allows water and solutes to enter mitochondria that will result in increased matrix volume with subsequent rupture of the OMM. The latter facilitates release of cytochrome *c* which in turn promotes apoptotic cell death. Moreover MPTP induction contributes to the loss of electrochemical gradient which in turn causes ATP synthase to work in reverse, consuming ATP. This process may be preceded by a transient but massive ROS production and calcium overload and culminate in necrotic cell death (Carreira et al., 2011). Finally, autophagy is another form of cell death that has been shown to play a role in I/R injury. Autophagic cell death was commonly observed in the heart with acute and chronic ischemia, heart failure, and aging (Hein et al., 2003). In conclusion, ischemia reperfusion injury appears to be a mixture of apoptotic, necrotic and autophagic cell death in which mitochondria are important mediators and regulators (Murphy and Steenbergen, 2008).

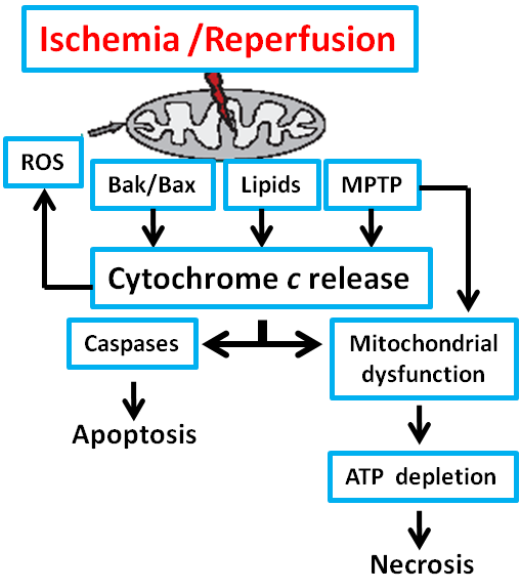

Figure 5 - Mechanisms and consequences of ischaemia-induced cytochrome c release from mitochondria. During ischaemia, mitochondrial cytochrome c may be released into the cytosol by mechanisms involving Bcl-2 proteins, lipids, or MPTP opening. In the cytosol, cytochrome c can participate in the activation of caspases, leading to apoptosis. Loss of cytochrome c from mitochondria may result in increased production of ROS, which, in turn, may lead to further oxidative damage to mitochondria. Loss of cytochrome c from mitochondria may result in mitochondrial dysfunction and ATP depletion, causing necrosis. From Barutaite et al., 2013

3.3 Mitochondrial shape and dynamics

Mitochondria are highly dynamic and heterogeneous organelles. Their morphology, size and distribution are actively controlled to respond to the functional needs of the cell. Studies from electron microscopy have shown that mitochondrial content and morphology can be highly variable across tissues and exhibit distinct patterns of fuel use and biosynthetic capacities (Vafai and Mootha, 2012). Morphology of mitochondria differs among different cell types.

In fibroblasts mitochondria are usually long filaments, whereas in hepatocytes are more spheres or ovoids, and can be solitary. In epithelial cells, mitochondria are tubular and they form an intricate network, while in native vascular smooth muscle mitochondria are ovoid or rod-shaped organelles. Mitochondria can vary even within individual cells. In skeletal muscle two populations of mitochondria can be retrieved: they are mostly globular in the perinuclear region, while subsarcolemal mitochondria are rod shaped and smaller than the ones embedded among myofibrilis. In pancreatic acinar cells there are three different regional groups of functionally unconnected mitochondria; one group in the peripheral basolateral region close to the plasma membrane, another around the nucleus and a third positioned in the periphery of the granular region separating the granules from the basolateral area (McCarron et al., 2013; Scorrano, 2013).

Mitochondrial shape ranges from spherical, grain-like, individual entities to long, branched filaments that, ultimately, might form interconnected tubules, depending on environmental conditions, cell type, and organism. (Fig. 6 A, B) (Dimmer and Scorrano, 2006). Mitochondrial morphology appears to be determinant of mitochondrial function,(Youle and van der Bliek, 2012; Shutt et al., 2012) which is precisely reflected by mitochondrial dynamics (Sjostrand, 1953). Mitochondrial dynamics refers to the fusion and fission cycles that constantly remodel mitochondrial network (Fig. 6 C,D).

Fission cuts a tubule into two while fusion can link two tubules together to form a longer tubule or a branch. In addition to complete fusion, a transient form of fusion was recently identified in which two mitochondria come into close

apposition, exchange soluble IMS and matrix proteins, and separate, maintaining the original morphology. Transient fusion, called “kiss-and-run”, supports mitochondrial motility and metabolism (Youle and van der Bliek, 2012).

Finally, mitochondria move along cytoskeletal tracks to sites of high-energy demand, and change their shapes change continually through the combined actions of fission, fusion and motility in response to the cellular environment and differentiation (Chang et al., 2006; Hollenbeck and Saxton, 2005; Saxton and Hollenbeck, 2012). Mitochondrial morphology and ultrastructure are determined by mitochondria-shaping proteins that include both pro-fusion an pro-fission members (Griparic and van der Bliek, 2001). Several members of the mitochondrial-shaping protein family are dynamin related proteins (DRPs), that are required to maintain mitochondrial morphology via a balance between continuous fusion and fission. DRPs are a special class of GTPases, well conserved between yeast, flies, and mammals (Hoppins et al., 2007), by hydrolyzing GTP they provide the mechanical forces necessary for fusion and division of two lipid bilayer that surround mitochondria. Mitochondria-shaping proteins impinge on the equilibrium between fusion and fission, thus controlling mitochondrial shape transition and form the core morphogenesis machinery.

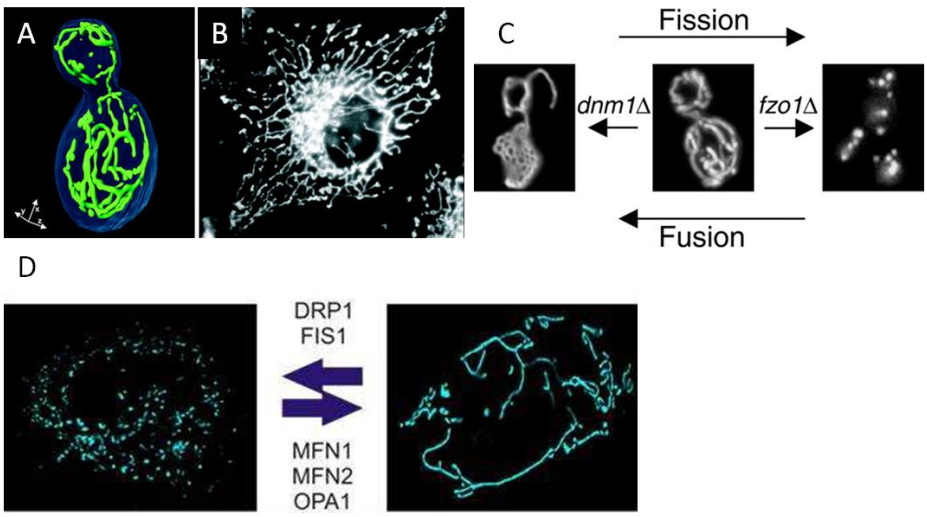

Figure 2 -Mitochondrial networks and fusion fission (A) Three-dimensional reconstruction of a mitochondrial network (green) in a *Saccharomyces cerevisiae* **(B)** Fluorescently labeled mammalian mitochondrial network in a cultured fibroblast cell from an African green monkey. Adapted from Westerman et al., 2002 **(C)** cartoon depicting the structure of mitochondrial network in *S.cerevisiae and the* relative mitochondrial shaping proteins regulating fusion and fission processes. Adapted from Mozdy A et al. J Cell Biol 2000 **(D)** cartoon depicting the different shape of mitochondrial network in mammals and the dynamin related proteins that regulate these processes

3.3.1 Mitochondrial-fission proteins

3.3.1.1 Dnm1/ DLP1/ DRP1

The key component of the mitochondrial fission machinery in mammals is constituted by the cytoplasmic dynamin-related protein 1 (DRP1) (Smirnova et al., 2001). Dnm1 in yeast, DRP1 in *Caenorhabditis elegans* and dynamin-like protein 1 (DLP1)/DRP1 in mammals are homologues and present similarities with dynamin, a large GTPase that participates in membrane scission in multiple endocytic and secretory organelles (Praefcke and McMahon, 2004). DRP1 contains a dynamin-

like-central domain and a carboxy-terminal GTPase effector domain, in addition to its amino-terminal GTPase. Intra-molecular interactions between the GTPase and GED regions appear to be required for full GTPase and fission activities (Zhu et al., 2004). Given its similarities with dynamin, DRP1 was proposed to couple GTP hydrolysis with mitochondrial membrane constriction and fission (Hinshaw, 1999; Smirnova et al., 2001). Althought DRP1 is a cytosolic protein, it is found in spots on mitochondria at sites of constriction of the OMM (Labrousse et al., 1999; Smirnova et al., 2001).

DRP1 is able to oligomerize *in vitro*, into ring-like structures after being recruited to the OMM by a mounting number of proteins: FIS1, Mff and MID 49 and 51.

3.3.1.2 Fis1/ FIS1

FIS1 is an outer membrane protein homogenously distributed on the surface of mitochondria (James et al., 2003). Its amino-terminal domain is exposed to the cytosol and forms a tetratricopeptide (TPR)-like domain, predicted to allow protein–protein interactions (Suzuki et al., 2003). The carboxy-terminal domain of FIS1 possesses a TM domain and a short stretch of amino acids facing the IMS. FIS1 overexpression induces mitochondrial and peroxisome fragmentation, although the protein does not possess any enzymatic activity. FIS1 probably recruits DRP1 to punctuate structures on mitochondria during mitochondrial fission, being therefore considered the limiting factor in the fission reaction. Accordingly, DRP1 and FIS1 seem to interact, as judged by crosslinking and co-immunoprecipitation (Yoon et al., 2003). Indeed, downregulation of FIS1 only partially diminishes DRP1

recruitment to mitochondria (Lee et al., 2004b). This pointed out whether FIS1 is the only protein needed for DRP1-dependent fission. In yeast FIS1 orthologue displays the same structural properties and is called Fis1. During assembly of the yeast mitochondrial fission complex, Fis1 recruits Dnm1 to mitochondria. Although a direct physical interaction between Fis1 and Dnm1 has been reported (Wells et al., 2007), a third player is essential for mitochondrial fission in yeast – Mdv1 (Tieu and Nunnari, 2000) or its paralog Caf4 (Griffin et al., 2005).

These proteins constitute adaptors, acting as scaffolds for the assembly of dynamins on membranes (Koirala et al., 2010). In mammals new fission adaptor proteins have recently been discovered.

3.3.1.3 Mff

In 2008 Van der Bliek and colleagues identified a new fission regulator protein named mitochondrial fission factor (MFF). This protein is anchored to the OMM with the C-terminal trans membrane domain, extruding the bulk of the N-terminal portion containing two short amino acids repeats in the N-terminal half and a coiled-coil domain just upstream of the trans membrane domain into the cytosol. The N-terminal cytosolic region is the one required for Drp1 recruitment, similarly to Fis1. It is able to both control mitochondrial and peroxisome elongation (Gandre-Babbe and van der Bliek, 2008) and its downregulation is able to diminish the number of Drp1 puncta on mitochondrial surface (Otera et al., 2010). This indicates that Mff and Fis1 share a similar function but act independently.

3.3.1.4 MID49 MID 51

Other components of the mitochondrial fission machinery are the MiD49 and MiD51 (also called mitochondrial elongation factor 1) of 49 and 51 KDa respectively (Palmer et al., 2013). They are amino-terminally anchored in the mitochondrial outer membrane with a cytosolic C-terminus. In contrast with Fis1 and Mff, both MiD49 and MiD51 are localized exclusively to the OMM and are not influencing peroxisome tabulation. Two independent studies have demonstrated that MiD49/51 are able to recruit Drp1 to the mitochondrial surface independently of other anchor proteins such as Fis1 and Mff (Loson et al., 2013; Palmer et al., 2013). Moreover MiD overexpression causes mitochondrial elongation which is due to a sequestration and consequent inactivation of Drp1 at the OMM with consequent unopposed fusion events (Palmer et al., 2013). Finally Fis1, Mff and MID49/51 can promote mitochondrial fission by recruiting Drp1 to the OMM. These proteins can act independently, but it remains possible that they can function together in orchestrating this process. Further studies are needed to elucidate whether these anchoring proteins operate in particular cellular types or stress conditions.

3.3.2 Mitochondrial-fusion proteins

3.3.2.1 Mitofusins, the OMM DRPs

Mitofusins, the DRPs that mediate fusion of OMM, are termed Mfn1 and Mfn2 in mammals, Fzo and Marf/Dmfn in flies, FZO-1 in the worm and Fzo1 in budding yeast. The first known protein mediator of mitochondrial fusion was discovered by Hales and Fuller. They used genetic approaches to identify in *Drosophila melanogaster fuzzy onions* (*fzo*) gene that encodes for Fuzzy onions 1 protein, a member of mitofusin GTPase family, required for developmentally regulated mitochondrial fusion event during spermatogenesis (Hales and Fuller, 1997). The *Saccharomyces cerevisiae* orthologue of *Drosophila* Fzo, Fzo1p, is required for the mitochondrial fusion during mitotic growth and yeast mating and for the maintenance of mitochondrial DNA (Hermann et al., 1998). Besides Fzo1, *Drosophila melanogaster* possesses another mitofusin homologue, the mitochondrial assembly regulatory factor (Marf) which is expressed ubiquitously in males and females. Muscle tissue specific knock-down of Marf induces fragmentation and alteration of mitochondrial ultrastructure (Deng et al., 2008). In mammals, two Fzo homologues, Mfn1 and Mfn2, are widely expressed in many tissues (Eura et al., 2003; Rojo et al., 2002; Santel et al., 2003). Mfn1 and Mfn2 are localized in the OMM, and display similar molecular structure that contains an N-terminal GTPase domain, two transmembrane domains spanning the MOM, and separating two heptad repeat regions (HR1 and HR2) (Chen et al., 2003a; Legros et al., 2002; Rojo et al., 2002; Santel and Fuller, 2001; Santel et al., 2003). The C-

terminal HR2 functions in mitochondrial tethering. Specifically when Mfn1 and 2 form homodimers or heterodimers to tether the outer membranes of adjacent mitochondria together, the HR2 region mediates mitofusin oligomerization by assembling a dimeric, antiparallel coiled coil. Two MFNs on opposing membranes can bind in *trans* to bridge mitochondria, maintaining a distance of 95 Å between the two membranes (Koshiba et al., 2004). The GTPase domain is required for the fusion process. It has been shown that Mfn1 exhibits much higher GTPase activity compared with Mfn2 during GTP-dependent membrane tethering, although its affinity for GTP is lower. In agreement with this, MFN1 exhibits a higher capacity to induce fusion (Chen et al., 2003a). In addition, a genetic analysis revealed that OPA1 requires MFN1 but not MFN2 to induce mitochondrial fusion, showing the first functional differences between the two mitofusins (Cipolat et al., 2004).

It has been suggested that Mfn1 is the main tethering protein, whereas Mfn2 may have a regulatory role (Detmer and Chan, 2007). Cell lines deficient for Mfn1 and Mfn2 completely lack mitochondrial fusion and show severe cellular defects, including poor cell growth, widespread heterogeneity of mitochondrial membrane potential, and decreased cellular respiration (Chen et al., 2005b). Knockout mice for either Mfn1 or Mfn2 die in midgestation, indicating that these genes are essential for embryonic development (Chen et al., 2003a). While mitofusins are known as mitochondrial fusion proteins, they may be involved in other cellular functions. Mfn2 may function as a cell proliferation suppressor, which is independent of its mitochondrial fusion activity (Chen et al., 2014). Furthermore our laboratory demonstrated a role for Mfn2 in regulating the shape of the

endoplasmic reticulum (ER) and as the first molecularly identified tether between mitochondria and the ER. Mfn2 is also enriched at the endoplasmic reticulum (ER)-mitochondria interface, where it tethers ER to mitochondria and facilitates their interaction for efficient mitochondrial calcium uptake (de Brito and Scorrano, 2008). Mutations in MFN2 are responsible for Charcot-Marie-Tooth 2A (CMT2A) (Zuchner et al., 2004) an inherited neuropathy characterized by moderate weakness and wasting of tibial muscles with lower limb hyporeflexia and mild distal sensory loss (Lawson et al., 2005). Most MFN*2* mutations in CMT2A cluster within the GTPase and the p21RAS-binding domains and are missense mutations (Lawson et al., 2005; Zuchner et al., 2004; Kijima et al., 2005). More recently mutations in MFN2 has been found to be responsible for mitochondrial DNA instability and optic atrophy 'plus' phenotype (Rouzier et al., 2012).

3.3.2.2 OPA1 an IMM DRP

Since this thesis aims at characterizing the role of OPA1 in vivo, we will discuss this protein in details.

Optic Atrophy 1 (OPA1), the mammalian homologue of *S.cerevisiae* Mgm1p, is the only dynamin related protein so far identified in the mitochondrial inner membrane (Olichon et al., 2002). Its name stems from its implication in autosomal dominant optic atrophy (ADOA), which affects retinal ganglion cells and the axons forming the optic nerve, leading to progressive visual loss (Delettre et al., 2000; Alexander et al., 2000).

Gene structure

Human and mouse *OPA1* gene display a very high homology level (~90%) (Delettre et al., 2000). Human *OPA1* ORF is built from 30 exons (31 exons in the case of mouse) distributed across more than 90 kb of genomic DNA on chromosome 3q28-q29 (chromosome 1 6 B2; 16 20.65 cM for mouse). *OPA1* is expressed ubiquitously, with the highest levels in retina, brain, liver, heart and pancreas (Alexander et al., 2000; Delettre et al., 2000; Misaka et al., 2002). Human Opa1 exhibits 8 transcripts which differ in their 3' UTR and result from the alternative splicing of exons 4, 4b and 5b. The relative abundance of these eight OPA1 splice variants shows tissue specificity (Delettre et al., 2001; Olichon et al., 2007a; Guillery et al., 2008). However, unlike in humans, in mouse only exons 4b and 4a, (and not exon 4) are involved in alternative splicing, leading to only 4 splice variants (Akepati et al., 2008). Of note, in lower eukaryotes such as in invertebrates, no alternative splicing has been reported for OPA1 orthologous genes (Olichon et al., 2007a).

Protein structure

OPA1 mRNA variants encode proteins of 924-1014 amino-acids. OPA1, and its yeast orthologues, belongs to the dynamins family, with which it shares three conserved regions: a GTPase domain, a middle domain, and a carboxy-terminus coiled-coil domain predicted to act as a GTPase effector. The latter is involved in the oligomerization and activation of the dynamins. The amino-terminal region of OPA1, preceding the GTPase domain, harbors a mitochondrial import sequence

(MIS)(Olichon et al., 2002). This MIS is followed by a transmembrane domain (TM1) required to anchor OPA1 to the inner mitochondrial membrane (IMM). Next, the splicing region, and in particular the domains corresponding to exons 4b and 5b , which are specific to vertebrate, encode a second (TM2a) and a third transmembrane domain (TM2b) plus a coiled coil domain (CC). CC0 is involved in hetero interaction with CC1. CC1 is located downstream of the alternatively spliced region and CC2 in the GED could be responsible for the formation of homotypic complexes between distinct OPA1 molecules (Duvezin-Caubet et al., 2007; Olichon et al., 2007a; Akepati et al., 2008; Belenguer and Pellegrini, 2013) (Fig.6). In addition to these post-transcriptional regulations, OPA1 expression is also regulated at post-translational level.

This later includes proteolytic processing of OPA1/Mgm1p. OPA1 precursors translated from the eight *OPA1* mRNA are targeted to mitochondria through their MIS which is cleaved by the mitochondrial processing peptidase (MPP) upon import, to give rise to long isoforms (L-OPA1) (Olichon et al., 2002; Satoh et al., 2003). Each L-OPA1 is then subjected to a limited proteolysis generating one or two short isoforms (S-OPA1) (Song et al., 2007). In physiological conditions, 50% of the L-isoforms containing exon 4 and 5b peptides, and 100% of L-isoforms containing exon 4b peptide are cleaved in S-isoforms, thus eliminating TM1 domain and those included in exon4b and 5b domains. Both short and long isoforms of OPA1 are associated to mitochondrial membrane, although it is proposed that L-OPA1 is anchored to the IMM while S-OPA1, lacking TM1, is peripherally attached to the IMM, a fraction of it having the possibility to diffuse in

the inter-membrane space (IMS) and to associate to OMM (Olichon et al., 2002; Griparic et al., 2004; Satoh et al., 2003; Ishihara et al., 2006; Cipolat et al., 2006).

Several studies have suggested that three mitochondrial proteases are involved in S-OPA1 generation, via two cleavage sites: S1 and S2. First, the rhomboid protease *PARL* (the mammalian counterpart of Pcp1p that cleaves Mgm1p) participates to the generation of low abundant S-OPA1 isoforms soluble in the IMS (Cipolat and Scorrano, 2006). Its knock-down/out does not affect however the ratio of L- to S-OPA1. The matricial AAA (m-AAA) metalloprotease paraplegin was proposed to cleave OPA1 at S1. Duvezin-Caubet and colleagues in 2007 demonstrated that the protease involved in OPA1 processing in not paraplegin, but subunits of the *m-AAA metalloprotease isozymes complex* composed of murine Afg3l1, Afg3l2, or human AFG3L2 and SPG7 subunits (Duvezin-Caubet et al., 2006; Duvezin-Caubet et al., 2007; Ishihara et al., 2006; Griparic et al., 2007; Guillery et al., 2008). In addition, prohibitins, regulators of m-AAA proteases activity, are also regulating OPA1 processing (Merkwirth et al., 2008). Finally, it was shown that the intermembrane space AAA *(i-AAA) metalloprotease* YME1L is responsible for cleavage at S2, but interestingly, exon 4b and 5b seem also to present an additional cleavage site for the i-AAA Yme1L (Song et al., 2007; Griparic et al., 2007).

To make this picture even more complex, it has been shown that dissipation of mitochondrial membrane potential and induction of apoptosis are able to stimulate the cleavage of OPA1 (Ishihara et al., 2006; Song et al., 2007; Griparic et al., 2007; Guillery et al., 2008). OMA1 an ATP-independent peptidase converts long into short OPA1 under these stress conditions (Ehses et al., 2009).

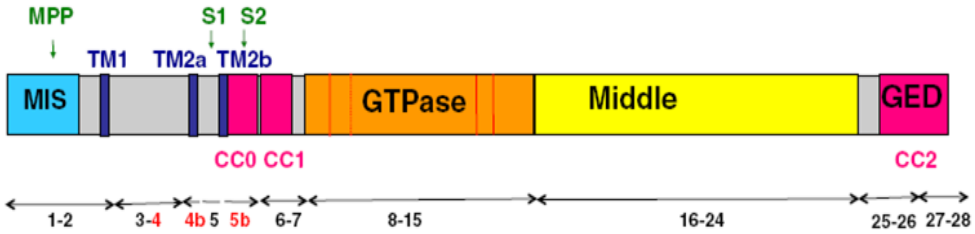

Figure 6 - Schematic representation of OPA1 structure. OPA1 shares several structural features with dynamins. These include a GTPase domain containing the three consensus GTP binding sequences (red bars) and the dynamin signature (red hatched bar), a middle domain and a GTPase effector domain (GED) containing a coiled-coil region (CCII). Before the GTPase domain, Opa1 displays amitochondrial import sequence (MIS) followed by a predicted transmembrane region (TM1), hydrophobic segments (TM2a and TM2b), and coiled-coil regions (CC). These domains are found in OPA1 all splice variants while TM2a, TM2b, and CC-0 are only present in spliced exons 4b and 5b. OPA1 exons (numbers) are schematized by double arrow. Intra-mitochondrial proteolytic cleavage sites for mitochondrial processing peptidase (MPP), paraplegin (S1) and YME1L (S2) are indicated. From (P. Belenguer, L. Pellegrini / Biochimica et Biophysica Acta 2012)

OPA1 functions

Involvement in mitochondrial fusion

OPA1 orthologues in yeast were initially identified as actors involved in maintaining the mitochondrial network fused (Guan et al., 1993; Pelloquin et al., 1999). A similar function was also reported for OPA1. Indeed, silencing all OPA1 variants, or those specifically including exon4, by RNAi or gene knock-out causes fragmentation of the tubular mitochondrial network (Cipolat et al., 2004; Griparic et al., 2004; Song et al., 2009).

Conversely, OPA1 overexpression induces mitochondrial elongation in cells with punctuated mitochondria (Cipolat et al., 2004), but surprisingly, promotes fragmentation in cells with tubular mitochondria, suggesting that very high OPA1

levels counteract its physiological pro-fusion activity (Misaka et al., 2002) This could be explained by two non-exclusive phenomena: 1) the disruption of the mitochondrial membrane potential, which is required for the fusion process (Legros et al., 2002), and 2) OPA1 interaction with OMM pro-fusion partners: Mfn1 and Mfn2 (Cipolat et al., 2004; Guillery et al., 2008), thus affecting the fusion machinery. The profusion activity of OPA1 was confirmed by experiments showing that mitochondrial fusion is impaired in OPA1 depleted cells (Song et al., 2007; Song et al., 2009; Cipolat et al., 2004; Chen and Chan, 2005; Lee et al., 2004a). Interestingly, both L- and S- forms are required for mitochondrial fusion, each one having separately little activity (Song et al., 2007). In addition, a functional role for exon 4 peptide has been revealed in the maintenance of mitochondrial membrane and fusion of the mitochondrial network (Davies et al., 2007).

Furthermore, levels of OPA1 can differentially induced two types of fusion: a transient fusion that results in rapid exchange of soluble components without affecting the mitochondrial morphology, and a complete fusion that allows the exchange of all mitochondrial components and affects its morphology (Liu et al., 2009).

It is important to note that while loss of OPA1/Mgm1p ultimately leads to mitochondrial fragmentation, data obtained in yeast and mammals indicate that consistent to its localization, OPA1 functions primarily in fusion of the inner membrane. Thus, OPA1 depletion does not abolish OM fusion both in vitro and ex vivo.

Furthermore multi-matrix structures accumulation reflecting OMM fusion without IMM fusion have been revealed by EM in *Opa1*$^{-/-}$ cells (Song et al., 2009; Meeusen et al., 2006).

It was recently reported that OPA1 pro-fusion activity is crucial for a mitochondrial quality control process, the so-called "kiss-and-run" process that involves transient fusions between mitochondria. Mitochondria that are affected for OPA1 activity, with consequently reduced fusion competency and low membrane potential, will be destinated to an active degradation by autophagy (Twig et al., 2008). Conversely, excess of OPA1 fusion activity, although transiently protective for some specific stresses (Tondera et al., 2009), leads to a senescence process, when sustained, by over-production of oxygen species and mitochondrial genome damage (Lee et al., 2007).

Involvement in energetic metabolism

As the IMM is structured in cristae and in a layer facing the OMM called inner boundary membrane, it has been suggested that OPA1 provides a dynamic intra-mitochondrial skeleton, a function that has been postulated in yeast for Mgm1p in relation with the oligomerization of ATP synthase (Amutha et al., 2004; Paumard et al., 2002; Arselin et al., 2004). Consistent with this implication, OPA1/Mgm1 is localized on cristae, as confirmed both by biochemical experiments (Griparic et al., 2004; Olichon et al., 2003; Pelloquin et al., 1999; Wong et al., 2000) and immuno-EM (Misaka et al., 2002; Olichon et al., 2002; Satoh et al., 2003; Vogel et al., 2006). Furthermore, it has been shown that OPA1 might be involved in cristae

maintenance since EM analysis of Mgm1/OPA1-depleted cells showed disorganized cristae with irregular shape, and for some of them presenting large cristae junctions (Olichon et al., 2003; Griparic et al., 2004; Sesaki et al., 2003). In 2006, our laboratory demonstrated that *Opa1* depleted cells reveal profoundly disorganized IMM structure with misshapen baggy cristae, whereas oligomers that contain a soluble and a membrane-bound form of OPA1 keep the cristae junctions tight, independently from OPA1 role in fusion (Frezza et al., 2006; Cipolat et al., 2006) RNAi depleted OPA1 cells show a severe reduction of endogenous respiration, no stimulation upon addition of an uncoupler and a diminution of oxygen consumption driven by complexes I, II and IV of the respiration complex (Chen et al., 2005a). In addition, it has been shown that OPA1 physically interact with Complex I, II and III of the respiration complex (Zanna et al., 2008).

We therefore investigated the role of OPA1 in cristae shape and mitochondrial respiratory chain assembly in vivo showing that conditional ablation of Opa1 alters cristae shape and respiratory chain supercomplexes assembly, whereas OPA1 overexpression increases RCS assembly (see results).

Involvement in the control of apoptosis

In addition to mitochondrial fragmentation, downregulation of OPA1, or expression of pathogenic mutants, increases cell sensitivity to spontaneous and induced apoptosis (Song et al., 2009; Lee et al., 2004b; Olichon et al., 2007b). These observations lead to propose that OPA1 functions as an anti-apoptotic protein, providing link between mitochondrial dynamics, energetic metabolism

and apoptosis. Indeed, overexpression of OPA1, protects cells from death induced by intrinsic signal, independently of its pro-fusion activity by inhibiting cytochrome *c* release (Frezza et al., 2006). Uncoupling of fusogenic and apoptotic functions of OPA1 could also be observed upon knockdown of particular splice variants, revealing that isoforms containing exon 4 peptide are important for fusion whereas those containing either exon 4b or 5b regulate cytochrome c release (Olichon et al., 2007a). In addition, OPA1 can regulate cristae morphology organizing into high molecular weight complexes that are target by BID during apoptosis. This correlates with the remodeling of the cristae that occurs during apoptosis (Scorrano et al., 2002; Frezza et al., 2006; Sun et al., 2007). Other studies have also implicated OPA1 in the sequestration of cytochrome c within the cristal space (Frezza et al., 2006; Yamaguchi et al., 2008).

This ability of OPA1 to sequester the cytochrome c is attributed to the existence of OPA1-containing complexes that maintain the diameter of cristae junctions in a basal state enough to retain cytochrome c within the intracristal space. It has also been proposed that OPA1 complexes at the junctions may act as a diffusion barrier (Perkins et al., 2009). Upon incubation with BH3-only proteins, OPA1 complexes rapidly dissociate, leaving holes large enough to allow the mobilization of cytochrome c from the cristae store to the IMS and subsequent release into the cytosol. This release could be counteracting upon OPA1 overexpression (Frezza et al., 2006). Interestingly, Baricault and colleagues demonstrated that apoptosis induction and PTP opening, as well as DeltaPsi(m) dissipation induce OPA1 cleavage. Decreased mitochondrial ATP levels, generated by apoptosis induction,

depolarization or inhibition of ATP synthase appear as the common and crucial stimulus that controls OPA1 processing (Baricault et al., 2007).

Involvement in mtDNA maintenance

OPA1 has also been involved in mtDNA stability. Missense mutations in OPA1 cause accumulation of multiple deletions in skeletal muscle (Amati-Bonneau et al., 2008; Hudson et al., 2008). In yeast, early works proposed that *mgm1-1* temperature sensitive mutant leads to a defect in mtDNA synthesis leading to a diminution of the number of molecules per cell at each division (Jones and Fangman, 1992; Pelloquin et al., 1999). It is proposed that it is through the changes in cristae morphology, that OPA1 inactivation perturbs mtDNA anchoring to the IMM and thus influences its replication and expression (Hudson et al., 2008). Unravelling the mechanisms by which OPA1 may affect mtDNA integrity will be another major challenge.

Thus, OPA1 has distinct function in the regulation of mitochondrial network morphology, organelle dysfunction and inner membrane cristae structure.

3.4 Mitochondrial shape and apoptosis

Mitochondria continually fuse and divide to form a dynamic interconnected network. This network disintegrates during apoptosis at the time of cytochrome *c* release, and upstream to caspase activation. Mitochondria fragment giving rise to numerous and smaller mitochondria, and undergo cristae remodeling to achieve

complete release of cytochrome *c.* (Frank et al., 2001; Scorrano et al., 2002; Suen et al., 2008). The regulation of mitochondrial morphology is a key factor in the process of apoptosis, and mitochondria shaping proteins seems to play a role. Mitochondrial fission represent a key step in apoptosis. In the early stages of apoptosis, DRP1 translocates from the cytosol to mitochondria there is required for the apoptotic mitochondrial fragmentation, before the release of cytochrome *c*. Inhibition of DRP1 by overexpression of a dominant-negative mutant suppress apoptosis and prevent cytochrome *c* release (Frank et al., 2001). Another study showed that downregulation of DRP1 delays but does not inhibit completely apoptosis (Estaquier and Arnoult, 2007). Similarly, FIS1 is also a player in apoptosis. Inhibition of FIS1 suppresses apoptosis, while its overexpression results in cytochrome *c* release and cell death (Lee et al., 2004, James). Conversely mitochondrial fusion is blocked during the BAX activation phase of apoptosis (Karbowski et al., 2004). Moreover overexpression of MFN1 and MFN2 inhibits cytochrome *c* release by intrinsic stimuli (Sugioka et al., 2004) and downregulation of OPA1 results in mitochondrial fragmentation, accompanied by cytochrome c release and mitochondrial dysfunction (Olichon et al., 2003). Mitochondrial ultrastructure changes dramatically in the early stages of apoptosis,

to allow the complete release of cytochrome *c* (Fig. 7). Two pools of cytochrome *c* are present in the mitochondria. One in the IMS and another is stored in the cristae. The IMS is very narrow, the average distance between OM and IM boundary membranes is only 20 nm(Frey and Mannella, 2000).

Accordingly only 15 %-20% of total cytochrome *c* is available in the IMS (Bernardi

and Azzone, 1981). The major part of cytochrome *c* is stored in the cristae compartment where the oxidative phosphorilation takes place, and is separated by IMS by narrow tubular junctions (Frank et al., 2001) The pathway of cristae remodeling is characterized by the widening of the narrow tubular junction and fusion of individual cristae, with subsequent cytochrome *c* mobilization from the cristae compartment towards the IMS and eventually to the cytosol (Scorrano et al., 2002; Germain et al., 2005; Mootha et al., 2001). The mitochondrial shaping protein OPA1 seems to play a key role in the regulation apoptotic cristae remodeling. OPA1 forms oligomers that participate in formation and maintenance of cristae junctions. During apoptosis these complexes are disrupted leading to widening of cristae junctions and subsequent redistribution of cytochrome c (Frezza et al., 2006).

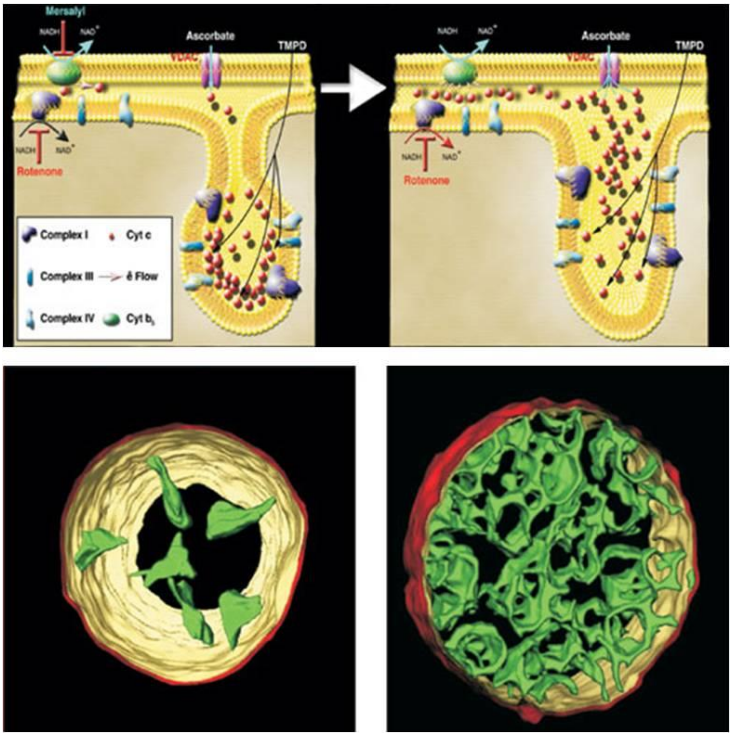

Figure 7- schematic (top panel) and representative 3D tomographic reconstruction of electron microscopy of mitochondria before (bottom left) or after (bottom right panel) induction of apoptosis showing the remodeling of the cristae and the consequences on accessibility of cytochrome *c* to the outer membrane. In the bottom panels, cristae are pseudocolored in green, outer membrane in red, inner boundary membrane in yellow. From (Scorrano et al., Dev Cell, 2002)

3.5 Mitochondrial shape and atrophy

Mitochondrial morphology has been shown to be altered during conditions of muscle use and disuse. Skeletal muscle mitochondria form a reticulum which increases in response to endurance training (Kirkwood et al., 1987). In contrast, chronic muscle disuse induced by denervation reduces mitochondrial content and produces muscle atrophy (Adhihetty et al., 2007). Chronic contractile activity induces an increase in mitochondrial content and upregulation of fusion proteins in rat skeletal muscle, while on the other side, denervation downregulates fusion proteins to a greater extent than the fission proteins (Iqbal et al., 2013). Moreover muscles from aged animals showed decrease in mitochondrial content, upregulation of fission proteins, and downregulation of fusion protein Mfn1 without changes in Opa1 levels, that have been shown to be significantly reduced in human skeletal muscle with aged related sarcopenia (Joseph et al., 2012). Mitochondria dramatically change their shape and dimension during fasting and denervation. Overexpression of DRP1 and Fis1 promotes muscle atrophy, while inhibition of fission proteins protects from muscle loss (Romanello et al., 2010).

In addition, skeletal muscle specific Mfn1 and Mfn2 deficient mice display severe muscle atrophy characterized by mitochondrial dysfunction, loss of mtDNA and compensatory mitochondrial proliferation (Chen et al., 2010). Impairment of autophagy leads to the accumulation of damaged and dysfunctional mitochondria and to a corresponding increase in intracellular ROS levels (Wu et al., 2009). Several conditions involved in muscle atrophy and loss of innervation are associated with dramatic increases in mitochondrial production of ROS (Muller et al., 2007), that contribute to muscle atrophy by denervation as potent triggers of mitochondria-mediated apoptosis (Adhihetty et al., 2007). In conclusion mitochondrial dysfunction contributes to muscle atrophy, mainly through increase in ROS production, inhibition of protein synthesis and activation of apoptosis.

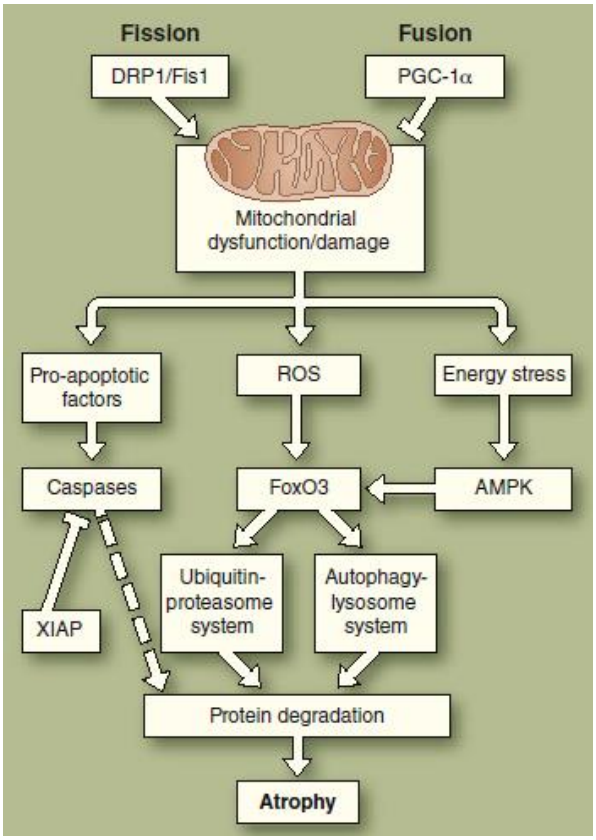

Figure 8- Scheme that represents the effects of mitochondrial fission and fusion on signaling pathways that control protein degradation systems. The dotted line depicts an action whose molecular mechanisms and role in adult skeletal muscle has not yet been completely defined. AMPK adenosine monophosphate–activated protein kinase; DRP1 dynamin-related protein 1; PGC-1α peroxisome proliferatoractivated receptor (PPAR)-γ coactivator-1α; XIAP x-linked inhibitor of apoptosis protein. From (Romanello and Sandri 2010).

Results

Sara Cogliati, Christian Frezza, Maria Eugenia Soriano, Tatiana Varanita, Ruben Quintana-Cabrera, Mauro Corrado,Sara Cipolat, Veronica Costa, Alberto Casarin, Ligia C. Gomes,Ester Perales-Clemente, Salviati, Patricio Fernandez-Silva, Jose A. Enriquez,and Luca Scorrano

Mitochondrial Cristae Shape Determines Respiratory Chain Supercomplexes Assembly and Respiratory Efficiency

Cell. 2013 Aug; *155*, 160-171.

Cell

Mitochondrial Cristae Shape Determines Respiratory Chain Supercomplexes Assembly and Respiratory Efficiency

Sara Cogliati,[1,2] Christian Frezza,[1] Maria Eugenia Soriano,[1,2] Tatiana Varanita,[1,2] Ruben Quintana-Cabrera,[1,2] Mauro Corrado,[1,3] Sara Cipolat,[1] Veronica Costa,[1] Alberto Casarin,[4] Ligia C. Gomes,[1] Ester Perales-Clemente,[5] Leonardo Salviati,[4] Patricio Fernandez-Silva,[6] Jose A. Enriquez,[5,*] and Luca Scorrano[1,2,3,*]

[1]Dulbecco-Telethon Institute, Venetian Institute of Molecular Medicine, Via Orus 2, 35129 Padova, Italy
[2]Department of Biology, University of Padova, Via U. Bassi 58B, 35121 Padova, Italy
[3]IRCCS Fondazione Santa Lucia, Via Ardeatina 306, 00143 Rome, Italy
[4]Clinical Genetics Unit, Department of Woman and Child Health, University of Padova, Via Giustiniani 3, 35128 Padova, Italy
[5]Centro Nacional de Investigaciònes Cardiovasculares Carlos III, Melchor Fernàndez Almagro 3, 28029 Madrid, Spain
[6]Departamento de Bioquìmica y Biologia Molecular y Celular, Facultad de Ciencias, Universidad de Zaragoza, Pedro Cerbuna 12, 50009 Zaragoza, Spain
*Correspondence: jaenriquez@cnic.es (J.A.E.), luca.scorrano@unipd.it (L.S.)
http://dx.doi.org/10.1016/j.cell.2013.08.032

SUMMARY

Respiratory chain complexes assemble into functional quaternary structures called supercomplexes (RCS) within the folds of the inner mitochondrial membrane, or cristae. Here, we investigate the relationship between respiratory function and mitochondrial ultrastructure and provide evidence that cristae shape determines the assembly and stability of RCS and hence mitochondrial respiratory efficiency. Genetic and apoptotic manipulations of cristae structure affect assembly and activity of RCS in vitro and in vivo, independently of changes to mitochondrial protein synthesis or apoptotic outer mitochondrial membrane permeabilization. We demonstrate that, accordingly, the efficiency of mitochondria-dependent cell growth depends on cristae shape. Thus, RCS assembly emerges as a link between membrane morphology and function.

INTRODUCTION

Mitochondria are key organelles in intermediate cellular metabolism, energy conversion, and calcium homeostasis (Dimmer and Scorrano, 2006). They also integrate and amplify apoptosis induced by intrinsic stimuli, releasing cytochrome *c* and other proapoptotic factors required for the activation of caspases (Green and Kroemer, 2004). Cytochrome *c* release is regulated by proteins of the BCL-2 family that control the permeabilization of the outer membrane (OMM) (Danial and Korsmeyer, 2004).

Energy conversion occurs at the inner mitochondrial membrane (IMM) that can be further divided into two subcompartments: the so-called "boundary membrane" and the cristae, separated from the former by narrow tubular junctions (Frey and Mannella, 2000). The cristae shape is dynamic: upon activation of mitochondrial respiration, "orthodox" mitochondria become "condensed," with an expanded cristae space (Hackenbrock, 1966). During apoptosis, the curvature of the cristae membrane is inverted in a remodeling process required for the complete release of cytochrome *c*, normally confined in the cristae (Scorrano et al., 2002; Frezza et al., 2006; Yamaguchi et al., 2008). Cristae remodeling occurs in response to proapoptotic BH3-only BCL-2 family members, such as BID, BIM-S, and BNIP3, and independently of the outer membrane multidomain BCL-2 family members BAX and BAK (Scorrano et al., 2002; Cipolat et al., 2006; Yamaguchi et al., 2008). Whether changes in morphology of the cristae, where respiratory chain complexes (RCCs) mainly localize (Vogel et al., 2006), affect oxidative phosphorylation efficiency, as originally predicted (Hackenbrock, 1966), is unclear. This issue is further complicated by the assembly of RCC in supercomplexes (RCS) (Schägger, 1995; Acín-Pérez et al., 2008), quaternary supramolecular structures that, by channeling electrons among individual RCCs, allow the selective use of RCC subsets for nicotine adenine dinucleotide (NADH)- or flavin adenine dinucleotide-derived electrons (Lapuente-Brun et al., 2013). Such a supramolecular organization is common in cristae: also, the mitochondrial ATP synthase is assembled into dimers with greater adenosine triphosphatase (ATPase) activity (Campanella et al., 2008; Gomes et al., 2011). Interestingly, cristae shape and ATPase dimers are linked: in yeast mutants where the ATPase cannot dimerize, cristae are disorganized (Paumard et al., 2002; Minauro-Sanmiguel et al., 2005; Strauss et al., 2008), whereas in mammalian cells, increased cristae density favors ATPase dimerization during autophagy (Gomes et al., 2011). On the contrary, despite their importance in mitochondrial bioenergetics,

the relationship between RCS and cristae shape remains unclear.

Mitochondrial morphology and ultrastructure depends on "mitochondria-shaping" proteins that regulate organellar fusion and fission (Griparic and van der Bliek, 2001). Mitofusins (MFN) 1 and 2, highly homologous dynamin-related proteins of the OMM, orchestrate fusion (Santel and Fuller, 2001; Legros et al., 2002; Chen et al., 2003; Santel et al., 2003). MFN1 primarily participates in fusion, cooperating with the IMM dynamin-related protein optic atrophy 1 (OPA1) (Cipolat et al., 2004), whereas MFN2 also tethers mitochondria to the endoplasmic reticulum (de Brito and Scorrano, 2008). Mitochondrial fission is regulated by the cytoplasmic dynamin-related protein 1 that, upon calcineurin-dependent dephosphorylation, translocates to mitochondria (Yoon et al., 2001; Smirnova et al., 2001; Cereghetti et al., 2008). Genetic depletion of OPA1 leads to disorganization of the cristae (Frezza et al., 2006), and oligomers that contain a soluble and a membrane-bound form of OPA1 keep the cristae junctions tight, independently from OPA1 role in fusion (Frezza et al., 2006; Cipolat et al., 2006). During apoptosis, these oligomers are early targets of BID, BIM-S, and BNIP3, as well as of intrinsic death stimuli (Frezza et al., 2006; Yamaguchi et al., 2008; Landes et al., 2010; Costa et al., 2010). Whereas our knowledge of the molecular determinants of cristae shape and their role in apoptosis is increasing, the relationship between cristae morphology and mitochondrial function remains unexplored. We therefore set out to genetically dissect whether and how cristae shape regulates mitochondrial respiration. We show that cristae morphology determines assembly and stability of RCS and hence optimal mitochondrial respiratory function during life and death of the cell.

RESULTS

Genetic Dissection of Outer Membrane Permeabilization from Cristae Remodeling

Whether apoptotic cristae remodeling that maximizes cytochrome *c* release from mitochondria affects mitochondrial function is unclear, mainly because it occurs around the same time as outer membrane permeabilization (Scorrano et al., 2002). In order to genetically dissociate the two processes, we inspected the primary structure of the prototypical cristae remodeling inducer BCL-2 family member BID for homology with peptides known to perturb the mitochondrial inner membrane, like mastoparan, a 14 amino acid wasp venom component (Pfeiffer et al., 1995). Interestingly, BID membrane inserting α6 helix as well as the transmembrane domains of Bnip3 and BimS that also remodel cristae (Yamaguchi et al., 2008; Landes et al., 2010) displayed homology to mastoparan (Figures S1A and S1B available online). To exploit the role of this homologous sequence in cristae remodeling, we mutagenized the two highly conserved 157 and 158 Lys *H. sapiens* BID residues to Ala (BID^{KKAA}) (Figure S1C). Because this mutation did not impair caspase-8 cleaved recombinant BID (cBID) integration in purified mouse liver mitochondria (MLM) (Wei et al., 2000; Figure S1D), we could measure its biological activity using an established quantitative, specific cytochrome *c* release ELISA (Scorrano et al., 2002). cBID efficiently released cytochrome *c* from purified mitochondria, whereas a BH3 domain G94E mutant was, as expected, inactive (Wei et al., 2000) and the $cBID^{KKAA}$ mutant released ~25%–30% more cytochrome *c* than the baseline (Figure 1A), a figure close to the amount of free intermembrane space cytochrome *c* (Scorrano et al., 2002). BAK oligomerization was superimposable in cBID or $cBID^{KKAA}$-treated mitochondria (Figure 1B); conversely, two established assays of intramitochondrial cytochrome *c* redistribution, the cytochrome b_5-dependent extramitochondrial NADH oxidation and the ratio of ascorbate-driven over tetramethyl-p-phenylenediamine (TMPD)-driven respiration (Scorrano et al., 2002), indicated that $cBID^{KKAA}$ mobilized the cristae cytochrome *c* pool less efficiently than cBID (Figures 1C and 1D). Indeed, $cBID^{KKAA}$ was unable to remodel mitochondrial cristae, as indicated by morphometric analysis of electron micrographs of mitochondria treated with the BID mutants (Figures 1E and 1F) (Scorrano et al., 2002). Cristae remodeling is associated with the disruption of high molecular weight (HMW) OPA1 oligomers (Frezza et al., 2006). Western blots of blue native gel electrophoresis (BNGE) of mitochondrial proteins revealed four major OPA1-containing complexes. Upon treatment with cBID, OPA1 rapidly disappeared from ~720 kDa HMW complexes (Figures 1G, S1E, and S1F). These HMW forms of OPA1 were similarly targeted by $cBID^{G94E}$ but significantly less by $cBID^{KKAA}$, as determined by BNGE (Figure 1H, quantification in [I]). Chemical crosslinking experiments (Frezza et al., 2006) further confirmed that the OPA1-containing oligomer is disrupted by the mutants of cBID able to induce cristae remodeling (Figures S1G and S1H). Finally, we measured the killing efficiency of these truncated BID (tBID) mutants expressed in mouse embryonic fibroblasts (MEFs). Only tBID efficiently killed MEFs: $tBID^{KKAA}$ and $tBID^{G94E}$ elicited comparable low levels of cell death, whereas the double $tBID^{KKAA,G94E}$ mutant appeared completely ineffective (Figure 1J), suggesting that both outer membrane permeabilization and mitochondrial cristae remodeling are required for BID-induced apoptosis. In conclusion, BID^{KKAA} is deficient in cristae remodeling, cytochrome *c* release, and induction of apoptosis.

RCS Disassemble during Cristae Remodeling

The BID^{KKAA} mutant dissociates outer membrane permeabilization from cristae remodeling and can be used to investigate the relationship between the latter and mitochondrial function. We therefore measured the effect of the BID mutants on the respiratory control ratio (RCR), an index of respiratory efficiency, of mitochondria incubated with excess exogenous cytochrome *c* and NADH (to compensate for the potential effects of inner membrane or outer membrane [OM] permeabilization). cBID reduced RCR only when mitochondria were energized with substrates for complex I (glutamate/malate) but not when they were fed with substrates entering the electron transport chain at complex II (succinate) or complex IV (ascorbate + TMPD) (Figure 2A; data not shown). Interestingly, these changes were recapitulated by the BH3 domain mutant $cBID^{G94E}$ that does not permeabilize the OM but not by the cristae remodeling-deficient mutants $cBID^{KKAA}$ and $cBID^{KKAA,G94E}$ (Figure 2B). Maximal (uncoupled) respiration was similarly affected by the cBID mutants tested, ruling out that BID alters RCR, because it affects ATPase or activity or ATP/ADP exchange (Figure S2A). These experiments

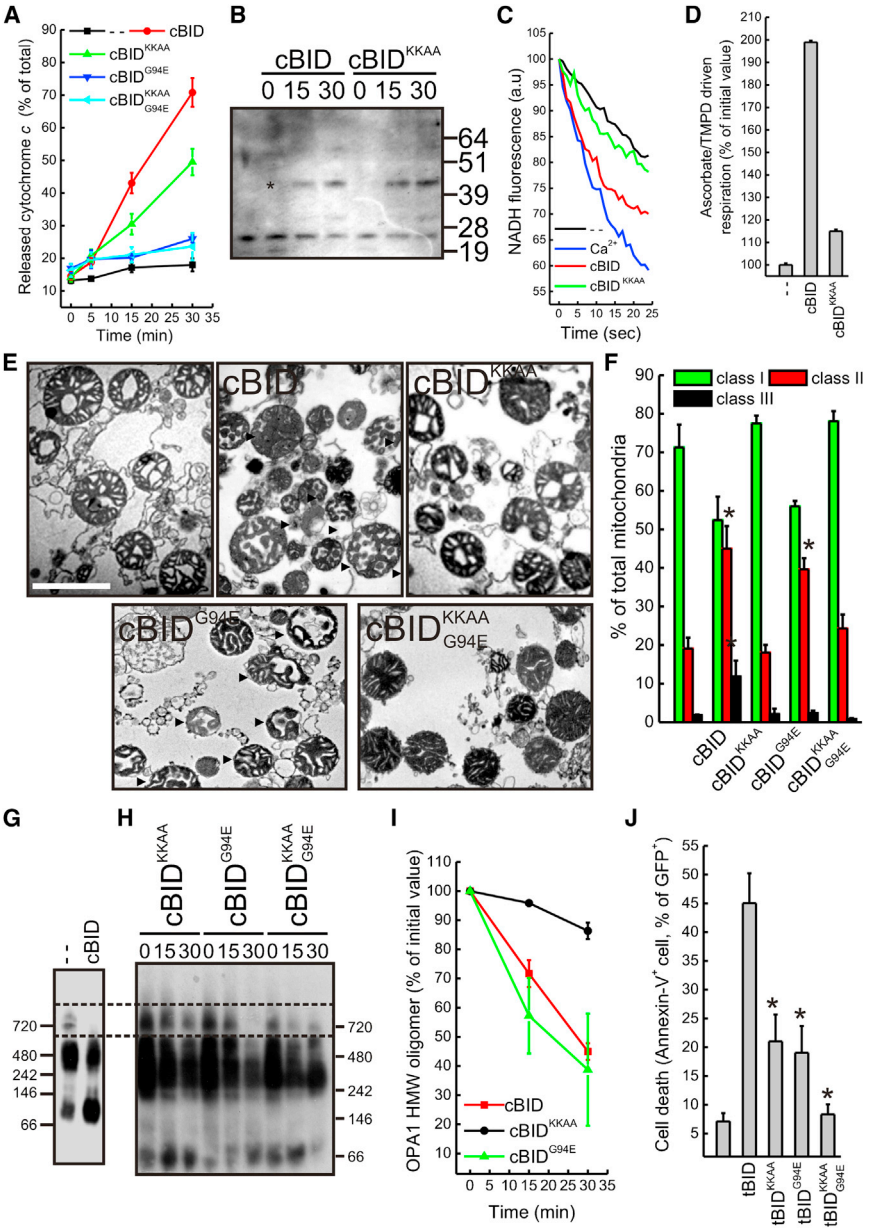

Figure 1. Two Conserved Lys in BID α6 Helix Are Required for Cristae Remodeling

(A) Mitochondria were treated for the indicated times with the indicated mutants of cBID, and cytochrome *c* release was measured by ELISA. Data represent average ± SEM of five independent experiments.

(B) Mitochondria treated with the indicated mutants of cBID for the indicated min were cross-linked with 1 mM BMH for 30 min, spun, and the pellets were separated by SDS-PAGE and immunoblotted using anti-BAK antibody. The asterisks denote BAK oligomers.

(C) Mitochondria were treated as indicated (Ca^{2+}, 200 μM), and cytochrome b_5-dependent NADH fluorescence changes were recorded. a.u., arbitrary units.

(D) Mitochondria were treated for 15 min with the indicated BID mutants, transferred into the chamber of a Clark's type O_2 electrode, and the ascorbate/TMPD-driven respiration ratio was determined. Data represent average ± SEM of four independent experiments.

(E) Representative electron microscopy fields of mitochondria treated for 15 min with the indicated cBID mutants. Arrows indicate class II and III mitochondria. The scale bar represents 450 nm.

(F) Blind morphometric analysis of randomly selected EM of mitochondria treated with the indicated cBID mutants (as in [E]). Mitochondria were assigned to morphological classes I–III as in Scorrano et al. (2002). Data represent average ± SEM of three independent experiments. The asterisk denotes $p < 0.05$ in a paired sample Student's t test versus untreated.

(G and H) BNGE analysis of OPA1 oligomers in MLM treated for 30 min (G) or for the indicated minutes (H), as indicated. The boxed area indicates the HMW complexes of OPA1.

(I) Densitometric analysis of OPA1 HMW complexes. Experiments were as in (H). Data represent average ± SEM of four independent experiments.

(J) MEFs were transfected with the pMIG plasmid containing the indicated insert and after 48 hr cell death was determined cytofluorimetrically as the percentage of Annexin-V^+, GFP^+ cells. Data represent average ± SEM of four independent experiments. The asterisk denotes $p < 0.05$ in a paired sample Student's t test versus tBID.

See also Figure S1.

suggest that cristae remodeling causes complex I-dependent changes in mitochondrial bioenergetics.

Complex I is further assembled in quaternary functional RCS with complexes III and IV (I + III and I + III + IV), whereas most complex II is not found in RCS (Acín-Pérez et al., 2008). Thus, the reduction in complex I-supported respiration could be a consequence of specific inhibition of complex I or of issues in RCS function. Even after 30 min of acute BID treatment, the specific complex I NADH-ubiquinone reductase activity of purified mitochondria was unaltered (data not shown), prompting us to investigate RCS assembly and stability in situ. We therefore took advantage of *Bax*$^{-/-}$, *Bak*$^{-/-}$ (DKO) MEFs, resistant to mitochondrial permeabilization, cytochrome *c* release, and apoptosis triggered by expression of tBID (Wei et al., 2001). Upon transduction of metabolically labeled DKO MEFs with tBID but not with $tBID^{KKAA}$ that does not cause cristae remodeling (Figure S2B), the RCS radioactivity signal as well as the RCS/complex V radioactivity ratio were reduced (Figures 2C and 2D), and we observed a reduction in the autoradiographic signal of cytochrome *b* retrieved in RCS compared to that in free complex III (Figures 2E and 2F). Whereas this result could suggest that complex III was incorporated less efficiently into RCS, immunoblotting for the complex I subunit NDUFA9 revealed that RCSs were also destabilized in DKO cells (Figure 2G). Functionally, only cBID and $cBID^{G94E}$ that cause cristae remodeling but not $cBID^{KKAA}$ reduced glutamate-supported RCR in DKO mitochondria (Figure 2H). Thus, BID destabilizes RCS and selectively reduces glutamate-dependent RCR.

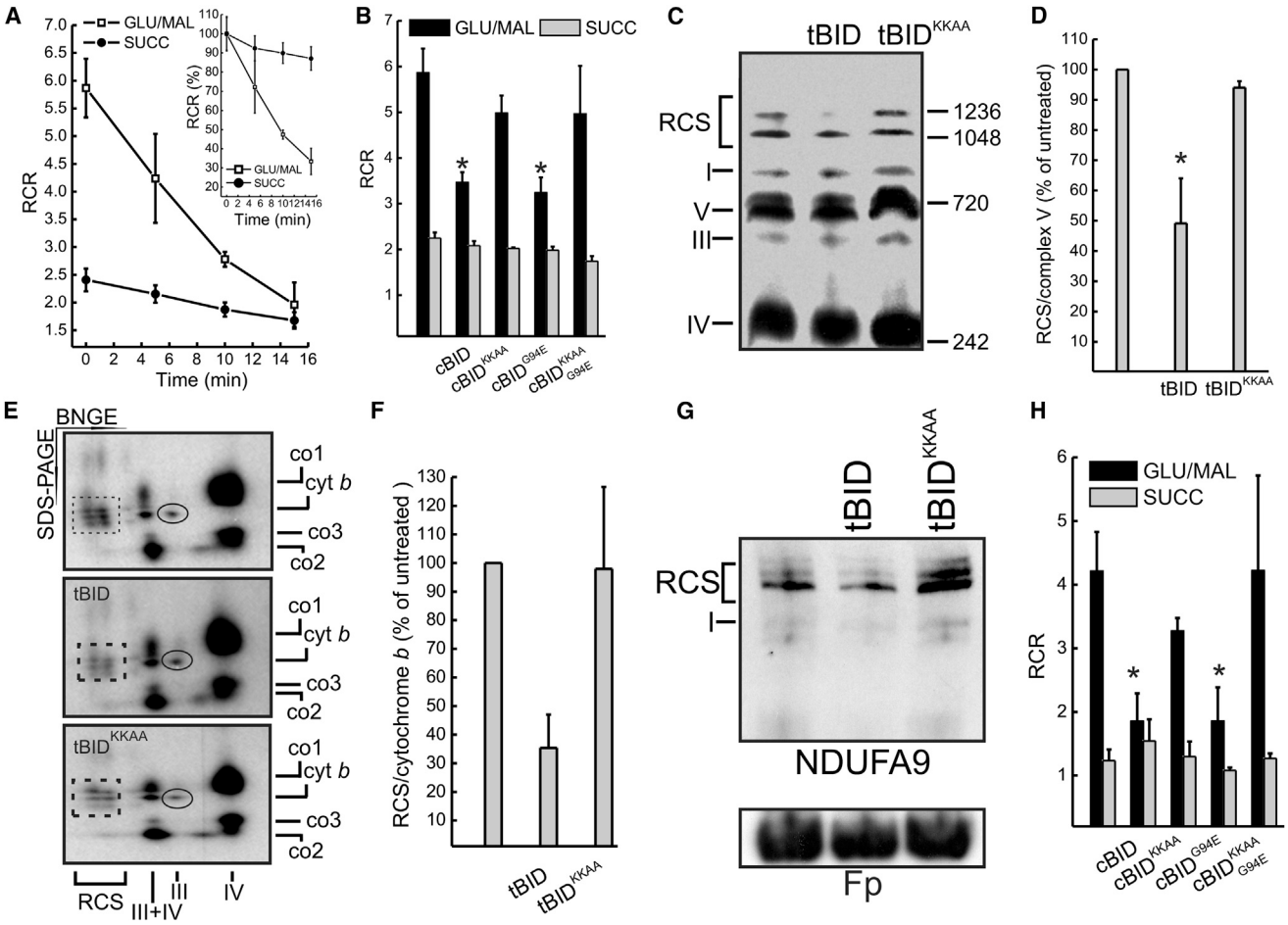

Figure 2. Respiratory Chain Supercomplexes Are Disassembled during Cristae Remodeling

(A) RCR of mitochondria energized with 5 mM/2.5 mM glutamate/malate (GLU/MAL) or 10 mM succinate (SUCC) treated for the indicated times with cBID. Data represent average ± SEM of five independent experiments. Inset, RCR values normalized to t = 0.

(B) Experiments were as in (A), except that mitochondria were incubated with the indicated mutants of cBID for 15 min. Data represent average ± SEM of four independent experiments. The asterisk denotes $p < 0.05$ in a paired sample Student's t test versus untreated.

(C) BNGE of mitochondrial OXPHOS protein from DKO MEFs transduced as indicated and, after 2 days, metabolically labeled for 2 hr and lysed after 24 hr. Equal amounts of protein (100 μg) were separated by BNGE, and radioactivity was detected in the fixed and dried gels for 1 week. RCC and RCS of the respiratory chain are indicated.

(D) Densitometric analysis of the autoradiographic RCS/complex V signal ratio. Data represent average ± SEM of three independent experiments performed as in (E). The asterisk denotes $p < 0.05$ in a paired sample Student's t test versus untreated.

(E) 2D BN/SDS PAGE analysis of mitochondrial OXPHOS proteins from DKO MEFs transduced as indicated, metabolically labeled for 2 hr, and lysed after 24 hr. Equal amount (50 μg) of proteins were separated in native condition, and then the lanes were excised and proteins separated by a second dimension SDS-PAGE. The gels were dried and the signal was detected following 1 week of exposure. RCC and RCS of the respiratory chain as well as the single-labeled proteins are indicated. Boxes and circles indicate RCS and cytochrome *b*, respectively.

(F) Densitometric analysis of the ratio of autoradiographic signal between supercomplex (boxed) and complex assembled cytochrome *b* (circled). Data represent average ± SEM of three independent experiments. The asterisk denotes $p < 0.05$ in a paired sample Student's t test versus untreated.

(G) BNGE analysis of OXPHOS proteins in mitochondria from DKO MEFs transduced as indicated. Equal amounts (100 μg) of proteins were separated in native conditions, transferred onto PVDF membranes, and probed with the indicated antibodies. RCC and RCS are indicated.

(H) RCR of DKO mitochondria energized with 5 mM/2.5 mM GLU/MAL or 10 mM SUCC treated for 15 min with the indicated cBID mutants. Data represent average ± SEM of four independent experiments. The asterisk denotes $p < 0.05$ in a paired sample Student's t test versus untreated.

See also Figure S2.

Conditional Ablation of *Opa1* Alters Cristae Shape and RCS Assembly

To verify whether RCS disorganization was a general consequence of altered cristae shape, we turned to cells lacking *Opa1*, a key regulator of cristae morphology (Frezza et al., 2006). However, chronic *Opa1* depletion impaired mitochondrial DNA (mtDNA) levels and translation (Figures S3A and S3B), complicating the analysis of the relationship between *Opa1* and RCS and calling for a model of conditional *Opa1* ablation. We produced, by homologous recombination, C57BL6/J

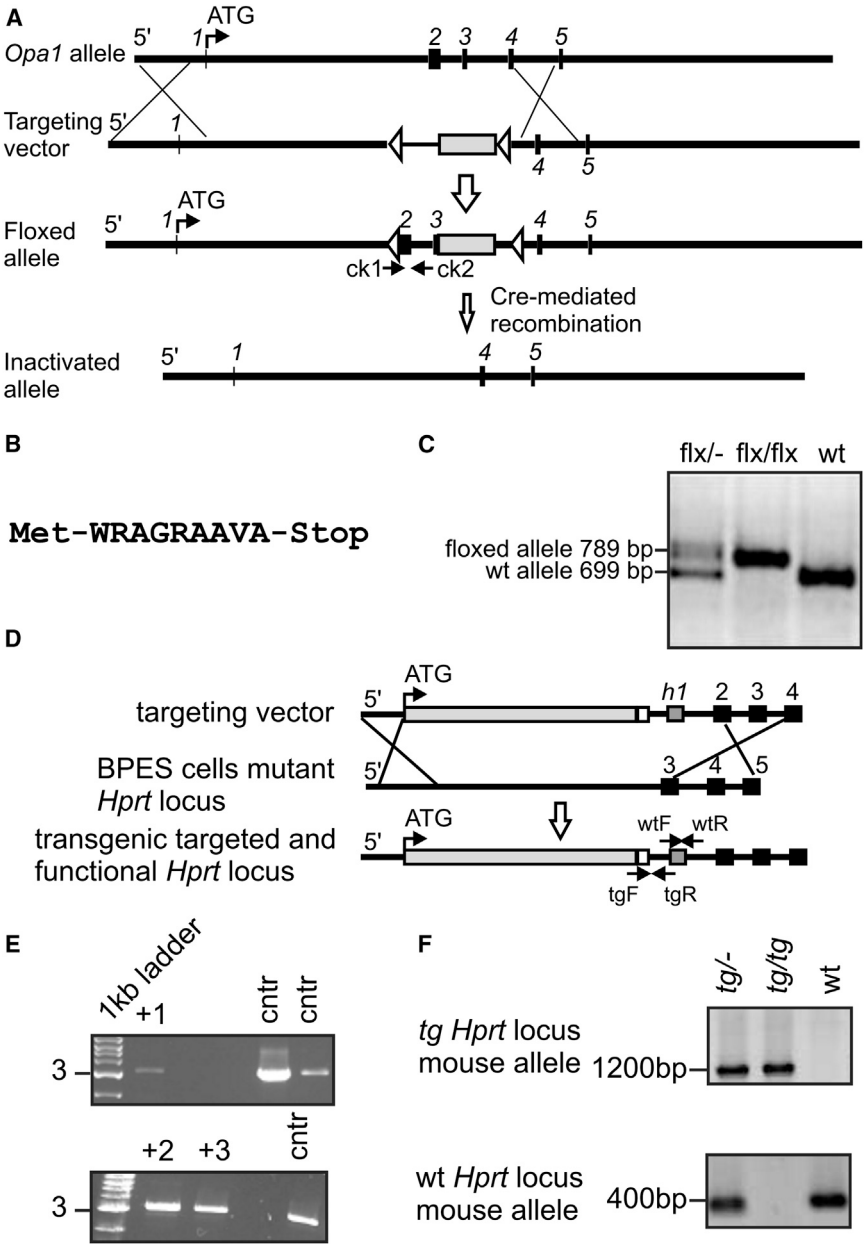

Figure 3. Generation of *Opa1*$^{flx/flx}$ and *Opa1*^{tg} Mice

(A) Maps of the wild-type *Opa1* allele, the targeting vector, the conditional floxed allele, and the inactivated *Opa1* allele. The 5′ UTR, exons (black boxes), LoxP sites (white arrows), FRT recombination sites, and PGK-neomycin cassette (white box) are indicated. The locations of PCR primers (*ck1 = primer check1 forward, ck2 = primer check2 reverse*) are indicated. Dimensions are not in scale.

(B) Prediction of the maximal possible aberrant OPA1 protein.

(C) RT-PCR analysis of transcripts in heterozygous (flx/−), homozygous (flx/flx), and WT mice.

(D) Maps of the targeting vector, the mutant *Hprt* locus of BPES cells, and the transgenic targeted and functional *Hprt* locus. The 5′ UTR, the human *β-ACTIN* promoter and *Opa1* gene (light gray box), poly A (white box), *human* exon 1 of *Hprt* locus (*h1*, dark gray box), and *Hprt* locus exons (black boxes) are indicated. The locations of PCR primers (WTF, WT forward; WTR, WT reverse; tgF, transgenic forward; tgR, transgenic reverse) are indicated. Dimensions are not in scale.

(E) RT-PCR screening of ESC clones. The positive clones are indicated.

(F) RT-PCR analysis of transcripts in heterozygous (tg/−), homozygous (tg/tg), and WT mice.

See also Figure S3.

embryonic stem cells with loxP sites inserted in the *Opa1* gene (*Opa1*$^{flx/flx}$), which were then microinjected in C57BL6/J blastocysts to generate *Opa1*$^{flx/flx}$ mice. Following Cre-mediated recombination, the deletion of exons 2 and 3 resulted in an aberrant exon1–exon4 transcript with a stop codon immediately after exon 1, producing a predicted 10 amino acid (aa) residual protein (Figures 3A and 3B). Chimerism and germ-line transmission of the offspring was tested by PCR, and germ-line transmittants were bred to homozygosity (Figure 3C). Fibroblasts isolated from the diaphragm of homozygous *Opa1*$^{flx/flx}$ 7-week-old male mice (MAFs) were immortalized and used for subsequent analysis. OPA1 was completely ablated 24 hr after adenoviral delivery of Cre recombinase (Figure 4A) and, as expected, mitochondria were fragmented (Figures 4B and 4C) with defects in cristae shape (Figures 4D and 4E). Four days after Cre-mediated *Opa1* ablation, mtDNA copy number (Figure 4F) and translation (Figures 4G and 4H) were unaffected, allowing us to specifically address the role of OPA1 and cristae shape in RCS assembly using an assay based on the incorporation of radiolabeled mtDNA-encoded proteins into RCC and RCS (Acín-Pérez et al., 2008). Upon acute *Opa1* ablation, the assembly of mtDNA-encoded subunits into RCC was not affected (data not shown). We therefore followed the RCS assembly rate (measured as the ratio between RCS and complex V radioactivity throughout the chase period) that resulted ~8-fold slower when Opa1 was ablated from *Opa1*$^{flx/flx}$ MAFs (Figures 4I and 4J). A similar reduction in the RCS assembly rate was observed in *Opa1*$^{-/-}$ MEFs (Figure S3C), suggesting that, in absence of *Opa1*, RCC are less superassembled, irrespective of their initial levels. To test if acute *Opa1* ablation altered RCS in vivo, we tail vein-injected Cre-expressing adenoviruses in *Opa1*$^{flx/flx}$ animals. After 72 hr, OPA1 levels in liver mitochondria were reduced by ~50% (Figure S4A), cristae morphology was abnormal (Figure S4B), RCS were reduced (Figure S4C), and glutamate/malate RCR was impaired (Figure 4K). These experiments of conditional ablation of *Opa1* identify a role for cristae shape in RCS assembly in vitro and in vivo.

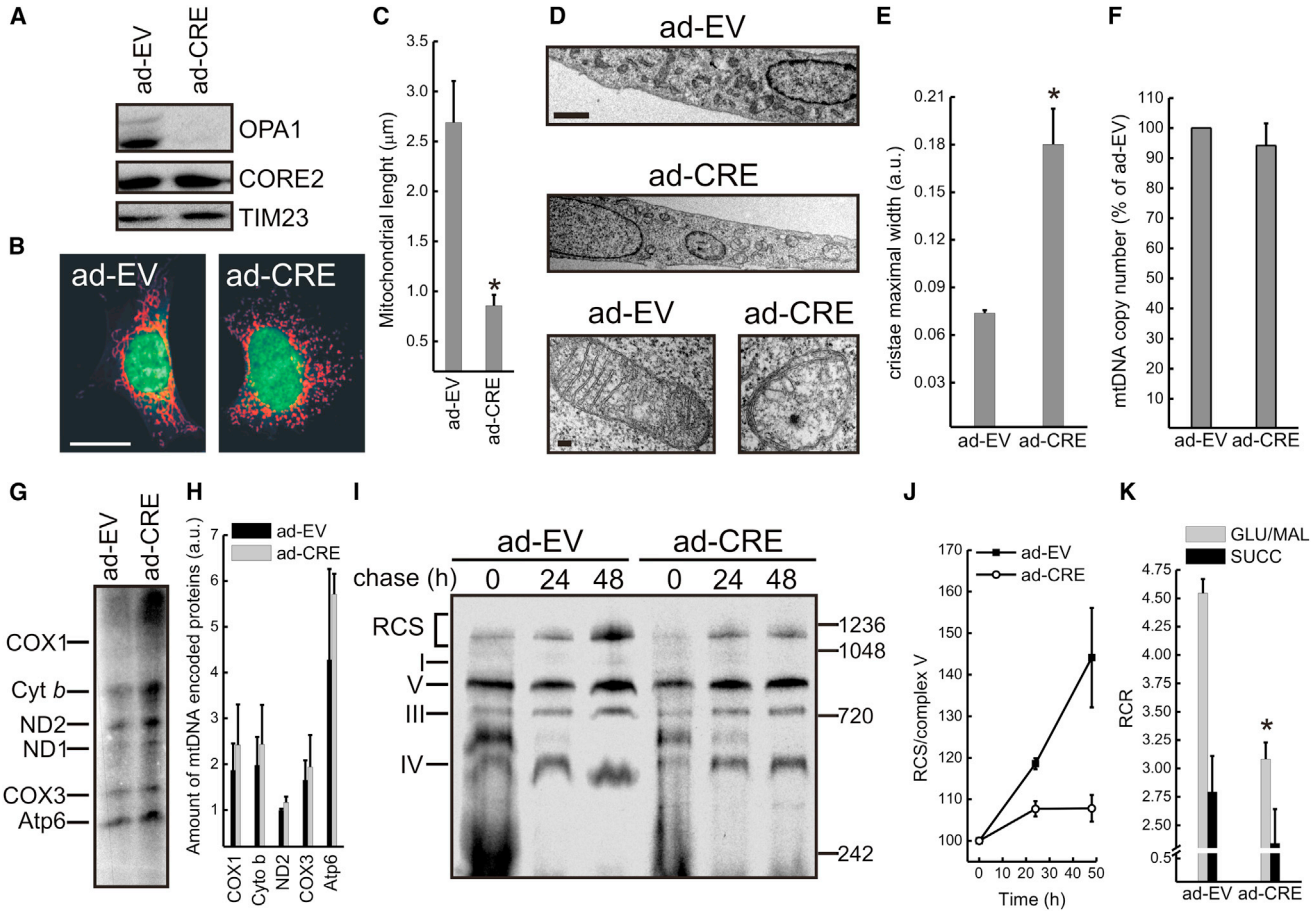

Figure 4. Acute Ablation of *Opa1* Alters Mitochondrial Morphology, Cristae Shape, and RCS Assembly

(A) *Opa1*$^{flx/flx}$ MAFs were infected with bicistronic adenoviruses carrying the indicated insert (EV, empty vector; CRE, Cre recombinase) upstream of GFP and, after 24 hr, equal amounts of proteins (20 μg) were separated by SDS-PAGE and immunoblotted with the indicated antibodies.

(B) *Opa1*$^{flx/flx}$ MAFs were infected with the indicated adenoviruses and, after 24 hr, fixed, immunostained using an anti-TOM20 antibody, and representative confocal images acquired. The green cytoplasmic staining identifies the coexpression of GFP. The scale bar represents 20 μm.

(C) Average mitochondrial major axis length. Experiments were as in (B). Data represent average ± SEM of four independent experiments (five mitochondria per cell, at least 50 cells/experiment). The asterisk denotes $p < 0.05$ in a paired sample Student's t test versus ad-EV.

(D) *Opa1*$^{flx/flx}$ MAFs were infected with the indicated adenoviruses and, after 24 hr, fixed and processed for electron microscopy. The scale bars represent 2 μm (top) and 200 nm (bottom).

(E) Morphometric analysis of cristae width in 40 randomly selected mitochondria of *Opa1*$^{flx/flx}$ MAFs infected with the indicated adenoviruses. Data represent average ± SEM of three independent experiments. The asterisk denotes $p < 0.05$ in a paired sample Student's t test versus ad-EV.

(F) Mitochondrial DNA copy number quantification. mtDNA was amplified by RT-PCR from total DNA of *Opa1*$^{flx/flx}$ MAFs infected with the indicated adenoviruses. Data are normalized to MAFs infected with control adenovirus and represent average ± SEM of four independent experiments.

(G) mtDNA translation assay. *Opa1*$^{flx/flx}$ MAFs infected as indicated were metabolic labeled in presence of emetine and lysed after 30 min. Protein samples (40 μg) were separated by SDS-PAGE, and the radioactivity was detected in the fixed and dried gels for 3 days. The mtDNA encoded proteins are indicated.

(H) Densitometric analysis of the mtDNA-encoded proteins. Experiments are as in (G). Data represent average ± SEM of four independent experiments.

(I) RCS assembly assay. *Opa1*$^{flx/flx}$ MAFs were infected as indicated and, after 24 hr, metabolically labeled for 2 hr and then chased for the indicated times. Equal amounts of protein (100 μg) were separated by BN PAGE, and radioactivity was detected in the fixed and dried gels for 1 week. RCC and RCS of the respiratory chain are indicated.

(J) Densitometric analysis of the incorporation rate of radioactivity into supercomplexes. Values are normalized for the autoradiographic signal of complex V. Data represent average ± SEM from three independent experiments performed as in (H).

(K) RCR of mitochondria isolated from livers of *Opa1*$^{flx/flx}$ mice 3 days after tail-vein injection of the indicated adenoviruses, energized with 5 mM/2.5 mM GLU/MAL or 10 mM SUCC. Data represent average ± SEM of four independent experiments. The asterisk denotes $p < 0.05$ in a paired sample Student's t test versus ad-EV.

See also Figure S4.

Overexpression of *Opa1* Increases RCS Assembly

The model linking cristae shape to RCS predicts that higher OPA1 levels should favor RCS assembly. To verify this hypothesis, we wanted to generate a mouse model of *Opa1* overexpression. Very high OPA1 levels are, however, toxic, causing paradoxical mitochondrial fragmentation (Cipolat

et al., 2004): we therefore targeted, by homologous recombination in the murine X chromosome *Hprt* region, a transgene-carrying mouse variant 1 *Opa1* under the human *β-actin* promoter (*Opa1*^{tg}) (Figure 3D). The integration into microinjected BPES embryonic stem cells was verified by PCR (Figure 3E), and the cells were microinjected into C57BL6/J blastocysts. Six generated agouti chimeras with a chimerism exceeding 90% were bred with C57BL6/J mates and tested for germline transmission by fur color and transgene PCR analysis (Figure 3F). Mice were viable, fertile, grew normally, and resisted to different forms of tissue damage (T.V., M.E.S., V. Romanello, S.C., V.C., R. Menabò, M. Sandri, F. Di Lisa, and L.S., unpublished data). Immortalized MAFs prepared from the diaphragm of hemizygous *Opa1*^{tg} 7-week-old C57BL6/J male mice displayed an ~1.5 increase in OPA1 levels compared to age- and sex-matched littermate controls MAFs (wild-type [WT]; Figure 5A). Mitochondria were slightly elongated (Figures 5B and 5C) and cristae tighter (Figures 5D and 5E), without any difference in mtDNA levels (Figure 5F) and translation (Figures 5G and 5H). Importantly, in *Opa1*^{tg} MAFs, RCS assembly (Figures 5I and 5J) and glutamate-supported RCR (Figure 5K) were increased. In vivo, an ~50% increase in liver mitochondria OPA1 levels (Figure S5A) was similarly associated to tighter cristae (Figure S5B) and increased RCS levels (Figure S5C). Taken together, these results indicate that RCS assembly is facilitated by increased OPA1 levels and tighter cristae.

Mitochondria-Supported Cell Growth Is Controlled by Cristae Shape

We next wished to address if cristae shape affects mitochondrial-dependent cell growth. We therefore measured the growth of DKO cells (resistant to BID-induced outer membrane permeabilization, caspase-dependent mitochondrial damage, and apoptosis) in galactose media, where most of cellular ATP comes from the respiratory chain (Acín-Pérez et al., 2004). WT and G94E tBID impaired growth in galactose, whereas cells transduced with tBID^{KKAA} that does not cause cristae remodeling did not display any defect (Figure 6A).

We next turned to genetic models of cristae shape changes. Growth in galactose-containing media was impaired upon acute ablation of *Opa1* in MAFs, whereas it was normal for fusion-deficient *Mfn1*$^{-/-}$, *Mfn2*$^{-/-}$ MEFs (Figures 6B and 6C), where mitochondrial fusion is also inhibited. In *Mfn1*$^{-/-}$, *Mfn2*$^{-/-}$ MEFs, mtDNA copy number was reduced (Figure S6A), but cristae shape (Figures S6B and S6C), mtDNA translation (Figure S6D), RCS stability (Figure S6E), and assembly (Figure S6F) were not affected. Thus, the galactose growth defect is not the consequence of impaired fusion but correlates with altered cristae shape and RCS. Finally, *Opa1*^{tg} MAFs grew faster than their WT counterparts in galactose media (Figure 6D), further confirming the link between cristae shape, RCS levels, and mitochondria-dependent cellular growth. In conclusion, cristae shape correlates with the efficiency of mitochondria-dependent cell growth.

DISCUSSION

Respiratory chain supercomplexes have been considered BNGE artifacts until direct respirometric experiments on purified RCS identified them as the functional mitochondrial respiratory units (Acín-Pérez et al., 2008). Since then, RCS have been directly visualized in intact cristae by electron tomography (Davies et al., 2011), complex IV assembly factors that favor RCS formation have been identified (Chen et al., 2012; Vukotic et al., 2012; Strogolova et al., 2012; Lapuente-Brun et al., 2013), and the role of RCS in mitochondrial utilization of reducing equivalents has been demonstrated (Lapuente-Brun et al., 2013). However, the relationship between cristae shape and RCS, as well as between RCS and mitochondrial function, remained obscure. Our results demonstrate that cristae shape regulates respiratory chain supercomplexes stability and assembly, impacting on respiratory efficiency and respiratory cell growth.

To dissect the role of cristae shape in RCS structure and function, we genetically ablated the master cristae shape regulator OPA1. Individual respiratory chain units associate with OPA1 (Zanna et al., 2008), and mitochondrial metabolism is deranged in dominant optic atrophy caused by *OPA1* mutations (Lodi et al., 2004). However, the defect in ATP production in *OPA1* haploinsufficient cells was unexplained: OPA1 is not essential for assembly of respiratory chain complexes and mtDNA levels as well as activities of individual respiratory chain complexes are normal in dominant optic atrophy (Zanna et al., 2008). Conversely, the reduction in mtDNA copy number has been invoked to explain the mitochondrial dysfunction of fusion-deficient cells from *Mfn1*, *Mfn2*-deficient mice (Chen et al., 2010). Our results challenge this hypothesis: upon acute *Opa1* ablation, mtDNA levels are normal, whereas cristae shape, RCS, complex-I-dependent respiration, and respiratory growth are impaired. Conversely, in *Mfn1*$^{-/-}$, *Mfn2*$^{-/-}$ cells, mtDNA copy number is reduced, but cristae shape, RCS, and respiratory growth are normal. Thus, RCS disorganization shall be regarded as a key mechanism of mitochondrial dysfunction accompanying altered organelle morphology.

The role of OPA1 and cristae shape in RCS organization is further supported by mouse models of *Opa1* conditional ablation and mild overexpression. The first tool allowed us to dissociate cristae biogenesis from mtDNA maintenance: whereas chronic *Opa1* depletion reduces mtDNA copy number and translation, upon acute *Opa1* ablation, mtDNA levels are normal, but cristae are disorganized, impacting on RCS assembly and respiratory function and growth. Thus, mtDNA reduction appears to be a consequence of chronic fusion inhibition in *Opa1*$^{-/-}$ (and double *Mfn*$^{-/-}$) cells. We can therefore predict that the *Opa1*$^{flx/flx}$ cells will be useful to elucidate how prolonged inhibition of mitochondrial fusion results in mtDNA levels reduction. *Opa1* mild overexpression lends further support to the model linking RCS organization to cristae shape: RCS assembly and respiratory function and growth are increased in *Opa1*^{tg} cells without any measurable change in mtDNA levels and translation. The *Opa1*^{tg} mouse will be instrumental to investigate the role of *Opa1* and cristae shape in vivo.

Apoptotic cristae remodeling further supports the relationship between cristae shape and RCS. The role and mechanisms of cristae remodeling in apoptosis are controversial (Scorrano et al., 2002; Germain et al., 2005; Frezza et al., 2006; Yamaguchi et al., 2008; Merkwirth et al., 2008; Costa et al., 2010). Despite that OPA1-mediated stabilization of cristae shape inhibits

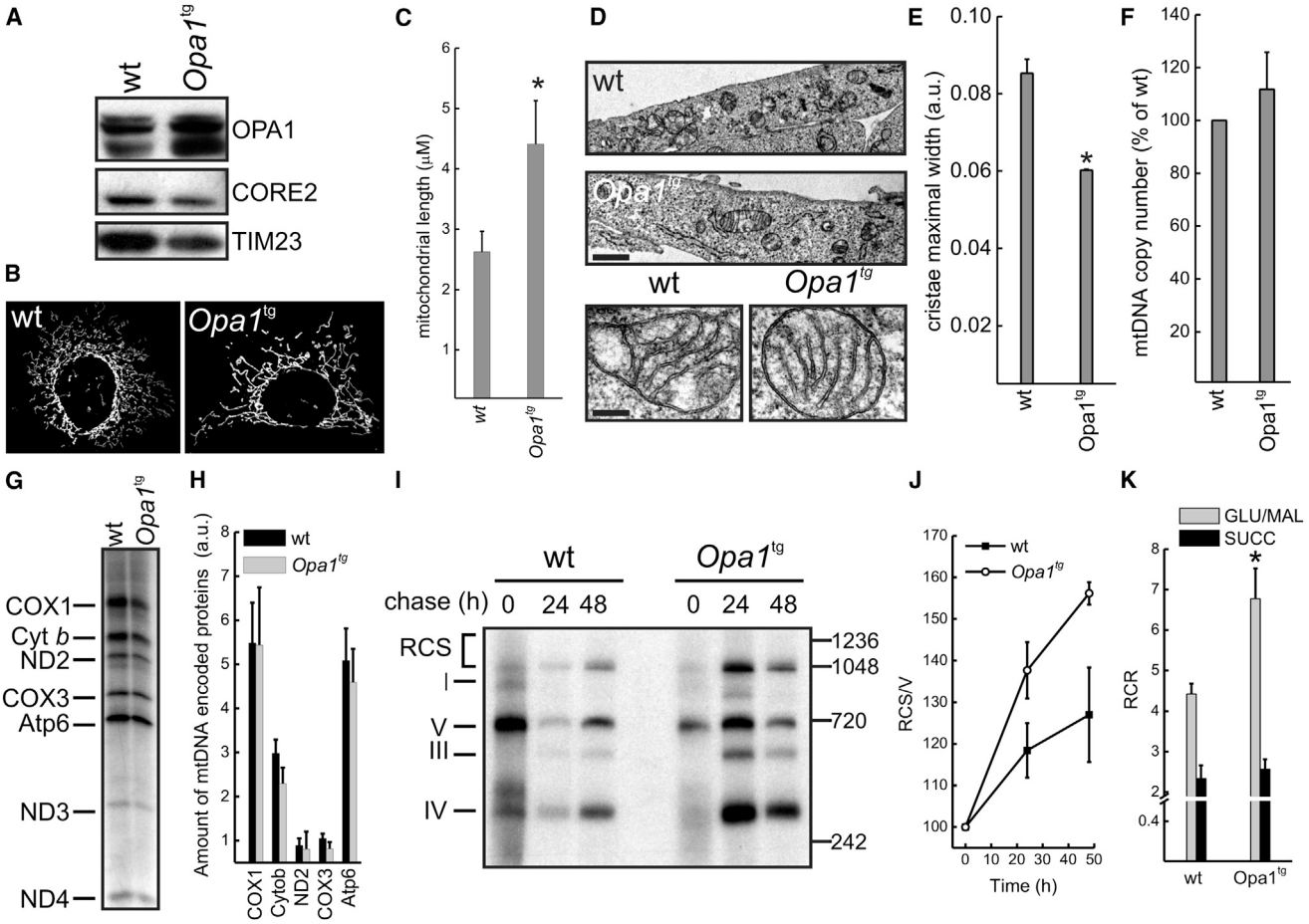

Figure 5. Transgenic Overexpression of OPA1 Increases RCS Assembly

(A) Equal amounts of proteins (20 μg) from MAFs of the indicated genotypes were separated by SDS-PAGE and immunoblotted with the indicated antibodies.

(B) Representative confocal micrographs of mitochondrial morphology in WT and Opa1^{tg} MAFs. Mitochondria were visualized by anti-TOM20 immunostaining. The scale bar represents 20 μM.

(C) Average mitochondrial major axis length. Experiments were as in (B). Data represent average ± SEM of four independent experiments (five mitochondria per cell, at least 50 cells/experiment). The asterisk denotes $p < 0.05$ in a paired sample Student's t test versus WT.

(D) Electron micrographs of MAFs of the indicated genotype. The scale bars represent 2 μm (top) and 200 nm (bottom).

(E) Morphometric analysis of cristae width in 40 randomly selected mitochondria of MAFs of the indicated genotype. Data represent average ± SEM of three independent experiments. The asterisk denotes $p < 0.05$ in a paired sample Student's t test versus WT.

(F) Mitochondrial DNA copy number quantification. mtDNA was amplified by RT-PCR from total DNA of MAFs of the indicated genotype. Data are normalized to WT MAFs and represent the average ± SEM of four independent experiments.

(G) mtDNA translation assay. MAFs of the indicated genotype were metabolic labeled in presence of emetine and lysed after 30 min. Protein samples (40 μg) were separated by SDS-PAGE, and the radioactivity was detected in the fixed and dried gels for 3 days. The mtDNA-encoded proteins are indicated.

(H) Densitometric analysis of the mtDNA-encoded proteins. Experiments are as in (G). Data represent average ± SEM of four independent experiments.

(I) RCS assembly assay. MAFs of the indicated genotype were metabolically labeled for 2 hr and then chased for the indicated times. Equal amounts of protein (100 μg) were separated by BN PAGE, and radioactivity was detected in the fixed and dried gels for 1 week. Individual complexes and supercomplexes of the respiratory chain are indicated.

(J) Densitometric analysis of the incorporation rate of radioactivity into RCS. Values are normalized for the autoradiographic signal of complex V. Data represent average ± SEM of three independent experiments performed as in (H).

(K) RCR of mitochondria isolated from livers of mice of the indicated genotype energized with 5 mM/2.5 mM GLU/MAL or 10 mM SUCC. Data represent mean ± SEM of four independent experiments. The asterisk denotes $p < 0.05$ in a paired sample Student's t test versus WT.

See also Figure S5.

intrinsic apoptosis (Frezza et al., 2006; Yamaguchi et al., 2008; Costa et al., 2010), cristae remodeling has been reckoned as a mere feedback mechanism in situ, occurring after caspase activation (Sun et al., 2007). Our results suggest that, in addition to its role in cytochrome *c* release, cristae remodeling also impairs mitochondrial function to precipitate apoptosis. The BID α6 mutant generated here, which does not induce cristae changes and cytochrome *c* mobilization but permeabilizes the outer

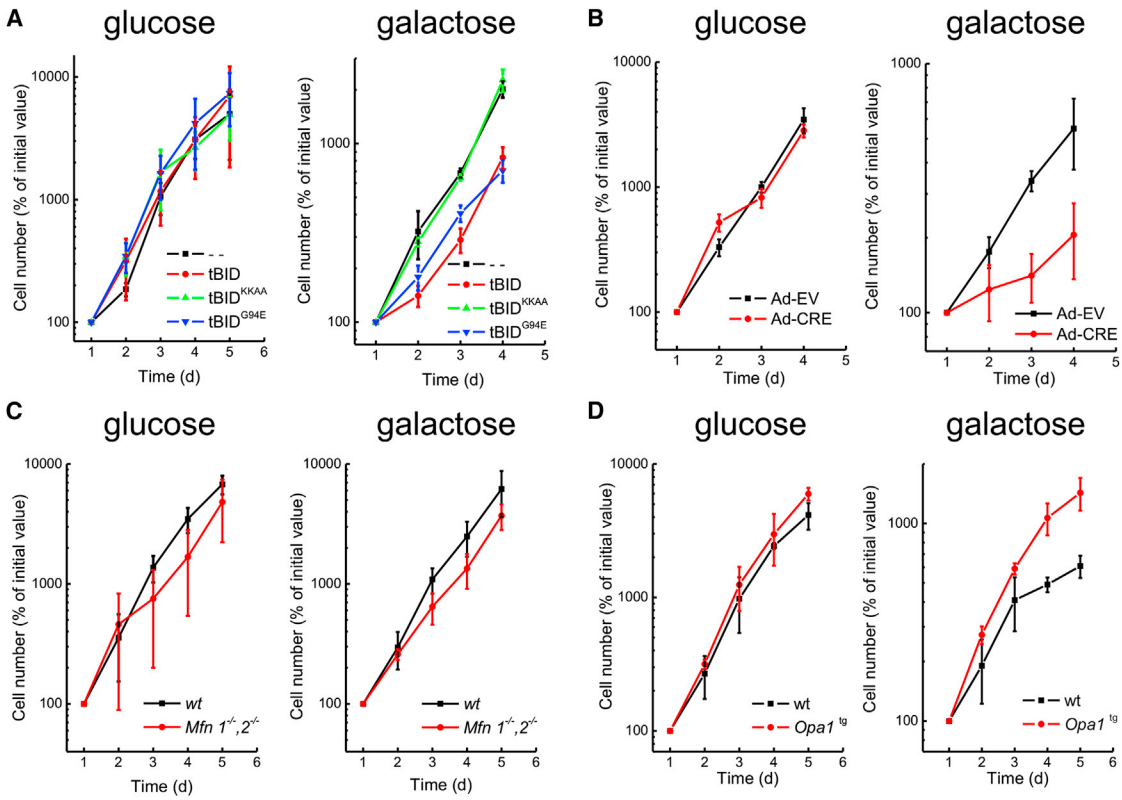

Figure 6. Mitochondria-Dependent Cellular Growth Requires Assembled RCS

(A) Growth curves of DKO MEFs transduced with the indicated retroviruses and grown in DMEM supplemented with the indicated monosaccharides. Data represent mean ± SEM of five independent experiments.

(B–D) Growth curves of the indicated cell lines cultured in DMEM supplemented with the indicated monosaccharides. Data represent mean ± SEM of five independent experiments.

See also Figure S6.

membrane, can be a useful tool to dissect in vivo the involvement of cristae remodeling in developmental and homeostatic apoptosis. We think that cristae remodeling influences RCS by targeting OPA1 (Frezza et al., 2006), not by altering membrane potential that is normal during cristae remodeling (Scorrano et al., 2002) or by inhibiting mtDNA translation and insertion of mtDNA-encoded subunits that similarly appear normal in DKO cell-expressing BID (data not shown).

Our work unravels a role for cristae shape in RCS assembly and stability, mitochondrial respiratory efficiency, and respiratory growth, suggesting that shape of biological membranes can influence membrane protein complexes. Moreover, our data highlight the importance of RCS in respiration by complex I-feeding substrates. Finally, we unveil how OPA1 regulates mitochondrial respiratory efficiency. The pathogenesis of dominant optic atrophy where OPA1 is mutated (Alexander et al., 2000) or of other mitochondrial diseases where OPA1 is degraded (Duvezin-Caubet et al., 2006) could also depend on this unexpected OPA1 function. In these latter settings, stabilization of OPA1 could correct RCS and therefore mitochondrial dysfunction, opening novel therapeutic perspectives for currently intractable diseases.

EXPERIMENTAL PROCEDURES

Generation of *Opa1*$^{flx/flx}$ and *Opa1*^{tg} Mice

To generate *Opa1*$^{flx/flx}$ mice, a mouse Bac clone containing the *Opa1* gene was isolated from the C57BL/6J ES BAC clone library. An 11 kb HpaI DNA restriction fragment containing the 5 kb upstream-exon3 was subcloned in a pUC-8 vector. The OPA1 fragment was excised with EcoRV and XmaI to generate blunt ends and inserted into a pKO4.4a-LoxP cut with XhoI and SalI. A LoxP site was introduced between intron1 and exon2 of *Opa1* and a phosphoglycerate kinase (PGK) promoter-driven neomycin resistance gene, flanked by two FRT sequences and with one LoxP sequence downstream, was inserted in intron3. The targeting vector was linearized and electroporated into C57BL6 embryonic stem cells (ESCs). Neomycin-resistant ESC clones were tested for homologous recombination. Three mutated ESC lines were microinjected into C57BL6 blastocytes and implanted in host mice to obtain chimeric mice, which were then bred with C57BL6 mates and their offspring tested by PCR for germline transmission. Colonies were established in a C57BL6 background.

To generate *Opa1*^{tg} mice, the human β-actin promoter was extracted from pDRIVE-hβ-ACTIN (InvivoGen) using SpeI and NcoI and cloned in pENTRY. The complementary DNA of mouse isoform 1 *Opa1* and polyA extracted from pcDNA3.1-OPA1 (Cipolat et al., 2004) using Nhe1 and EciI was ligated into pENTRY using Quick Ligase (Ozyme). The transgene was then inserted by homologous recombination in a pDEST vector containing part of the human hypoxanthine phosphoribosyltransferase locus. The resulting vector was

linearized using PvuI and electroporated into C57BL6 BPES cells by Nucleis (France). Homologous recombinants were selected on stringent hypoxanthine aminopterin-thymidine-supplemented medium. Three positive ESC recombinant clones were microinjected into C57BL6 blastocysts and implanted into host pseudopregnant female C57BL6 to obtain chimeric mice. Six chimeras (identified by fur agouti color) were bred with C57BL6 mates, and germline transmission was verified by fur color and PCR. Colonies were established in a C57BL6 and in a Sv129 background by crossbreeding. Details on mouse genotyping and handling can be found in the Extended Experimental Procedures.

BNGE, 2D BN/BNGE, and 2D BN/SDS PAGE

Mitochondria (10 mg/ml) were suspended in buffer D (1 M 6-aminohexanoic acid, 1.25% V/V digitonin, 50 mM Bis-Tris-HCl, pH 7) and centrifuged. The supernatant was collected, and 5% Serva Blue G dye in 1 M 6-aminohexanoic acid was added to 1/3 of the final sample volume. Equal amounts (100 μg) of mitochondrial proteins were separated by 3%–13% gradient BNGE (Schägger, 1995). For RCS detection, the concentration of digitonin in buffer D was 4% (V/V).

For two-dimensional (2D) Blue Native (BN)/BNGE, the lane cut from the first-dimension BNGE was casted on top of a native 3%–14% gradient gel in 1% (V/V) dodecyl maltoside. For 2D BN/SDS PAGE, the lane cut from the first-dimension BNGE was incubated for 1 hr at 25°C in 1% SDS and 1% β-mercaptoethanol and then casted on top of an 8% or a 16.5% denaturing gel. After electrophoresis, the complexes were electroblotted on a polyvinylidene fluoride (PVDF) membrane and probed with the indicated antibodies.

To detect RCS from radiolabelled cells, samples were treated as described above, and after electrophoresis, the gels were dried and the signal was detected following exposure for 3–6 days.

Pulse-Chase Experiments

Labeling of mtDNA-encoded proteins was performed with [^{35}S]-methionine and cysteine (EXPRE^{35}S^{35}S Protein Labeling Mix, Perkin Elmer Life Sciences). Cells were preincubated for 12 hr in the presence of 40 μg/ml chloramphenicol in uridine-supplemented medium and then exposed for 2 hr to the [^{35}S] protein labeling mix (pulse) in the presence of 50 μg/ml cycloheximide. Cells were washed for four times with PBS and cold Dulbecco's modified Eagle's medium (DMEM) and then cultured for the indicated time (chase) prior to lysis and protein separation by BNGE.

To assay basal mtDNA translation, equal protein amounts (40 μg) from cells metabolically labeled as described above treated for 30 min with 50 μg/ml emetine were separated by SDS-PAGE.

Mitochondrial Assays

Mitochondria from liver of mice and from the indicated cell lines were isolated as in Frezza et al. (2007). Cytochrome *c* release, ascorbate/TMPD-driven respiration and cytochrome b_5-dependent NADH oxidation were determined as described (Scorrano et al., 2002). Details can be found in the Extended Experimental Procedures.

Biochemistry

For protein crosslinking, mitochondria treated as indicated were incubated with 1 mM 1-ethyl-3-[3-dimethylaminopropyl]carbodiimide hydrochloride (EDC) or 1 mM bismaleimidohexane (BMH), as previously described (Frezza et al., 2006). Carbonate extraction was performed as previously described (Dimmer et al., 2008). Details and procedures for SDS-PAGE and immunoblotting can be found in the Extended Experimental Procedures.

Molecular Biology

The retroviral vector pMIG-tBid was described previously (Cheng et al., 2001). KKAA, G94E, and G94EKKAA mutants were generated by site-direct mutagenesis using KOD polymerase (Biolabs). Details can be found in the Extended Experimental Procedures.

To measure mtDNA copy number, total cellular DNA was amplified using specific oligodeoxynucleotides for *mt-Co2* and *Sdha* by real-time PCR. Details can be found in the Extended Experimental Procedures.

Cell Biology

MEFs and human embryonic kidney 293 cells (HEK293) cells were cultured as described (Gomes et al., 2011). When indicated, in DMEM, glucose was substituted with 0.9 mg/ml galactose. Ecotropic viruses were generated as described (Cheng et al., 2001). WT, *Opa1*$^{flx/flx}$, *Opa1*^{tg}, and MAFs SV40 transformed cell lines were generated from the diaphragm of the respective 7-week-old mouse killed by cervical dislocation. Details on the procedure can be found in the Extended Experimental Procedures. Acute *Opa1* ablation in *Opa1*$^{flx/flx}$ MAFs was obtained by infection with adenoviruses expressing cytomegalovirus (CMV)-Cre-GFP (ad-CRE; 300 pfu/cell; Vector Biolabs). CMV-GFP (ad-EV)-expressing adenoviruses were used as control.

Cell growth was determined by counting viable cells for the indicated time. *Opa1*$^{flx/flx}$ MAFs were infected and DKO MEFs were transduced 24 or 16 hr before the growth was assessed.

Apoptosis was measured by flow cytometric detection (FACSCalibur) of the Annexin-V-PE positive events in the GFP-positive population. Details can be found in the Extended Experimental Procedures.

Imaging and Transmission Electron Microscopy

For mitochondrial imaging, cells stained with a rabbit polyclonal anti-TOM20 (Santa Cruz; 1:200), as previously described (Frezza et al., 2006), were analyzed by confocal microscopy. Adenovirus-infected cells were identified by GFP expression. Electron microscopy (EM) was performed as described (Scorrano et al., 2002). Details can be found in the Extended Experimental Procedures.

SUPPLEMENTAL INFORMATION

Supplemental Information includes Extended Experimental Procedures and six figures and can be found with this article online at http://dx.doi.org/10.1016/j.cell.2013.08.032.

ACKNOWLEDGMENTS

We thank A. Gross (Weizmann Institute) for anti-BID antibody, A. Latorre-Pellicer (CNIC) for mtDNA RT-PCR, and M. Albiero (VIMM) for tail vein injections. L.S. is a senior scientist of the Dulbecco-Telethon Institute. This work is supported by Telethon Italy (GGP12162, GPP10005B, and TCR02016), AIRC Italy, MOH Italy (GR 09.021), and Swiss National Foundation (31-118171). J.A.E. is supported by MINECO (SAF2012-32776 and CSD2007-00020), DGA (B55, PIPAMER O905), and CAM (S2011/BMD-2402). S.C. was supported by a Journal of Cell Science Travelling Fellowship. C.F. was supported by an AIRC Biennial Fellowship. The CNIC is funded by the Instituto de Salud Carlos III-MICINN and the Pro-CNIC Foundation.

Received: December 28, 2012
Revised: July 25, 2013
Accepted: August 19, 2013
Published: September 19, 2013

REFERENCES

Acín-Pérez, R., Bayona-Bafaluy, M.P., Fernández-Silva, P., Moreno-Loshuertos, R., Pérez-Martos, A., Bruno, C., Moraes, C.T., and Enríquez, J.A. (2004). Respiratory complex III is required to maintain complex I in mammalian mitochondria. Mol. Cell *13*, 805–815.

Acín-Pérez, R., Fernández-Silva, P., Peleato, M.L., Pérez-Martos, A., and Enriquez, J.A. (2008). Respiratory active mitochondrial supercomplexes. Mol. Cell *32*, 529–539.

Alexander, C., Votruba, M., Pesch, U.E., Thiselton, D.L., Mayer, S., Moore, A., Rodriguez, M., Kellner, U., Leo-Kottler, B., Auburger, G., et al. (2000). OPA1, encoding a dynamin-related GTPase, is mutated in autosomal dominant optic atrophy linked to chromosome 3q28. Nat. Genet. *26*, 211–215.

Campanella, M., Casswell, E., Chong, S., Farah, Z., Wieckowski, M.R., Abramov, A.Y., Tinker, A., and Duchen, M.R. (2008). Regulation of mitochondrial

structure and function by the F1Fo-ATPase inhibitor protein, IF1. Cell Metab. *8*, 13–25.

Cereghetti, G.M., Stangherlin, A., Martins de Brito, O., Chang, C.R., Blackstone, C., Bernardi, P., and Scorrano, L. (2008). Dephosphorylation by calcineurin regulates translocation of Drp1 to mitochondria. Proc. Natl. Acad. Sci. USA *105*, 15803–15808.

Chen, H., Detmer, S.A., Ewald, A.J., Griffin, E.E., Fraser, S.E., and Chan, D.C. (2003). Mitofusins Mfn1 and Mfn2 coordinately regulate mitochondrial fusion and are essential for embryonic development. J. Cell Biol. *160*, 189–200.

Chen, H., Vermulst, M., Wang, Y.E., Chomyn, A., Prolla, T.A., McCaffery, J.M., and Chan, D.C. (2010). Mitochondrial fusion is required for mtDNA stability in skeletal muscle and tolerance of mtDNA mutations. Cell *141*, 280–289.

Chen, Y.C., Taylor, E.B., Dephoure, N., Heo, J.M., Tonhato, A., Papandreou, I., Nath, N., Denko, N.C., Gygi, S.P., and Rutter, J. (2012). Identification of a protein mediating respiratory supercomplex stability. Cell Metab. *15*, 348–360.

Cheng, E.H., Wei, M.C., Weiler, S., Flavell, R.A., Mak, T.W., Lindsten, T., and Korsmeyer, S.J. (2001). BCL-2, BCL-X(L) sequester BH3 domain-only molecules preventing BAX- and BAK-mediated mitochondrial apoptosis. Mol. Cell *8*, 705–711.

Cipolat, S., Martins de Brito, O., Dal Zilio, B., and Scorrano, L. (2004). OPA1 requires mitofusin 1 to promote mitochondrial fusion. Proc. Natl. Acad. Sci. USA *101*, 15927–15932.

Cipolat, S., Rudka, T., Hartmann, D., Costa, V., Serneels, L., Craessaerts, K., Metzger, K., Frezza, C., Annaert, W., D'Adamio, L., et al. (2006). Mitochondrial rhomboid PARL regulates cytochrome c release during apoptosis via OPA1-dependent cristae remodeling. Cell *126*, 163–175.

Costa, V., Giacomello, M., Hudec, R., Lopreiato, R., Ermak, G., Lim, D., Malorni, W., Davies, K.J., Carafoli, E., and Scorrano, L. (2010). Mitochondrial fission and cristae disruption increase the response of cell models of Huntington's disease to apoptotic stimuli. EMBO Mol Med *2*, 490–503.

Danial, N.N., and Korsmeyer, S.J. (2004). Cell death: critical control points. Cell *116*, 205–219.

Davies, K.M., Strauss, M., Daum, B., Kief, J.H., Osiewacz, H.D., Rycovska, A., Zickermann, V., and Kühlbrandt, W. (2011). Macromolecular organization of ATP synthase and complex I in whole mitochondria. Proc. Natl. Acad. Sci. USA *108*, 14121–14126.

de Brito, O.M., and Scorrano, L. (2008). Mitofusin 2 tethers endoplasmic reticulum to mitochondria. Nature *456*, 605–610.

Dimmer, K.S., and Scorrano, L. (2006). (De)constructing mitochondria: what for? Physiology (Bethesda) *21*, 233–241.

Duvezin-Caubet, S., Jagasia, R., Wagener, J., Hofmann, S., Trifunovic, A., Hansson, A., Chomyn, A., Bauer, M.F., Attardi, G., Larsson, N.G., et al. (2006). Proteolytic processing of OPA1 links mitochondrial dysfunction to alterations in mitochondrial morphology. J. Biol. Chem. *281*, 37972–37979.

Frey, T.G., and Mannella, C.A. (2000). The internal structure of mitochondria. Trends Biochem. Sci. *25*, 319–324.

Frezza, C., Cipolat, S., Martins de Brito, O., Micaroni, M., Beznoussenko, G.V., Rudka, T., Bartoli, D., Polishuck, R.S., Danial, N.N., De Strooper, B., and Scorrano, L. (2006). OPA1 controls apoptotic cristae remodeling independently from mitochondrial fusion. Cell *126*, 177–189.

Germain, M., Mathai, J.P., McBride, H.M., and Shore, G.C. (2005). Endoplasmic reticulum BIK initiates DRP1-regulated remodelling of mitochondrial cristae during apoptosis. EMBO J. *24*, 1546–1556.

Gomes, L.C., Di Benedetto, G., and Scorrano, L. (2011). During autophagy mitochondria elongate, are spared from degradation and sustain cell viability. Nat. Cell Biol. *13*, 589–598.

Green, D.R., and Kroemer, G. (2004). The pathophysiology of mitochondrial cell death. Science *305*, 626–629.

Griparic, L., and van der Bliek, A.M. (2001). The many shapes of mitochondrial membranes. Traffic *2*, 235–244.

Hackenbrock, C.R. (1966). Ultrastructural bases for metabolically linked mechanical activity in mitochondria. I. Reversible ultrastructural changes with change in metabolic steady state in isolated liver mitochondria. J. Cell Biol. *30*, 269–297.

Landes, T., Emorine, L.J., Courilleau, D., Rojo, M., Belenguer, P., and Arnauné-Pelloquin, L. (2010). The BH3-only Bnip3 binds to the dynamin Opa1 to promote mitochondrial fragmentation and apoptosis by distinct mechanisms. EMBO Rep. *11*, 459–465.

Lapuente-Brun, E., Moreno-Loshuertos, R., Acín-Pérez, R., Latorre-Pellicer, A., Colás, C., Balsa, E., Perales-Clemente, E., Quirós, P.M., Calvo, E., Rodríguez-Hernández, M.A., et al. (2013). Supercomplex assembly determines electron flux in the mitochondrial electron transport chain. Science *340*, 1567–1570.

Legros, F., Lombès, A., Frachon, P., and Rojo, M. (2002). Mitochondrial fusion in human cells is efficient, requires the inner membrane potential, and is mediated by mitofusins. Mol. Biol. Cell *13*, 4343–4354.

Lodi, R., Tonon, C., Valentino, M.L., Iotti, S., Clementi, V., Malucelli, E., Barboni, P., Longanesi, L., Schimpf, S., Wissinger, B., et al. (2004). Deficit of in vivo mitochondrial ATP production in OPA1-related dominant optic atrophy. Ann. Neurol. *56*, 719–723.

Merkwirth, C., Dargazanli, S., Tatsuta, T., Geimer, S., Löwer, B., Wunderlich, F.T., von Kleist-Retzow, J.C., Waisman, A., Westermann, B., and Langer, T. (2008). Prohibitins control cell proliferation and apoptosis by regulating OPA1-dependent cristae morphogenesis in mitochondria. Genes Dev. *22*, 476–488.

Minauro-Sanmiguel, F., Wilkens, S., and García, J.J. (2005). Structure of dimeric mitochondrial ATP synthase: novel F0 bridging features and the structural basis of mitochondrial cristae biogenesis. Proc. Natl. Acad. Sci. USA *102*, 12356–12358.

Paumard, P., Vaillier, J., Coulary, B., Schaeffer, J., Soubannier, V., Mueller, D.M., Brèthes, D., di Rago, J.P., and Velours, J. (2002). The ATP synthase is involved in generating mitochondrial cristae morphology. EMBO J. *21*, 221–230.

Pfeiffer, D.R., Gudz, T.I., Novgorodov, S.A., and Erdahl, W.L. (1995). The peptide mastoparan is a potent facilitator of the mitochondrial permeability transition. J. Biol. Chem. *270*, 4923–4932.

Santel, A., and Fuller, M.T. (2001). Control of mitochondrial morphology by a human mitofusin. J. Cell Sci. *114*, 867–874.

Santel, A., Frank, S., Gaume, B., Herrler, M., Youle, R.J., and Fuller, M.T. (2003). Mitofusin-1 protein is a generally expressed mediator of mitochondrial fusion in mammalian cells. J. Cell Sci. *116*, 2763–2774.

Schägger, H. (1995). Native electrophoresis for isolation of mitochondrial oxidative phosphorylation protein complexes. Methods Enzymol. *260*, 190–202.

Scorrano, L., Ashiya, M., Buttle, K., Weiler, S., Oakes, S.A., Mannella, C.A., and Korsmeyer, S.J. (2002). A distinct pathway remodels mitochondrial cristae and mobilizes cytochrome c during apoptosis. Dev. Cell *2*, 55–67.

Smirnova, E., Griparic, L., Shurland, D.L., and van der Bliek, A.M. (2001). Dynamin-related protein Drp1 is required for mitochondrial division in mammalian cells. Mol. Biol. Cell *12*, 2245–2256.

Strauss, M., Hofhaus, G., Schröder, R.R., and Kühlbrandt, W. (2008). Dimer ribbons of ATP synthase shape the inner mitochondrial membrane. EMBO J. *27*, 1154–1160.

Strogolova, V., Furness, A., Robb-McGrath, M., Garlich, J., and Stuart, R.A. (2012). Rcf1 and Rcf2, members of the hypoxia-induced gene 1 protein family, are critical components of the mitochondrial cytochrome bc1-cytochrome c oxidase supercomplex. Mol. Cell. Biol. *32*, 1363–1373.

Sun, M.G., Williams, J., Munoz-Pinedo, C., Perkins, G.A., Brown, J.M., Ellisman, M.H., Green, D.R., and Frey, T.G. (2007). Correlated three-dimensional light and electron microscopy reveals transformation of mitochondria during apoptosis. Nat. Cell Biol. *9*, 1057–1065.

Vogel, F., Bornhövd, C., Neupert, W., and Reichert, A.S. (2006). Dynamic subcompartmentalization of the mitochondrial inner membrane. J. Cell Biol. *175*, 237–247.

Vukotic, M., Oeljeklaus, S., Wiese, S., Vögtle, F.N., Meisinger, C., Meyer, H.E., Zieseniss, A., Katschinski, D.M., Jans, D.C., Jakobs, S., et al. (2012). Rcf1 mediates cytochrome oxidase assembly and respirasome formation, revealing heterogeneity of the enzyme complex. Cell Metab. *15*, 336–347.

Wei, M.C., Lindsten, T., Mootha, V.K., Weiler, S., Gross, A., Ashiya, M., Thompson, C.B., and Korsmeyer, S.J. (2000). tBID, a membrane-targeted death ligand, oligomerizes BAK to release cytochrome c. Genes Dev. *14*, 2060–2071.

Wei, M.C., Zong, W.X., Cheng, E.H., Lindsten, T., Panoutsakopoulou, V., Ross, A.J., Roth, K.A., MacGregor, G.R., Thompson, C.B., and Korsmeyer, S.J. (2001). Proapoptotic BAX and BAK: a requisite gateway to mitochondrial dysfunction and death. Science *292*, 727–730.

Yamaguchi, R., Lartigue, L., Perkins, G., Scott, R.T., Dixit, A., Kushnareva, Y., Kuwana, T., Ellisman, M.H., and Newmeyer, D.D. (2008). Opa1-mediated cristae opening is Bax/Bak and BH3 dependent, required for apoptosis, and independent of Bak oligomerization. Mol. Cell *31*, 557–569.

Yoon, Y., Pitts, K.R., and McNiven, M.A. (2001). Mammalian dynamin-like protein DLP1 tubulates membranes. Mol. Biol. Cell *12*, 2894–2905.

Zanna, C., Ghelli, A., Porcelli, A.M., Karbowski, M., Youle, R.J., Schimpf, S., Wissinger, B., Pinti, M., Cossarizza, A., Vidoni, S., et al. (2008). OPA1 mutations associated with dominant optic atrophy impair oxidative phosphorylation and mitochondrial fusion. Brain *131*, 352–367.

Results

The multifunctional mitochondrial inner membrane protein Optic Atrophy 1 controls cellular damage in vivo

Tatiana Varanita[1], M.E. Soriano Garcìa Cuerva[1], Vanina Romanello[1,3], Tania Zaglia[1,3], Roberta Menabò[3], Veronica Costa[2], Sara Cogliati[1], Ruth Slack[4], Marco Mongillo[1,3], Marco Sandri[1,3], Fabio Di Lisa[3], and Luca Scorrano[1,2]

[1] *Dulbecco Telethon Institute, Venetian Institute of Molecular Medicine, Via Orus 2, 35129 Padova, Italy;*

[2] *Dept. of Biology, University of Padova, V.C. 3, 35121 Padova, Italy;*

[3] *Dept. of Biomedical Sciences, University of Padova, V.C. 3, 35121 Padova, Italy;*

[4] *Center for Neuroscience, University of Ottawa, Canada;*

Address correspondence to

Luca Scorrano. Email: luca.scorrano@unipd.it

Character count:

Summary

Mitochondrial morphological changes have been implied in apoptosis and autophagy in several in vitro models, but their relevance to tissue adaptation to damaging insults is unexplored. Here we show that controlled mild overexpression of Optic atrophy 1 (OPA1), an inner mitochondrial membrane protein that controls cristae remodeling and mitochondrial respiratory efficiency, protects multiple tissues from apoptotic, necrotic and atrophic stimuli. Targeted insertion of one copy of OPA1 in a permissive X chromosome locus does not interfere with mouse development, but it protects from ischemic damage in the heart and the brain, as well as from muscular atrophy and hepatocellular apoptosis. Mechanistically, OPA1 stabilizes the cristae, increasing mitochondrial respiratory efficiency, blunting cytochrome c release in vitro and in vivo as well as mitochondrial dysfunction. Our results indicate that the OPA1-dependent cristae remodeling pathway is an essential determinant of the cellular response to tissue damage in vivo.

Introduction

Mitochondria are crucial organelles mediating several key processes such as energy conversion and calcium homeostasis (Danial et al., 2003; Rizzuto et al., 2000). Impaired mitochondrial function is involved in cellular damage especially in tissues with high energy demand such as heart, skeletal muscle, and nervous system (DiMauro and Schon, 2003). Cellular damage is not only the consequence of the bioenergetic failure of mitochondria, since these organelles play also a crucial role in apoptosis. They integrate and release lethal signals leading to cell death (Green and Kroemer, 2004). In response to several stimuli mitochondria release cytochrome *c* and other pro-apoptotic proteins that execute the demise of the cell (Wang, 2001). Mitochondrial permeabilization during apoptosis is controlled by members of the Bcl-2 family and is accompanied by both morphological and ultrastructural changes of the organelle (Danial and Korsmeyer, 2004; Wasilewski and Scorrano, 2009). Mitochondrial network fragmentation and cristae remodeling with the widening of the cristae junction are both required for the complete release of cytochrome *c* (Scorrano et al., 2002; Yamaguchi et al., 2008).

Mitochondria are highly dynamic organelles that continuously fuse and divide. These processes are controlled by a family of Dynamin-related large GTPases (Griparic and van der Bliek, 2001). Mitochondrial fission is regulated by the recruitment of Dynamin related protein (DRP) 1 on the outer mitochondrial membrane (OMM) upon calcineurin dependent dephosphorylation (Cereghetti et al., 2008), where it binds to its adaptors on the OMM like fission 1 (Fis1),

mitochondrial fission factor (MFF) and mitochondrial division (Mid) 49 and 51 (Palmer et al., 2011). This fission process is counterbalanced by mitochondrial fusion, controlled by Mitofusins (MFN) 1 and 2, in the OMM, and by OPA1 in the inner mitochondrial membrane (IMM) (Chen et al., 2003; Santel et al., 2003; Cipolat et al., 2004). The IMM is the metabolically active site of the organelle and it can be divided in two subcompartments, the so-called "boundary membrane" and the cristae, separated from the former by narrow tubular junctions (Frey and Mannella, 2000). Cristae shape is not static, as it became apparent when the transition from the orthodox to the condensed morphology upon activation of mitochondrial respiration was discovered (Hackenbrock, 1966). A different modification occurs during apoptosis, when cristae membrane curvature is inverted and the tubular cristae junctions enlarge in a process that is required for the complete release of cytochrome *c* (Scorrano et al., 2002). Remodeling of mitochondrial cristae occurs in response to pro-apoptotic BH3-only BCL-2 family members such as BID, BIM-S and BNIP3 and independently of outer membrane permeabilization (Scorrano et al., 2002; Yamaguchi et al., 2008; Landes et al., 2010). In addition and independently to its role in mitochondrial fusion, OPA1 regulates mitochondrial apoptotic cristae remodeling (Frezza et al., 2006; Cipolat et al., 2006). OPA1 form oligomers that participate in formation and maintenance of cristae junctions. During apoptosis these complexes are disrupted leading to widening of cristae junctions and subsequent redistribution of cytochrome c (Frezza et al., 2006). Moreover, OPA1 has a direct metabolic effect, stabilizing

respiratory chain supercomplexes (RCS) by maintaining mitochondrial cristae morphology (Cogliati et al., 2013).

Cristae remodeling does not occur after the permeabilization of the outer membrane, but it appears to represent a subroutine engaged early in response to an apoptotic insult to mitochondria and not a part of a late amplificatory loop (Frezza et al., 2006; Yamaguchi et al., 2008; Cogliati et al., 2013). An elegant correlative light-electron tomography study reported instead that a caspase inhibitor blocked cristae remodeling but not the release of cytochrome *c*, albeit possible experimental artifacts associated with the use of a cytochrome *c*-4CYS reporter molecule, which in principle does not behave like the endogenous cytochrome *c* pool and requires harsh treatment to the cells in order to be visualized (Sun et al., 2007; Goldstein et al., 2005) could confound the conclusions of this report. Moreover, cristae remodeling has been so far described at best in cells and our understanding of its role in reversible and irreversible cell damage in vivo is at best scant. The identification of the key role of OPA1 in cristae remodeling suggests a potential approach to manipulate this process in the living animal; however, constitutive as well as conditional tissue specific OPA1 ablation is lethal (Zhang et al., 2011; Davies et al., 2007), while uncontrolled OPA1 overexpression is toxic (Cipolat et al., 2004), complicating the generation of suitable in vivo models.

To circumvent the difficulties related to in vivo models of cristae shape alteration, we recently generated a mouse model where a transgene in which expression of OPA1 isoform 1 under the control of the ubiquitous promoter human beta-actin

was purposely targeted to a permissive region of the X chromosome, without altering endogenous gene expression (Cogliati et al., 2013). We capitalized on this novel mouse model to investigate whether increased OPA1 levels that prevent cristae remodeling, changes the response to tissue damage in organs with high metabolic activity. Our data indicate that mild OPA1 overexpression is compatible with life, yet it ameliorates the tissue response to apoptotic, necrotic and atrophic stimuli. Mechanistically, OPA1 blunts cytochrome c release and mitochondrial dysfunction, highlighting the importance of cristae shape in the control of cell death in the adult animal.

Controlled OPA1 overexpression is compatible with embryonic development and does not affect lifespan.

OPA1 overexpressing mice were generated by targeting a single copy of murine *Opa1* isoform 1 driven by human β actin promoter immediately upstream of the *Hprt* locus, located in the X chromosome in the mouse (Cogliati et al., 2013) see also the general scheme of the targeted transgenesis strategy and the PCR analysis of genomic DNA in Figure 1 A, B. We chose to use the human β- actin promoter because when it is close to the *Hprt* locus, it directs moderate expression in a wide variety of tissues (Bronson et al., 1996), thereby avoiding the toxic side effects caused by very high levels of OPA1 overexpression (Cipolat et al., 2004). *Opa1*^{tg} mice were backcrossed for more than 10 generations in the genetic backgrounds C57/Bl6J and SV129. *Opa1*^{tg} mice were born at the expected Mendelian frequency,

developed and grew normally. The resulting *Opa1*^{tg} mice apparently indistinguishable from sex- and age-matched control wild type (Wt). A mild OPA1 overexpression, ~1,5 was detected by western blot analysis in different tissues like heart, muscle, liver, brain and cerebellum (Figure 1 C, D), without concomitant changes in the protein expression levels of the key proteins involved in fusion, fission, as well as in the pro-apoptotic and anti-apoptotic mitochondrial proteins (Figure 1S A, B). There were no differences in the body weight of the *Opa1*^{tg} compared with Wt littermates during the initial 60 days after birth. (Figure 1S C). However 5 months old males and females *Opa1*^{tg} mice bred in the C57/Bl6J background showed a slightly but significant reduction in body weight compared to their Wt littermate, which was maintained up to 9 months of age (Figure 1 E), without altering however the overall survival as shown by a Kaplan-Meyer censorial analysis (Figure 1 F, G). Conversely, OPA1 overexpression had no effect on body weight in the Sv129 background (Figure 1S D), where however it correlated with an increased incidence of hematological and solid tumors that significantly reduced lifespan (not shown). In conclusion *Opa1*^{tg} mice are viable and display no apparent major phenotype, indicating that a mild OPA1 overexpression is compatible with life and fertility.

OPA1 protects from age-associated atrophy

Opa1^{tg} animals appeared in a better general health condition than their Wt littermates, especially when aged above 6 months. To substantiate objectively this subjective observation, we analyzed morphologically and histologically several

organs. 9 months after birth, hearts of *Opa1*^{tg} mice appeared significantly bigger than their Wt littermates (Figure 2 A). This increase in heart size was supported by an increase in the heart weight / body weight ratio that was not apparent in younger animals (Figure 2 B) and by a significant increase in cardiomyocyte cross-sectional area at 9 months (Figure 2C,D), which again was not observed at 5 months (Figure 2S A, B). However, this apparent hypertrophic phenotype was not accompanied by echocardiographic signs of cardiac dysfunction at 9 (Figure 2 E, F) or 5 months (Figure 2S C). In accordance with the functional analysis, signs of hypertrophy were not retrieved in 9 months old *Opa1*^{tg} heart histology: (Figure 2 G) staining for the fetal genes associated with cardiac hypertrophy (Du, 2007) such as beta myosin heavy chain (β-MHC) (Figure H) and atrial natriuretic peptide (ANP) (Figure 2 I) was negative and no signs of interstitial fibrosis were detected (Figure 2S E), exactly as in 5 month old mice (Figure 2S D). Other organs, such as liver and kidney were not enlarged both at the ecographic and the histological inspection (Figure 2S F, G, H, I). Thus, old *Opa1*^{tg} mice display a non-pathological cardiac hypertrophy.

Opa1^{tg} mice are protected from muscular atrophy

We reasoned that the benign heart hypertrophy observed in old *Opa1*^{tg} mice could be explained if *Opa1*^{tg} muscular cells were less susceptible to the atrophic program, which requires changes in mitochondrial morphology (Romanello et al., 2010) and is exacerbated during aging when the atrophy accompanied by lipofuscinosis occurs (De Meyer et al., 2010). We therefore investigated if the

program of muscle atrophy was altered in *Opa1*^{tg} animals, by using the well-established model of ischiotomy (Sandri et al., 2006; Adhihetty et al., 2007). Histological analysis did not reveal signs of inflammation, degeneration or regeneration in gastrocnemius sections from control or 10 days denervated 5 months-old Wt and *Opa1*^{tg} mice (Figure 3 A). However, the loss muscular mass after denervation was significantly less in *Opa1*^{tg} mice, with a ~50% reduction in muscle atrophy (Figure 3B). This protection was not explained by differences in the expression of mitochondrial genes involved in fission and biogenesis, or in atrophy and autophagy related genes before as well as after denervation, as measured by real-time PCR (not shown). Conversely, succinate dehydrogenase (SDH) staining increased in *Opa1*^{tg} muscles (Figure 3 C), suggesting that mitochondria were untouched in the denervated *Opa1*^{tg} fibers. Since autophagy preferentially targets dysfunctional mitochondria (Narendra and Youle, 2011) and during muscle atrophy dysfunctional mitochondria that lost their membrane potential (Seo et al., 2010) accumulate, we turned to an established assay to unveil the latent mitochondrial dysfunction (Irwin et al., 2003) When we followed in real time the changes in the mitochondrial fluorescence of the potentiometric probe tetramethyl rhodamine methylester (TMRM) caused by the ATPase inhibitor oligomycin, we observed that in fibers isolated from denervated Wt muscles the ATPase inhibitor caused a paradoxical depolarization (as opposed to the expected hyperpolarization observed in healthy fibers where the ATPase consumes the electrochemical gradient to generate ATP), indicative of latent organellar dysfunction. In fibers from *Opa1*^{tg} mice conversely the recordings before or after

denervation were completely superimposable (Figure 3 D), suggesting that the mild OPA1 overexpression protects from denervation-induced mitochondrial dysfunction. Thus, OPA1 overexpression protects from atrophy by blocking mitochondrial dysfunction and clearance, without altering the autophagic program or inducing mitochondrial biogenesis.

Opa1^{tg} mice are protected from ischemic damage.

The mitochondria-specific protection from muscular atrophy provided by OPA1 overexpression prompted us to move to other models of tissue damage where mitochondria play a central role. Myocardial infarction, besides being the leading cause of death in the western world, encompasses profiles of central necrosis and of peripheral apoptosis, where mitochondrial dysfunction participates in the ischemic as well as in the reperfusion phase (Murphy and Steenbergen, 2008) By using a classical Langendorff perfused heart preparation, we subjected hearts of 5 month old mice to 40 minutes of ischemia followed by 15 minutes of reperfusion (Barbato et al., 1996) and we assessed cardiac injury by measuring lactate dehydrogenase (LDH) release during the reperfusion period. OPA1 overexpression drastically reduced the amount of released LDH in both C57/Bl6 (Figure 4 B) and SV129 (Figure 4C) as well as in male and female mice, thereby excluding potential confounding effects of animal genetic background and gender that influence the response to heart ischemia (Du, 2004). The protection was not confined to heart, since infarct volume , assessed in triphenyl tetrazolium chloride (TTC) stained serial

sections from brains three days after middle cerebral artery (MCAo) occlusion (Colak et al., 2011) was significantly reduced in *Opa1*^{tg} mice (Figure 4 D, E, F). These results indicate that mild OPA1 overexpression protects heart and brain from ischemic damage.

Opa1 ^{tg} are less susceptible to Fas-induced liver damage

The protection afforded by OPA1 from heart and brain ischemia corroborates early findings that implicated OPA1 and the OPA1-dependent cristae remodeling in cell death. However, we wished to test this model further by turning to a model of in vivo apoptosis. Fas receptor activation in the liver by means of tail vein injection of anti-Fas activating antibodies is a well characterized model of severe apoptotic liver damage (Ogasawara et al., 1993) where Fas-induced death is dependent on mitochondria (Yin et al., 1999; Wei et al., 2000). While liver histology was not different in 3 months old BL6 Wt and *Opa1*^{tg} mice, 24 hours after tail vain injection of an activating anti-Fas antibody (JO2), damage was greatly decreased in *Opa1*^{tg} livers, where the lobular architecture was preserved and the hemorrhagic infiltrates where reduced (Figure 5A). Accordingly, TUNEL staining revealed a significant reduction in apoptotic cell death in *Opa1*^{tg} livers (Figure 5 B, C). Mechanistically, the protection correlates with the inhibition of cytochrome *c* release from mitochondria, as revealed by the analysis of subcellular cytochrome *c* distribution in Fas-treated Wt and Opa1tg livers (Figure 5 D). Consistently, plasma levels of alanine and aspartate transaminases (ALT and AST), an indicator of liver

damage, were significantly reduced in blood samples from Fas-treated *Opa1*^{tg} mice compared to those from their Wt treated littermates (Figure 5 E, F). Thus, OPA1 overexpression inhibits mitochondrial dependent apoptosis in vivo.

Opa1^{tg} mitochondria are resistant to cristae remodeling and cytochrome c release

We next wished to address mechanistically how OPA1 overexpression protected from multiple and different death stimuli in vivo. In principle, OPA1 levels modulate mitochondrial fusion as well as cristae shape, by inhibiting the cristae remodeling pathway. Moreover, they control cristae tightness, respiratory chain supercomplexes assembly and hence the efficiency of mitochondrial respiration. Indeed, these morphological and metabolic changes were observed in immortalized MAFs prepared from diaphragms of *Opa1*^{tg} mice (Cogliati et al., 2013). We recapitulated the findings of slight mitochondrial elongation in primary myoblasts prepared from *Opa1*^{tg} diaphragms (Figure 6 A), and of tighter cristae in *Opa1*^{tg} hearts (Figure 6 B) as well as in other organs (not shown). Functionally, complex IV dependent respiration (Figure 3S A), calcium retention capacity (CRC), a sensitive indicator of the threshold for mitochondrial permeability transition that participates in cytochrome c release (Basso et al., 2005), cyclosporine A (CsA) sensitivity of CRC (Figure 3S B, C), as well as mitochondrial membrane potential (Figure 3S D) were superimposable in Wt and *Opa1*^{tg} purified mitochondria. However, when we turned to an established assay of cytochrome c release from

purified liver mitochondria treated with recombinant cleaved, active BID (cBID), (Scorrano et al., 2002; Frezza et al., 2006), we observed that *Opa1*^{tg} mitochondria were releasing less cytochrome c (Figure 6 C), despite that cBID caused the same extent of BAK activation (measured as its oligomerization) in wt and *Opa1*^{tg} mitochondria (Figure 3S E).We therefore turned to an established assay of cytochrome c mobilization from the cristae, measuring the ratio of ascorbate (asc) driven over tetramethy-p-phenyenediamine (TMPD) driven respiration (Scorrano et al., 2002). While basal asc/TMPD ratio was not affected in *Opa1*^{tg} mitochondria, the increase in the ratio caused by cBID was completely blocked in *Opa1*^{tg} mitochondria (Figure 6 D), indicating that the apoptotic redistribution of cytochrome *c* was blocked in *Opa1*^{tg} mitochondria. Accordingly, the OPA1 oligomers targeted by cBID to trigger cristae remodeling and cytochrome c redistribution were stabilized in in *Opa1*^{tg} mitochondria (Figure 6 E, F). Taken together these results indicate that a mild OPA1 overexpression is sufficient to protect from apoptotic cristae remodeling in vivo.

Discussion

The field of mitochondrial dynamics exploded when the processes of cristae remodeling and mitochondrial fragmentation during apoptosis were discovered (Scorrano et al., 2002; Frank et al., 2001; Martinou et al., 1999). The discovery that OPA1 controls cristae remodeling (Frezza et al., 2006) and RCS assembly and stability (Cogliati et al., 2013) offered a conceptual framework to explore whether

OPA1 overexpression interfered with cell death in vivo. Our results indicate that mild OPA1 overexpression is compatible with life and protects animals from multiple form of death, implicating cristae remodeling in myocardial and brain infarction, hepatocellular apoptosis and muscular atrophy.

Our strategy to investigate the role of cristae remodeling in vivo has been to modulate the levels of its master regulator OPA1. Not surprisingly, given the crucial role of this protein in mitochondrial physiology, its ablation is lethal early during intrauterine development (Davies et al., 2007) and its inducible deletion in differentiated tissues such as brain and skeletal muscle is similarly fatal (not shown). We therefore turned to a different approach and generated a mouse model of targeted, controlled OPA1 overexpression (Cogliati et al., 2013) where we could avoid the paradoxical toxic effects of high OPA1 expression (Cipolat et al., 2004).

OPA1 overexpression does not impair fertility, intrauterine development, adult life and even lifespan, a surprising lack of effect for a gene with a potential antiapoptotic effect. It shall be mentioned however that in the more permissive SV129 background the incidence of spontaneous cancer is significantly increased and lifespan is accordingly reduced. The overexpression of the bona fide apoptosis inhibitors Bcl-2 and Bcl-Xl is even less potent in promoting cancer per se (except for the expression restricted in the B cell compartment, (Frenzel et al., 2009)): for example, a BCl-Xl skin transgene did not show increased incidence of skin cancer or precancerous lesions (Pena et al., 1998). Moreover, mitochondrial apoptosis is required for the normal development (Wang, 2001) and OPA1 does not interfere

with the core apoptotic machinery of outer membrane permeabilization (here and (Frezza et al., 2006). Therefore, the finding of spontaneous cancer development remains to be accurately investigated from the molecular point of view.

The observation of non-pathological heart hypertrophy in *Opa1*^{tg} mice prompted us to verify if this trasngene had any effect on muscular atrophy. Chronic muscle disuse induced by denervation results in mitochondrial alterations and muscle atrophy (Adhihetty et al., 2007) Interestingly, disruption of the mitochondrial network is an essential loop of this muscular atrophy program (Romanello et al., 2010). The preservation of heart size during aging perfectly correlated with the anti-atrophic effect of OPA1 overexpression in the skeletal muscle: remarkably, while OPA1 overexpression did not impinge on mitochondrial biogenesis or autophagy, it sustained mitochondrial function and prevented their elimination. OPA1 expression indeed triggered a slight mitochondrial elongation, which was accompanied by a remarkable increase in respiratory capacity that correlated with the cristae tightness (Cogliati et al., 2013). Thus, amelioration of mitochondrial cristae seems a feasible strategy to counteract muscular atrophy, an emerging medical problem in the aging society.

In addition to skeletal muscle, brain and heart are also high energy demanding tissues where mitochondrial dysfunction is invariably detrimental. Indeed, ischemia and ischemia/reperfusion injury are associated with a dramatic change in mitochondrial morphology and ultrastructure (Calo et al., 2013). We observed that mild OPA1 overexepression was sufficient to improve enzymatic parameters associated with tissue damage in response to ischemic injury. In addition to its role

in apoptosis, mitochondrial dynamics has been recently implied in necrosis and necroptosis (Orogo and Gustafsson, 2013) (Wang et al., 2012). Our results suggest that cristae remodeling is central also to propagate the necrotic damage and that its prevention can ameliorate the ischemic damage outcome. Notably, OPA1 overexpression did not increase brain or heart vascularization, suggesting a direct effect on the mechanisms of ischemic cell damage.

One of the best characterized in vivo apoptotic pathways is that induced by the activation of Fas-R. The liver, where Fas is constitutively expressed on hepatocytes (Ogasawara et al., 1993) is not surprisingly very sensitive to Fas-mediated apoptosis.. Because hepatocytes are type II cells in which Fas-induced death is dependent on mitochondrial pathway, the model of liver apoptosis by Fas-R activation has been widely employed to study apoptosis in vivo (Rodriguez et al., 1996; Yin et al., 1999; Wei et al., 2001). In addition to muscular atrophy and ischemia/reperfusion, OPA1 overexpression also protected from hepatocellular apoptosis. The mechanistic analysis allowed to conclude that OPA1 expression does not interfere with Bax, Bak mediated outer membrane permeabilization, yet it protects from cytochrome c release in vitro and in vivo by counteracting the intramitochondrial redistribution that accompanies cristae remodeling. Our work unravels a role for cristae shape in multiple forms of cell death in vivo. The use of a mouse model of mild, controlled OPA1 overexpression allowed us to test the hypothesis that OPA1 and cristae remodeling modulate apoptosis. The analysis of this OPA1 overexpressing mouse extended the forms of death controlled by

mitochondrial remodeling and indicated a crucial role for mitochondrial ultrastructure in tissue adaptation to pathological stimuli.

Experimental procedures

In vivo experiments

Generation of OPA1 overexpressing mice

Experimental procedures for the generation of *Opa1*^{tg} mice was described in (Cogliati et al., 2013). *Opa1*^{tg} mice were initially developed in a mixed genetic background of C57BL/6 x Sv/129 and were backcrossed to C57BL/6 and SV/129 for more than 10 generations. The genotype is determined by analysis of DNA extracted from tail biopsy, via Polymerase Chain Reaction (PCR).

Echocardiography.

Echocardiography was performed in adult (5 and 9 month) *Opa1*^{tg} (n=6) and age- and sex-matched littermate controls (n=6), using a Vevo 2100™ (Visual Sonics, Toronto, Canada) system equipped with a 30 MHz transducer. Anesthesia was induced with 3% isoflurane, maintained with 1.5% isoflurane during constant monitoring of temperature, respiration rate, and ECG. Two-dimensional cine loops with frame rates of 200 frames/s of a long-axis view and a short-axis view at proximal-, mid- and apical level of the left ventricle (LV) were recorded. Inter ventricular septum (IVS) and LV posterior wall (LVPW) thicknesses, LV internal diameter (LVID) and maximal LV length were measured in systole (s) and in diastole (d) from the long axis B-mode image, according to standard procedures. Ejection fraction (EF) was determined by the following formula: Simp EF (%) = 100 x Simp Systolic Volume (SV)/ Simp LV volume; d. To assess changes in LV shape, the sphericity index (SI) was calculated at end-diastole (d) and end-systole (s) as

the volume of the LV divided by the volume of a sphere with a diameter equal to the LV longest axis (measured in the apical view) using the following formulas: SI: d = LV volume; d/(3/4*Π*(Simp Length; d)^3); SI: s = LV volume; s/(3/4*Π*(Simp Length; s)^3). As this ratio increases, the ventricle becomes more spherical. Echocardiographic image acquisition and analysis were performed by a single operator, blinded to the mouse genotype.

Muscle denervation

Denervation was performed by cutting sciatic nerve of the left hind limb, the right hind limb was used as control. 5 months old males were used. 10 days after denervation animals were killed by cervical dislocation and muscles were utilized for histological experiments or gene expression studies.

Heart Ischemia and Reperfusion

Heart Ischemia and Reperfusion was performed according to Langendorff experimental model. The hearts were removed from cervical dislocated 5 months sex matched animals and treated as follows : after 10 min of stabilization, experimental hearts were subjected to 40 min of global ischemia by stopping the coronary flow and 15 min of reperfusion. The hearts were perfused with bicarbonate buffer gassed with 95% O2-5% CO2 at 37 °C (pH 7.4) at a constant flux of 5 ml/min. Perfusion was performed in the nonrecirculating Langendorff model, as previously described (Barbato et al., 1996) The bicarbonate buffer contained (in mM) 118.5 NaCl, 3.1 KCl, 1.18 KH2PO4, 25.0 NaHCO3, 1.2 MgCl2, 1.4 CaCl2 and

5.6 glucose. Lactate dehydrogenase (LDH) accumulated in the coronary effluent during reperfusion period was collected for the quantification of myocardial cell damage. After reperfusion the hearts were quickly immersed into PBS supplemented with 0,5% Triton X100 and homogenized for measurement of total lactate dehydrogenase (LDH).

Brain Ischemia

Animals were sacrificed 3 days after Middle Cerebral Artery (MCA) occlusion. MCA ligation surgery in mice and 2,3,5 Triphenyltetrazolium chloride (TTC) staining for quantification of infarct volumes was performed exactly as described in (Colak et al., 2011).

Tail vein injection

Three months old mice were injected intravenously with anti-Fas antibody (Jo2 BD Pharmingen), at a dose of 0,25μg/g. Animals were observed and sacrificed 24 h after injection, for liver histology and biochemical analysis.

In vitro mitochondrial assays

Liver and muscle mitochondria from the indicated phenotype were isolated by standard differential centrifugation as described in (Frezza et al., 2007). Cytochrome *c* redistribution and release in response to recombinant cBID was determinate as described in (Scorrano et al., 2002). Mitochondrial oxygen consumption was measured with a Clark type oxygen electrode (Hansatech).

1mg/ml mitochondria in Experimental Buffer (EB: 150 mM KCl, 10 mM Tris Mops, 10 µM EGTA-Tris,), 5mM/2.5mM glutamate malate or 10mM succinate were added. Basal O2 consumption was recorded (state 2) and after 2 minutes 100 µM ADP was added (state 3), followed by 2.5 µg/mL oligomycin to determine state 4 respiration, FCCP was added to asses maximal respiration. Complex IV-driven respiration was determined with the addition of 3 mM ascorbate plus 150 mM TMPD in the presence 1mg/ml mitochondria in EB supplemented with 5 mM cytochrome *c* and 0,5□g/ml antimycin A.

Mitochondrial membrane potential

Mitochondrial membrane potential in isolated FDB (flexor digitorum brevis) muscle fibres was measured by intensity of TMRM fluorescence. Briefly, FDB myofibres were placed in 1ml Tyrode's buffer and loaded with 5 nM TMRM (Molecular Probes) supplemented with 1 mM cyclosporine H (a Pglycoprotein inhibitor) for 30 min at 37°C. Myofibres were then observed at Olympus IX81 inverted microscope (Melville, NY) equipped with a CellR imaging system. Sequential images of TMRM fluorescence were acquired every 60 s with a 4X objective (Olympus). At the times indicated by arrows, oligomycin (5 mM) (Sigma) or the uncoupler carbonyl cyanide p-trifluoromethoxyphenylhydrazone (FCCP, 4 mM) (Sigma) was added. TMRM fluorescence analysis over mitochondrial regions of interest was performed using ImageJ software.

Biochemistry

For protein crosslinking, mitochondria were treated as indicated with 1mM EDC or 1 mM BMH as previously described (Frezza et al., 2006). For SDS-PAGE, equal amounts of mitochondrial proteins (were separated on 3%-8% Tris-acetate or 4%-12% Tris-MES (NuPage, Invitrogen) polyacrilamide gel, transferred onto PVDF membranes (Biorad) and probed using the indicated primary antibodies and isotype matched secondary antibodies conjugated to horseradish peroxidase. Signal was detected with ECL (Amersham). Details on the antibodies used can be found in Supplemental data. Densitometry was performed

BN PAGE

To detect OPA1 oligomers, mitochondria were resuspended in an appropriated volume of Buffer D (1M 6-aminohexanoic acid, 1.25% V/V digitonin, 50mM Bis-Tris-HCl, pH 7) at a final concentration of 10 mg/ml. Following centrifugation, the supernatant was collected and 5% Serva Blue G dye in 1M 6-aminohexanoic acid was added to one-third of the final volume of the sample. Equal amounts (100 µg) of mitochondrial proteins were separated on a 3%-12% gradient BNGE Invitrogen as described in (Schagger, 1995).

Histology and immunofluorescence staining.

Heart, muscle and liver tissue from the indicated genotypes were fixed in 1% paraformaldehyde (PFA) (Sigma) at room temperature for 15 minutes, equilibrated in sucrose gradient, frozen in liquid nitrogen, sectioned and processed for

histological and immunofluorescence analyses. Livers also were, cut into small pieces and fixed overnight at 4°C in 4% paraformaldehyde in PBS, and then dehydrated through serial ethanol concentration for paraffin embedding. Paraffin embedded livers were used for TUNEL, haematoxylin and eosin staining.

Acknowledgements

LS is a Senior Scientist of the Dulbecco-Telethon Institute. Supported by Telethon Italy (GGP12162, GPP10005B, TCR02016), AIRC Italy, Swiss National Foundation (31-118171).

Figure Legends

Figure 1. Characterization of *Opa1*^{tg} mice

(A) Schematic representation of targeted transgenesis strategy into the permissive hypoxanthine phosporibosytransferese (HPRT) locus. The targeted vector include a 5' HPRT homology arm, β-actin promoter, the transgene cDNA OPA1 isoform1 and 3' HPRT homology arm including a part of HPRT promoter and an homologous region to the mouse HPRT locus. The targeting construct is linearized before electroporation into BPES cells. Homologous recombination of the 3' arm reconstitutes a functional HPRT gene, allowing the selection of targeted BPES cells on stringent hypoxanthine-aminopterin-thymidine (HAT) conditions.

(B) PCR analysis of genomic DNA from wild-type (Wt) mice, heterozygous (Opa1(+/-) and homozygous (Opa1(+/+) *Opa1*^{tg} mice tail.

(C) Equal amounts of protein from tissues of the indicated genotypes were separated by SDS-PAGE and immunoblotted with the indicated antibodies.

(D) Densitometric analysis of OPA1 protein level in tissue from heart and muscle. Data represent average ± SEM (n=7 for each group); asterisk denotes p<0,05 in an unpaired sample Student's test.

(E) Body weight is represented as average ± SEM of 5 months males (n= 34 for each group) and females (n= 13 for each group) and 9 months old males (n= 18 for each group) and females (n= 16 for each group) C57/Bl6 *Opa1*^{tg} and Wt littermates. The asterisk denotes p<0.05 in a two tailed ANOVA test.

(F, G) Kaplan-Meier survival curve of Wt and *Opa1*^{tg} males and females littermates (n=10) .

Figure 2. Non-pathological cardiac hypertrophy in 9 months old *Opa1^{tg}* mice

(A) Representative images of hearts dissected from 5 months (top) and 9 months (bottom) old Wt and *Opa1^{tg}* littermates.

(B) Evaluation of heart weight/body weight ratio in Wt and *Opa1^{tg}* mice. Data represent average ± SEM (n=8 for each group 5 months old mice and n=4 for each group 9 months old mice). Asterisk indicates $p<0.05$ in an unpaired sample Student's test versus 5 months old genotype matched dataset.

(C) Immunofluorescence analysis on ventricular cryosections from Wt and *Opa1^{tg}* mice stained for dystrophin. Images are details from the left ventricle.

(D) Cardiomyocyte cross-sectional area (CSA) (pixel) in cryosections from Wt and *Opa1^{tg}* 9 months old mice. Data are average ± SEM. (n=4 for each group). The asterisk denotes $p<0.05$ in an unpaired sample Student's test.

(E, F) Echocardiographic long axis view of hearts from 9 months old Wt and *Opa1^{tg}* littermates. LV: left ventricle; A: aorta. Percentage of cardiac ejection fraction (FE) and shortening (FS) are represented in (F).

(G) Haematoxilin-eosin staining of ventricular cryosections from Wt and *Opa1^{tg}* mice.

(H,I) Immunofluorescence analysis of ventricular cryosections from Wt and *Opa1^{tg}* mice stained for beta myosin heavy chain (β-MHC, H) and to antrial natriuretic peptide (ANP) (I).

Figure 3. Muscle atrophy induced by denervation is reduced in *Opa1^{tg}* mice

(A) Haematoxilin-eosin staining of control and 10 days denervated gastrocnemial crysections from C57/Bl6 Wt and *Opa1^{tg}* male littermates.

(B) Quantification of muscle loss 10 days after denervation by cross-sectional area (CSA) measurement of innervated and denervated fibers (n=5 for each group) Data are average ±SEM. The asterisk denotes $p<0.05$ in an unpaired sample Student's test.

(C) Representative images of succinate dehydrogenase (SDH) staining in control and denervated garstocnemius cryosections from Wt and *Opa1^{tg}* littermates.

(D) Quantitative analysis of TMRM fluorescence over mitochondrial regions in isolated fibers from *Opa1^{tg}* and Wt control and denervated FDB (flexor digitorum bevis) muscles. Data are average ± SEM. (n=5 for each group).

Figure 4. *Opa1^{tg}* mice are less susceptible to ischemic damage

(A) Schematic representation of the Langendorff experimental model used.

(B,C) Quantitative analysis of lactate dehydrogenase (LDH) released during reperfusion in the coronary effluent in 5 months old Wt and *Opa1^{tg}* males and females of the indicated background (n=8 for each group). Data represent average ±SEM. The asterisk denotes $p<0.05$ in a two tailed ANOVA test.

(D) Representative images of TTC stained whole brains from 3 months old females Wt and *Opa1^{tg}* SV129 mice 72h after middle cerebral artery occlusion (MCAo).

(E) Representative TTC stained 250μm brain sections, 72h after MCAo. Slices are aligned from anterior to posterior.

(F) Quantification of infarct volume 72h post MCAo. Data represent average ±SEM (n =4 for each group). The asterisk denotes $p<0.05$ in an unpaired sample Student's test.

Figure 5. Apoptotic liver damage is reduced in *Opa1*^{tg} mice

(A) Representative images of Hematoxylin-eosin stained paraffin embedded liver sections from Wt and *Opa1*^{tg} mice. Mice were tail vein injected with saline solution (control) or with 0,25□g/g body weight anti-Fas (Jo-2) , sacrificed after 24h and livers explanted for histology.

(B) TUNEL staining of paraffin embedded liver sections from Wt and *Opa1*^{tg} control and 24h following anti -Fas injection. Arrows represent TUNEL positive hepatocytes.

(C) Quantification of TUNEL positive hepatocyte per field in experiments as in (B). Data represent average ± SEM of four independent experiments (at least 30 images per group per experiment).

(D) Double-color immunohistochemistry of liver cryosections from control or anti-Fas injected Wt and *Opa1*^{tg} mice. Cytochrome c staining is in green, Tom 20 in red.

(E) Plasma ALT levels of the indicated genotypes at the indicated time point. Data represent average ±SEM (n=7 for each group). The asterisk denotes $p<0,05$ in an unpaired ANOVA tests.

(F) Plasma AST levels of the indicated genotypes at the indicated time point. Data represent average ±SEM (n=8 for each group). The asterisk denotes $p<0.05$ in an unpaired ANOVA test

Figure 6. Cytochrome c release is reduced from *Opa1^{tg}* mitochondria

(A) Representative images of mitochondrial network of primary myoblast from Wt and *Opa1^{tg}* after transfection with mito-YFP.

(B) Electron micrographs of heart mitochondria of the indicated genotype.

(C) Mitochondria isolated from livers of the indicated genotypes were treated for the indicated times with 40pmol/mg cBID and cytochrome *c* release was measured. Data represent average ±SEM of 5 independent experiments.

(D) Ascorbate/TMPD –driven respiration of Wt and *Opa1^{tg}* liver mitochondria treated where indicated for 15 min with cBID. Data represent average ±SEM of 4 independent experiments. The asterisk denotes $p<0.05$ in an unpaired Student's test.

(E) Muscle mitochondria were treated with cBID and 10 mM EDC was added at the indicated time. Mitochondrial proteins (30 μg) were analyzed by SDS-PAGE/Immunoblotting using anti-OPA1 antibody.

(H) BNGE analysis of OPA1 oligomers in muscle mitochondria of the indicated genotypes treated for the indicated times with cBID.

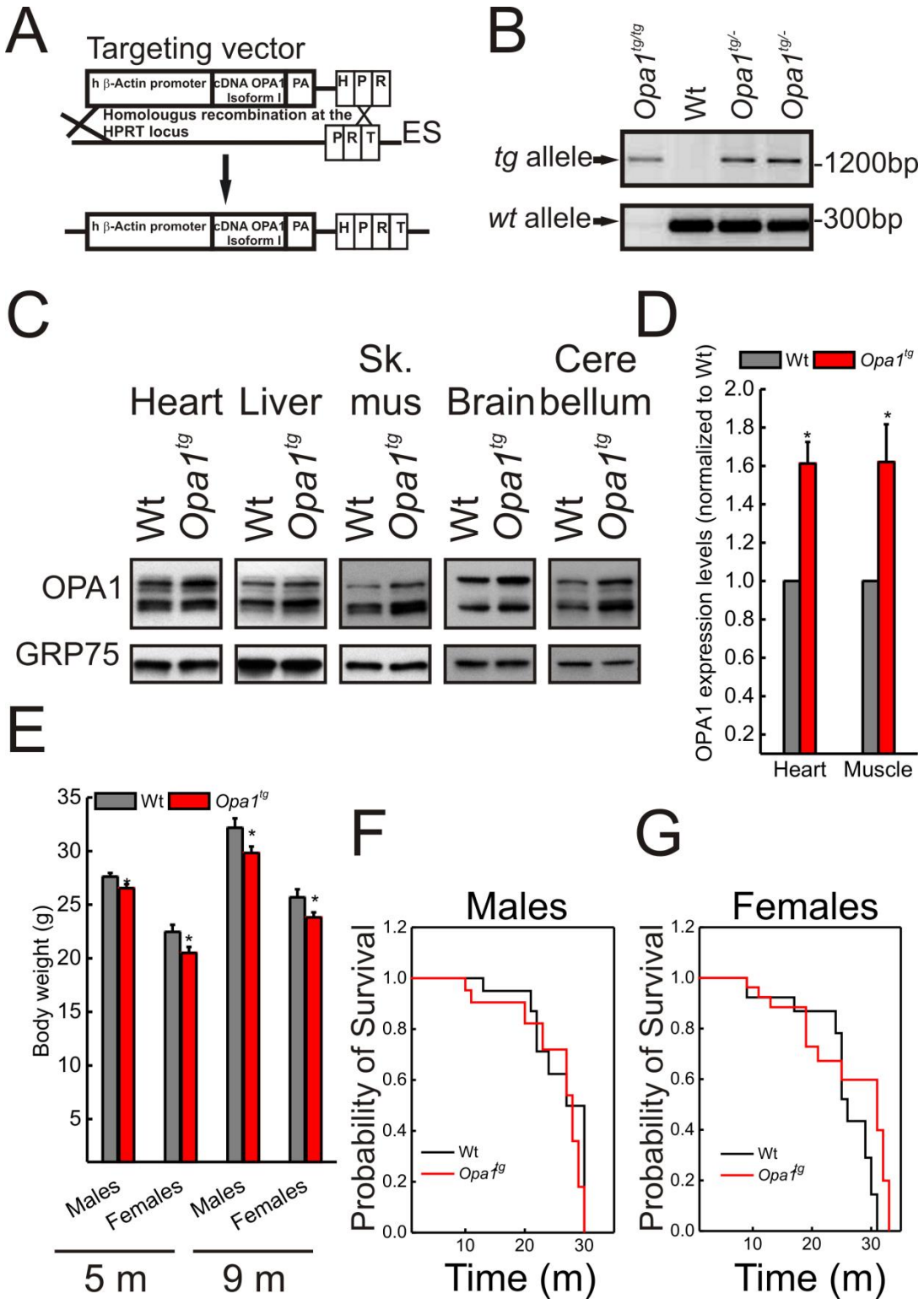
A
Targeting vector
h β-Actin promoter
cDNA OPA1 Isoform I
PA
H P R
Homologugus recombination at the HPRT locus
P R T
ES
B
Opa1tg/tg
Wt
Opa1tg/-
Opa1tg/-
tg allele
wt allele
-1200bp
-300bp
C
Heart
Liver
Sk. mus
Brain
Cere bellum
Wt
Opa1tg
OPA1
GRP75
D
Wt
Opa1tg
OPA1 expression levels (normalized to Wt)
Heart
Muscle
E
Wt
Opa1tg
Body weight (g)
Males
Females
Males
Females
5 m
9 m
F
Males
Probability of Survival
Wt
Opa1tg
Time (m)
G
Females
Probability of Survival
Wt
Opa1tg
Time (m)

Figure 1

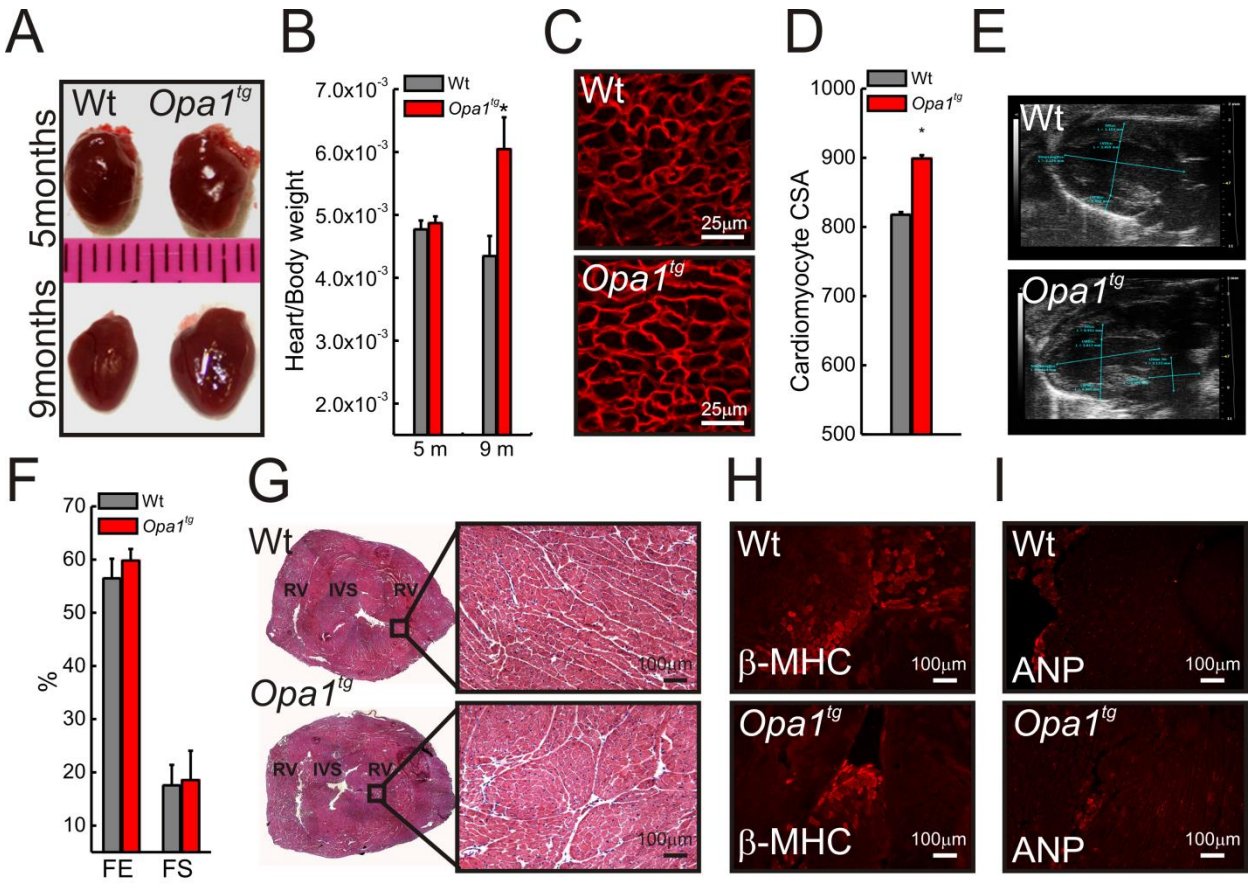
A
B
C
D
E
Wt
Opa1tg
5months
9months
Heart/Body weight
7.0x10-3
6.0x10-3
5.0x10-3
4.0x10-3
3.0x10-3
2.0x10-3
5 m
9 m
25µm
Cardiomyocyte CSA
1000
900
800
700
600
500
F
G
H
I
%
70
60
50
40
30
20
10
FE
FS
RV
IVS
100µm
β-MHC
ANP

Figure 2

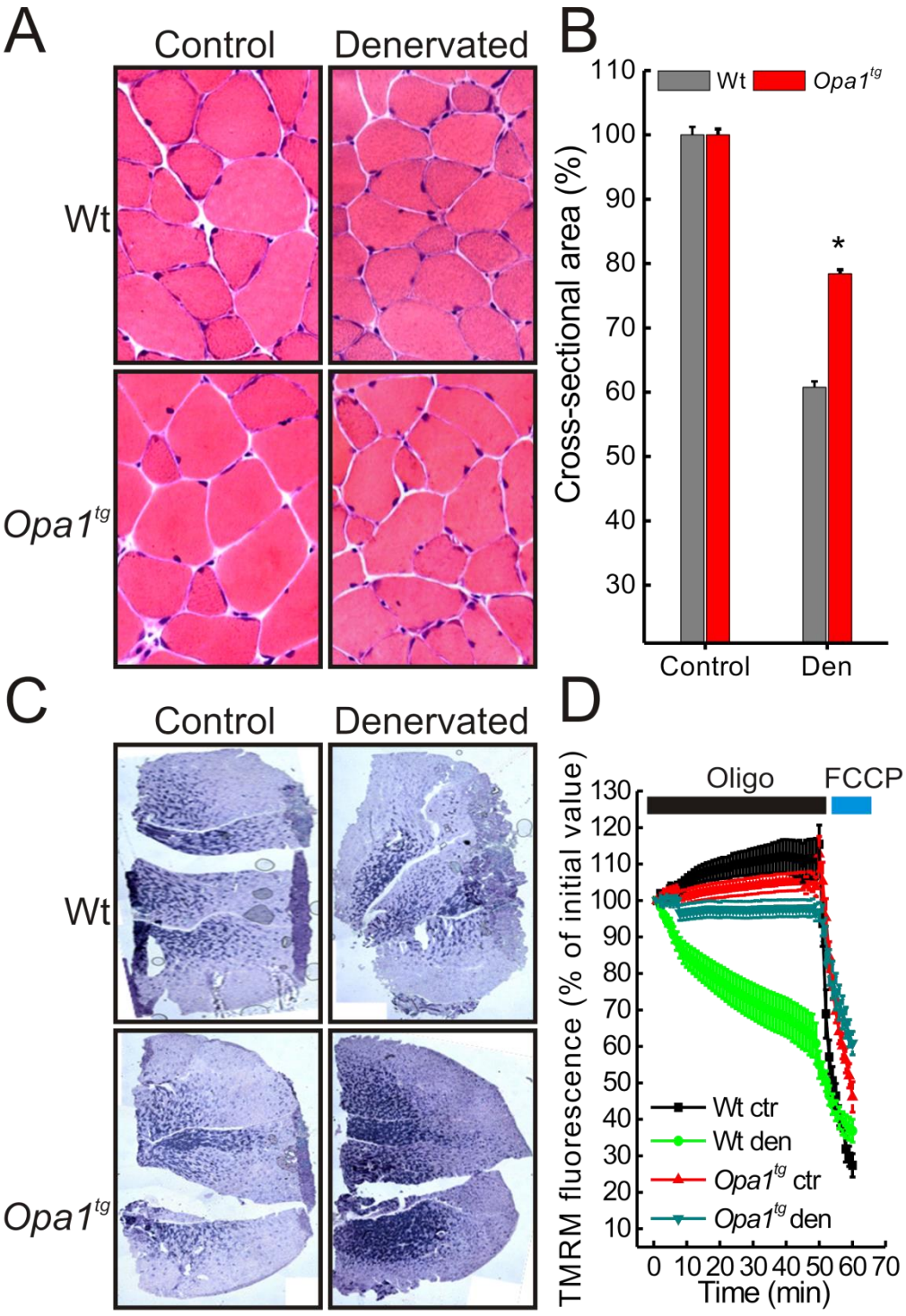
A
Control
Denervated
Wt
Opa1tg
B
Wt
Opa1tg
Cross-sectional area (%)
110
100
90
80
70
60
50
40
30
*
Control
Den
C
Control
Denervated
Wt
Opa1tg
D
Oligo
FCCP
TMRM fluorescence (% of initial value)
130
120
110
100
90
80
70
60
50
40
30
20
10
Wt ctr
Wt den
Opa1tg ctr
Opa1tg den
0 10 20 30 40 50 60 70
Time (min)

Figure 3

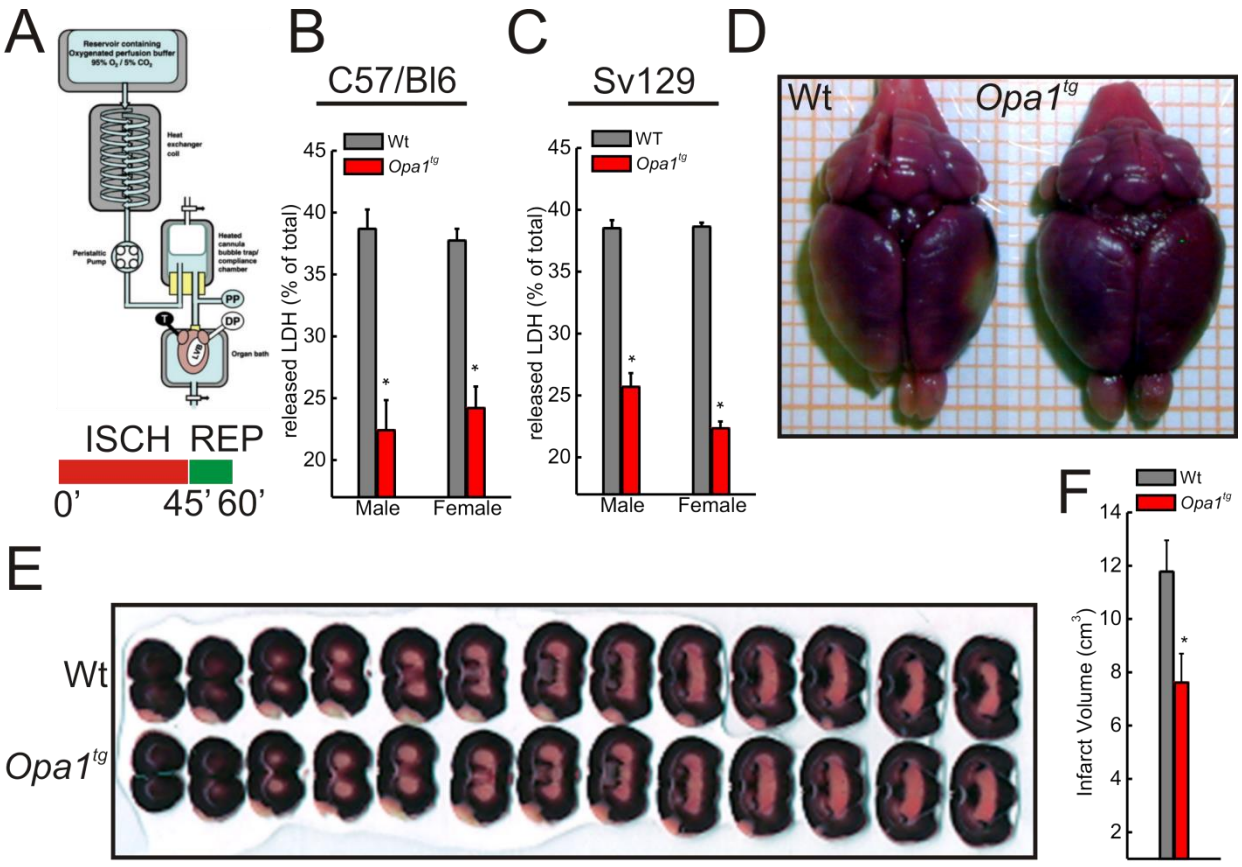
A
Reservoir containing Oxygenated perfusion buffer 95% O2 / 5% CO2
Heat exchanger coil
Peristaltic Pump
Heated cannula bubble trap/ compliance chamber
PP
DP
T
Organ bath
ISCH REP
0'
45' 60'
B
C57/Bl6
Wt
Opa1tg
released LDH (% of total)
45
40
35
30
25
20
Male
Female
C
Sv129
WT
Opa1tg
released LDH (% of total)
Male
Female
D
Wt
Opa1tg
E
Wt
Opa1tg
F
Wt
Opa1tg
Infarct Volume (cm3)
14
12
10
8
6
4
2

Figure 4

Figure 5

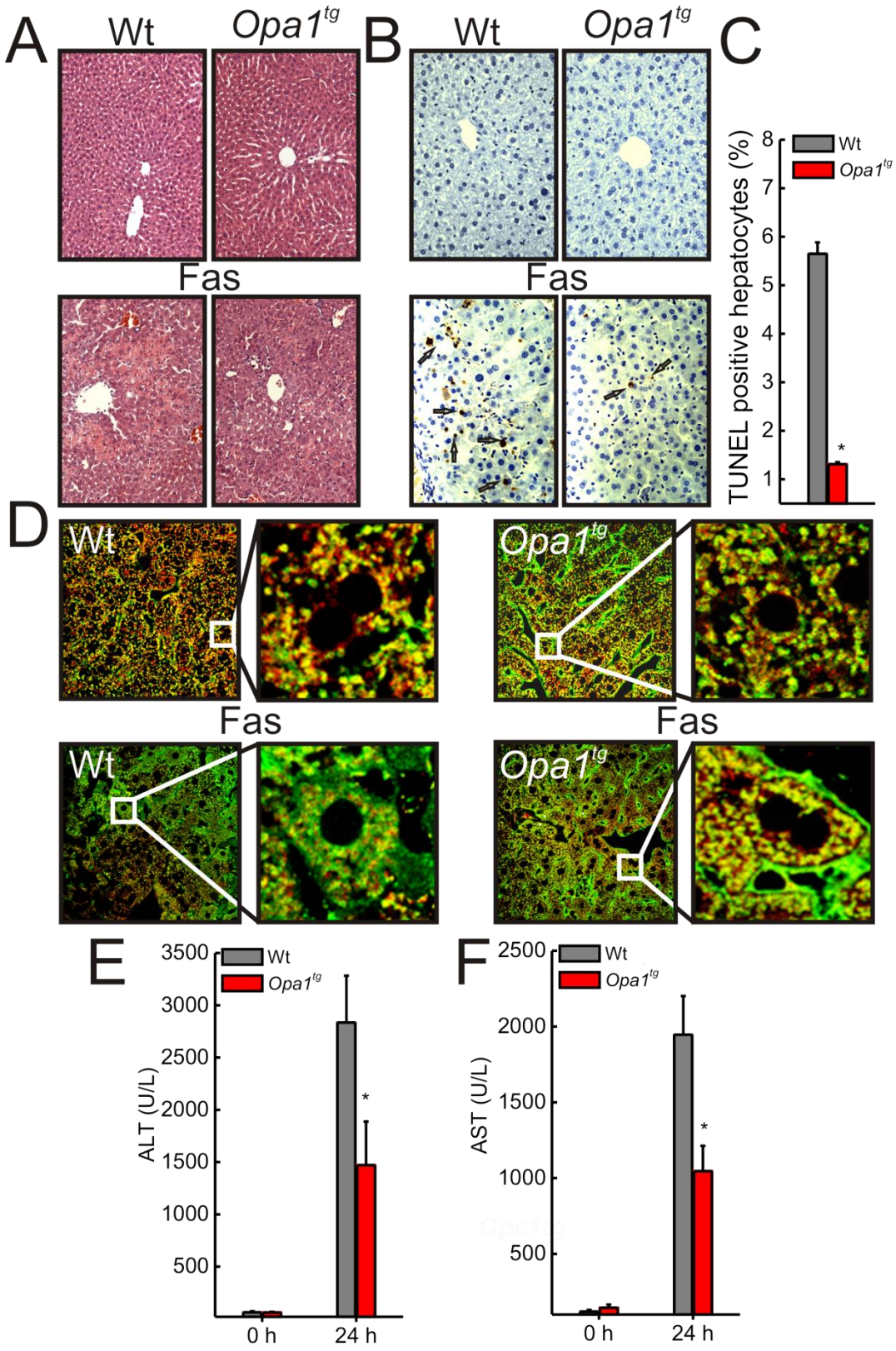
A
Wt
Opa1tg
Fas
B
Wt
Opa1tg
Fas
C
TUNEL positive hepatocytes (%)
Wt
Opa1tg
D
Wt
Opa1tg
Fas
Wt
Opa1tg
E
ALT (U/L)
Wt
Opa1tg
0 h
24 h
F
AST (U/L)
Wt
Opa1tg
0 h
24 h

Figure 6

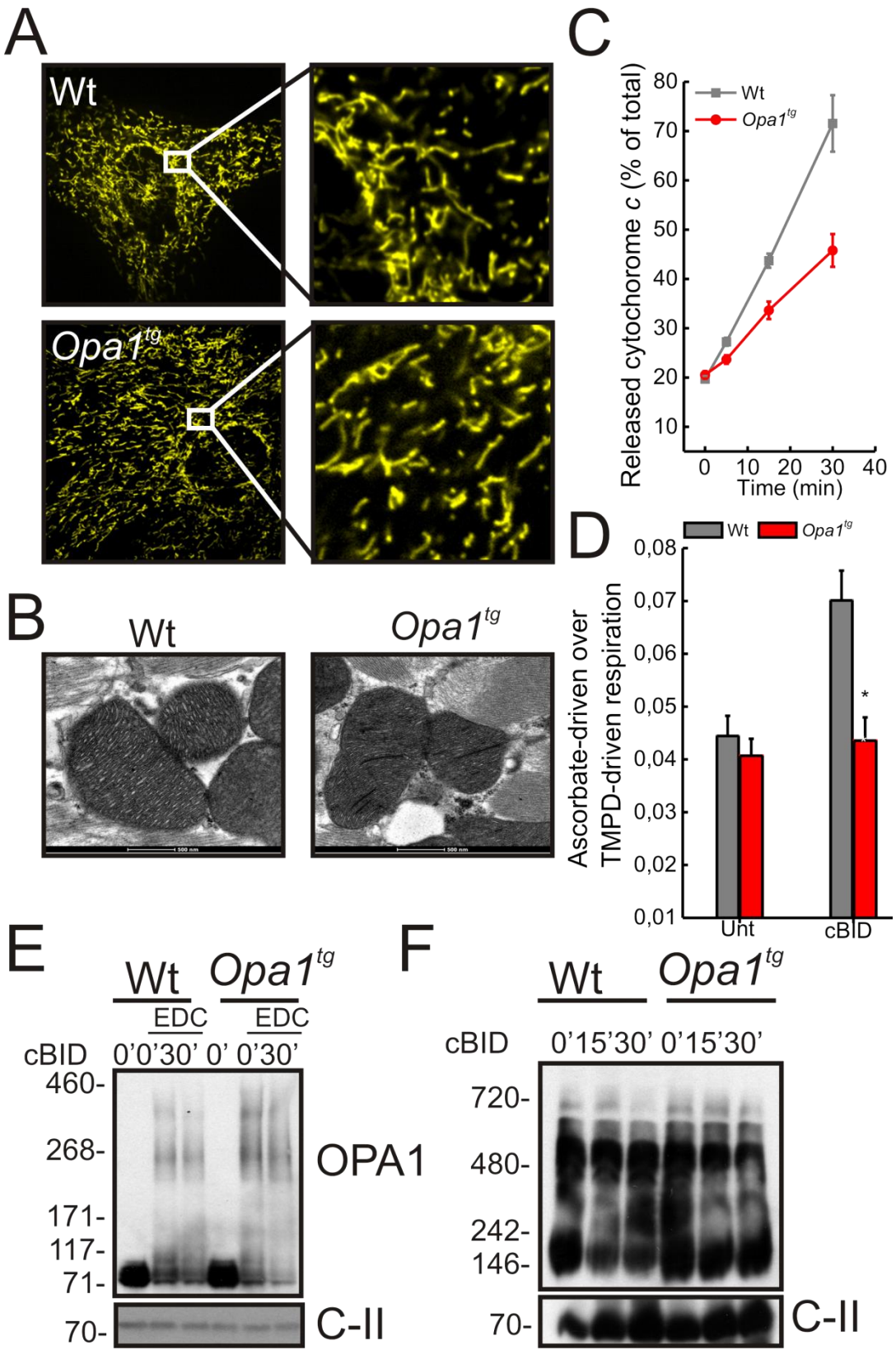
A
Wt
Opa1tg
B
Wt
Opa1tg
C
Released cytochorome c (% of total)
Time (min)
Wt
Opa1tg
D
Ascorbate-driven over TMPD-driven respiration
Wt
Opa1tg
Unt
cBID
E
Wt
Opa1tg
EDC
EDC
cBID
0'0'30' 0' 0'30'
460-
268-
171-
117-
71-
OPA1
70-
C-II
F
Wt
Opa1tg
cBID
0'15'30' 0'15'30'
720-
480-
242-
146-
70-
C-II

Reference List

Adhihetty,P.J., O'Leary,M.F.N., Chabi,B., Wicks,K.L., and Hood,D.A. (2007). Effect of denervation on mitochondrially mediated apoptosis in skeletal muscle. Journal of Applied Physiology *102*, 1143-1151.

Barbato,R., Menabo,R., Dainese,P., Carafoli,E., Schiaffino,S., and DiLisa,F. (1996). Binding of cytosolic proteins to myofibrils in ischemic rat hearts. Circulation Research *78*, 821-828.

Basso,E., Fante,L., Fowlkes,J., Petronilli,V., Forte,M.A., and Bernardi,P. (2005). Properties of the permeability transition pore in mitochondria devoid of Cyclophilin D. J. Biol. Chem. *280*, 18558-18561.

Bronson,S.K., Plaehn,E.G., Kluckman,K.D., Hagaman,J.R., Maeda,N., and Smithies,O. (1996). Single-copy transgenic mice with chosen-site integration. Proceedings of the National Academy of Sciences of the United States of America *93*, 9067-9072.

Calo,L., Dong,Y., Kumar,R., Przyklenk,K., and Sanderson,T.H. (2013). Mitochondrial Dynamics: An Emerging Paradigm in Ischemia-Reperfusion Injury. Current Pharmaceutical Design *19*, 6848-6857.

Cereghetti,G.M., Stangherlin,A., Martins de,B.O., Chang,C.R., Blackstone,C., Bernardi,P., and Scorrano,L. (2008). Dephosphorylation by calcineurin regulates translocation of Drp1 to mitochondria. Proc. Natl. Acad. Sci. U. S. A *105*, 15803-15808.

Chen,H., Detmer,S.A., Ewald,A.J., Griffin,E.E., Fraser,S.E., and Chan,D.C. (2003). Mitofusins Mfn1 and Mfn2 coordinately regulate mitochondrial fusion and are essential for embryonic development. J. Cell Biol. *160*, 189-200.

Cipolat,S., de Brito,O.M., Dal Zilio,B., and Scorrano,L. (2004). OPA1 requires mitofusin 1 to promote mitochondrial fusion. Proc. Natl. Acad. Sci. U. S. A *101*, 15927-15932.

Cipolat,S., Rudka,T., Hartmann,D., Costa,V., Serneels,L., Craessaerts,K., Metzger,K., Frezza,C., Annaert,W., D'Adamio,L., Derks,C., Dejaegere,T., Pellegrini,L., D'Hooge,R., Scorrano,L., and De Strooper,B. (2006). Mitochondrial Rhomboid PARL Regulates Cytochrome c Release during Apoptosis via OPA1-Dependent Cristae Remodeling. Cell *126*, 163-175.

Cogliati,S., Frezza,C., Soriano,M.E., Varanita,T., Quintana-Cabrera,R., Corrado,M., Cipolat,S., Costa,V., Casarin,A., Gomes,L.C., Perales-Clemente,E., Salviati,L., Fernandez-Silva,P., Enriquez,J.A., and Scorrano,L. (2013). Mitochondrial Cristae Shape Determines Respiratory Chain Supercomplexes Assembly and Respiratory Efficiency. Cell *155*, 160-171.

Colak,G., Filiano,A.J., and Johnson,G.V. (2011). The application of permanent middle cerebral artery ligation in the mouse. J. Vis. Exp.

Danial,N.N., Gramm,C.F., Scorrano,L., Zhang,C.Y., Krauss,S., Ranger,A.M., Datta,S.R., Greenberg,M.E., Licklider,L.J., Lowell,B.B., Gygi,S.P., and Korsmeyer,S.J. (2003). BAD and glucokinase reside in a mitochondrial complex that integrates glycolysis and apoptosis. Nature *424*, 952-956.

Danial,N.N. and Korsmeyer,S.J. (2004). Cell death: critical control points. Cell *116*, 205-219.

Davies,V.J., Hollins,A.J., Piechota,M.J., Yip,W., Davies,J.R., White,K.E., Nicols,P.P., Boulton,M.E., and Votruba,M. (2007). Opa1 deficiency in a mouse model of autosomal dominant optic atrophy

impairs mitochondrial morphology, optic nerve structure and visual function. Hum. Mol. Genet. *16*, 1307-1318.

De Meyer,G.R.Y., De Keulenaer,G.W., and Martinet,W. (2010). Role of autophagy in heart failure associated with aging. Heart Failure Reviews *15*, 423-430.

DiMauro,S. and Schon,E.A. (2003). Mitochondrial respiratory-chain diseases. N. Engl. J. Med. *348*, 2656-2668.

Du,X.J. (2004). Gender modulates cardiac phenotype development in genetically modified mice. Cardiovascular Research *63*, 510-519.

Du,X.J. (2007). Divergence of hypertrophic growth and fetal gene profile: the influence of beta-blockers. British Journal of Pharmacology *152*, 169-171.

Frank,S., Gaume,B., Bergmann-Leitner,E.S., Leitner,W.W., Robert,E.G., Catez,F., Smith,C.L., and Youle,R.J. (2001). The role of dynamin-related protein 1, a mediator of mitochondrial fission, in apoptosis. Dev. Cell *1*, 515-525.

Frenzel,A., Grespi,F., Chmelewskij,W., and Villunger,A. (2009). Bcl2 family proteins in carcinogenesis and the treatment of cancer. Apoptosis *14*, 584-596.

Frey,T.G. and Mannella,C.A. (2000). The internal structure of mitochondria. Trends. Biochem. Sci. *25*, 319-324.

Frezza,C., Cipolat,S., Martins,d.B., Micaroni,M., Beznoussenko,G.V., Rudka,T., Bartoli,D., Polishuck,R.S., Danial,N.N., De Strooper,B., and Scorrano,L. (2006). OPA1 Controls Apoptotic Cristae Remodeling Independently from Mitochondrial Fusion. Cell *126*, 177-189.

Frezza,C., Cipolat,S., and Scorrano,L. (2007). Organelle isolation: functional mitochondria from mouse liver, muscle and cultured fibroblasts. Nat. Protoc. *2*, 287-295.

Goldstein,J.C., Munoz-Pinedo,C., Ricci,J.E., Adams,S.R., Kelekar,A., Schuler,M., Tsien,R.Y., and Green,D.R. (2005). Cytochrome c is released in a single step during apoptosis. Cell Death. Differ. *12*, 453-462.

Green,D.R. and Kroemer,G. (2004). The pathophysiology of mitochondrial cell death. Science *305*, 626-629.

Griparic,L. and van der Bliek,A.M. (2001). The many shapes of mitochondrial membranes. Traffic *2*, 235-244.

Hackenbrock,C.R. (1966). Ultrastructural bases for metabolically linked mechanical activity in mitochondria. I. Reversible ultrastructural changes with change in metabolic steady state in isolated liver mitochondria. J. Cell Biol. *30*, 269-297.

Irwin,W.A., Bergamin,N., Sabatelli,P., Reggiani,C., Megighian,A., Merlini,L., Braghetta,P., Columbaro,M., Volpin,D., Bressan,G.M., Bernardi,P., and Bonaldo,P. (2003). Mitochondrial dysfunction and apoptosis in myopathic mice with collagen VI deficiency. Nature Genetics *35*, 367-371.

Landes,T., Emorine,L.J., Courilleau,D., Rojo,M., Belenguer,P., and rnaune-Pelloquin,L. (2010). The BH3-only Bnip3 binds to the dynamin Opa1 to promote mitochondrial fragmentation and apoptosis by distinct mechanisms. EMBO Rep. *11*, 459-465.

Martinou,I., Desagher,S., Eskes,R., Antonsson,B., Andre,E., Fakan,S., and Martinou,J.C. (1999). The release of cytochrome c from mitochondria during apoptosis of NGF-deprived sympathetic neurons is a reversible event. J. Cell Biol. *144*, 883-889.

Murphy,E. and Steenbergen,C. (2008). Mechanisms underlying acute protection from cardiac ischemia-reperfusion injury. Physiological Reviews *88*, 581-609.

Narendra,D.P. and Youle,R.J. (2011). Targeting Mitochondrial Dysfunction: Role for PINK1 and Parkin in Mitochondrial Quality Control. Antioxidants & Redox Signaling *14*, 1929-1938.

Ogasawara,J., Watanabefukunaga,R., Adachi,M., Matsuzawa,A., Kasugai,T., Kitamura,Y., Itoh,N., Suda,T., and Nagata,S. (1993). Lethal Effect of the Anti-Fas Antibody in Mice. Nature *364*, 806-809.

Orogo,A.M. and Gustafsson,A.B. (2013). Cell death in the myocardium: My heart won't go on. Iubmb Life *65*, 651-656.

Palmer,C.S., Osellame,L.D., Laine,D., Koutsopoulos,O.S., Frazier,A.E., and Ryan,M.T. (2011). MiD49 and MiD51, new components of the mitochondrial fission machinery. EMBO Rep. *12*, 565-573.

Pena,J.C., Rudin,C.M., and Thompson,C.B. (1998). A Bcl-xL transgene promotes malignant conversion of chemically initiated skin papillomas. Cancer Res. *58*, 2111-2116.

Rizzuto,R., Bernardi,P., and Pozzan,T. (2000). Mitochondria as all-round players of the calcium game. Journal of Physiology-London *529*, 37-47.

Rodriguez,I., Matsuura,K., Khatib,K., Reed,J.C., Nagata,S., and Vassalli,P. (1996). A bcl-2 transgene expressed in hepatocytes protects mice from fulminant liver destruction but not from rapid death induced by anti-Fas antibody injection. Journal of Experimental Medicine *183*, 1031-1036.

Romanello,V., Guadagnin,E., Gomes,L., Roder,I., Sandri,C., Petersen,Y., Milan,G., Masiero,E., Del,P.P., Foretz,M., Scorrano,L., Rudolf,R., and Sandri,M. (2010). Mitochondrial fission and remodelling contributes to muscle atrophy. EMBO J *29*, 1774-1785.

Sandri,M., Lin,J.D., Handschin,C., Yang,W.L., Arany,Z.P., Lecker,S.H., Goldberg,A.L., and Spiegelman,B.M. (2006). PGC-1 alpha a protects skeletal muscle from atrophy by suppressing Fox03 action and atrophy-specific gene transcription. Proceedings of the National Academy of Sciences of the United States of America *103*, 16260-16265.

Santel,A., Frank,S., Gaume,B., Herrler,M., Youle,R.J., and Fuller,M.T. (2003). Mitofusin-1 protein is a generally expressed mediator of mitochondrial fusion in mammalian cells. J. Cell Sci. *116*, 2763-2774.

Schagger,H. (1995). Native electrophoresis for isolation of mitochondrial oxidative phosphorylation protein complexes. Methods Enzymol. *260*, 190-202.

Scorrano,L., Ashiya,M., Buttle,K., Weiler,S., Oakes,S.A., Mannella,C.A., and Korsmeyer,S.J. (2002). A Distinct Pathway Remodels Mitochondrial Cristae and Mobilizes Cytochrome c during Apoptosis. Dev. Cell *2*, 55-67.

Seo,A.Y., Joseph,A.M., Dutta,D., Hwang,J.C.Y., Aris,J.P., and Leeuwenburgh,C. (2010). New insights into the role of mitochondria in aging: mitochondrial dynamics and more. Journal of Cell Science *123*, 2533-2542.

Sun,M.G., Williams,J., Munoz-Pinedo,C., Perkins,G.A., Brown,J.M., Ellisman,M.H., Green,D.R., and Frey,T.G. (2007). Correlated three-dimensional light and electron microscopy reveals transformation of mitochondria during apoptosis. Nat. Cell Biol. *9*, 1057-1065.

Wang,X. (2001). The expanding role of mitochondria in apoptosis. Genes Dev. *15*, 2922-2933.

Wang,Z.G., Jiang,H., Chen,S., Du,F.H., and Wang,X.D. (2012). The Mitochondrial Phosphatase PGAM5 Functions at the Convergence Point of Multiple Necrotic Death Pathways. Cell *148*, 228-243.

Wasilewski,M. and Scorrano,L. (2009). The changing shape of mitochondrial apoptosis. Trends Endocrinol. Metab *20*, 287-294.

Wei,M.C., Lindsten,T., Mootha,V.K., Weiler,S., Gross,A., Ashiya,M., Thompson,C.B., and Korsmeyer,S.J. (2000). tBID, a membrane-targeted death ligand, oligomerizes BAK to release cytochrome c. Genes Dev. *14*, 2060-2071.

Wei,M.C., Zong,W.X., Cheng,E.H., Lindsten,T., Panoutsakopoulou,V., Ross,A.J., Roth,K.A., MacGregor,G.R., Thompson,C.B., and Korsmeyer,S.J. (2001). Proapoptotic BAX and BAK: a requisite gateway to mitochondrial dysfunction and death. Science *292*, 727-730.

Yamaguchi,R., Lartigue,L., Perkins,G., Scott,R.T., Dixit,A., Kushnareva,Y., Kuwana,T., Ellisman,M.H., and Newmeyer,D.D. (2008). Opa1-mediated cristae opening is Bax/Bak and BH3 dependent, required for apoptosis, and independent of Bak oligomerization. Mol. Cell *31*, 557-569.

Yin,X.M., Wang,K., Gross,A., Zhao,Y., Zinkel,S., Klocke,B., Roth,K.A., and Korsmeyer,S.J. (1999). Bid-deficient mice are resistant to Fas-induced hepatocellular apoptosis. Nature *400*, 886-891.

Zhang,Z.Y., Wakabayashi,N., Wakabayashi,J., Tamura,Y., Song,W.J., Sereda,S., Clerc,P., Polster,B.M., Aja,S.M., Pletnikov,M.V., Kensler,T.W., Shirihai,O.S., Iijima,M., Hussain,M.A., and Sesaki,H. (2011). The dynamin-related GTPase Opa1 is required for glucose-stimulated ATP production in pancreatic beta cells. Molecular Biology of the Cell *22*, 2235-2245.

The multifunctional mitochondrial inner membrane protein Optic Atrophy 1 controls cellular damage in vivo

Tatiana Varanita, M.E. Soriano Garcìa Cuerva, Vanina Romanello, Tania Zaglia, Roberta Menabò, Veronica Costa, Sara Cogliati, Ruth Slack, Marco Mongillo, Marco Sandri, Fabio Di Lisa, and Luca Scorrano

Supplementary online material

Legends to supplementary figures

Supplementary Figure 1S. Characterization of *Opa1*^{tg} mice

(A) Equal amounts of protein from liver tissue of the indicated genotypes were separated by SDS-PAGE and immunoblotted with the indicated antibodies.

(B) Equal amounts of protein from liver tissue of the indicated genotypes were separated by SDS-PAGE and immunoblotted with the indicated antibodies.

(C) Growth rate of C57/Bl6 Wt and *Opa1*^{tg} males and females during the initial 60 days of life. Data represent average $\pm$ SEM (n=20 per each group).

(D) Body weight is represented as average $\pm$ SEM of 5 months males (n=17 for each group) and females (n= 10 for each group) and 9 months old males (n= 19 for each group) and females (n=8 for each group) SV129 *Opa1*^{tg} and Wt litettermates.

Supplementary Figure 2S. Histological and morphological characterization of heart, liver and kidney

(A) Immunofluorescence analysis on ventricular cryosections from Wt and *Opa1*^{tg} mice stained with an antibody to dystrophin. Images are details from the left ventricle.

(B) Evaluation of cardiomyocyte (CM) area in cryosections from Wt and *Opa1*^{tg} 5 months old hearts. Bars indicate average $\pm$ SEM. (n=5 for each group).

(C) Echocardiographic long axis view of hearts from 5 months old Wt and *Opa1*^{tg} littermates. LV: left ventricle; A: aorta.

(D) Haematoxilin-eosin staining in ventricular cryosections from 5 months Wt and *Opa1*^{tg} mice.

(E) Immunofluorescence analysis of heart cryosections from 9 months old Wt and *Opa1*^{tg} mice stained with an antibody to Collagene I (Col.I).

(F) Evaluation of liver weight/body weight ratio in 5 and 9 months old male mice. Wt and *Opa1*^{tg} . Bars indicate average ± SEM (n=10 for each group).

(G) Echographic view of the liver from 9 months old Wt and *Opa1tg* mice.

(H) Echographic short axis view of the left kidney from 9 months old Wt and *Opa1*^{tg} mice.

(I) Morphometric analysis of kidney from 9 months old Wt and *Opa1*^{tg} mice. Error bars indicate s.e.m. (n=6 for each group).

Suplimentary Figure 3S. *Opa1*^{tg} mitochondria are slightly elongated and contain tighter cristae

(A) Complex IV dependent respiration of mitochondria isolated from livers of the indicated genotypes. Data represent average ± SEM (n=4 for each group).

(B) Representative traces of Calcium Retention Capacity (CRC) of liver mitochondria isolated from 5 months old Wt and *Opa1*^{tg} mice. Where indicated, 2 µM CsA was present in the mediumCsA.

(C) Quantification of CRC in experiments as in (D).

(D) Representative traces of Rhodamine 123 fluorescence. Mitochondria isolated from livers of the indicated genotype (1 mg/mL, MLM) were treated where indicated (arrows) with 300 µM ADP and 200 nM FCCP.

(E) Mitochondria of the indicated genotype were treated with cBID for the indicated times. 10 mM BMH or DMSO was then added and after 30 min the crosslinking reaction was quenched. Equal amounts (40 g) of mitochondrial proteins were analyzed by SDS-PAGE/immunoblotting using anti-BAK antibody. Asterisks indicates BAK multimers.

Figure 1S

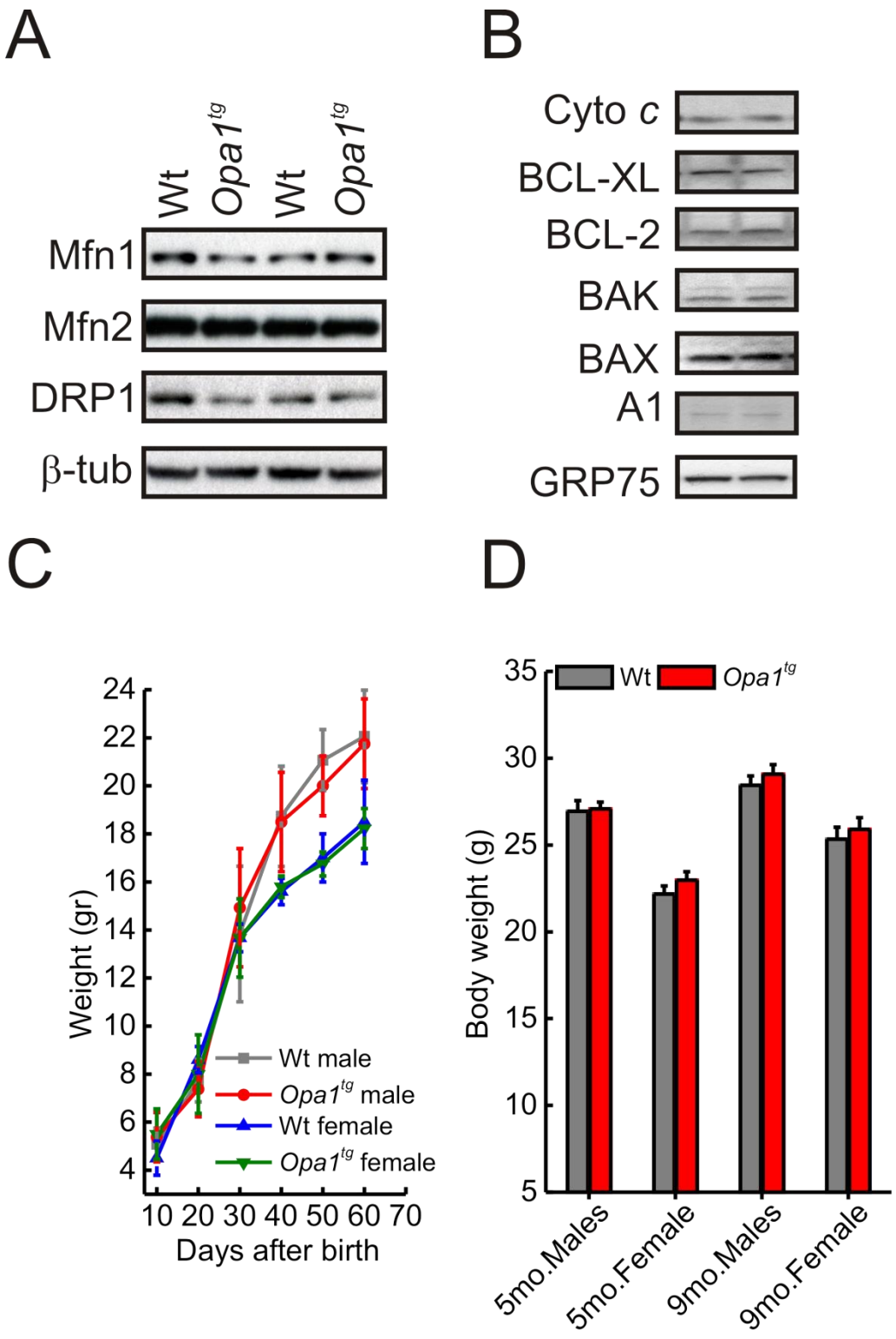
A
Wt
Opa1tg
Wt
Opa1tg
Mfn1
Mfn2
DRP1
β-tub
B
Cyto c
BCL-XL
BCL-2
BAK
BAX
A1
GRP75
C
Weight (gr)
24
22
20
18
16
14
12
10
8
6
4
10 20 30 40 50 60 70
Days after birth
Wt male
Opa1tg male
Wt female
Opa1tg female
D
Body weight (g)
35
30
25
20
15
10
5
Wt
Opa1tg
5mo.Males
5mo.Female
9mo.Males
9mo.Female

Figure 2S

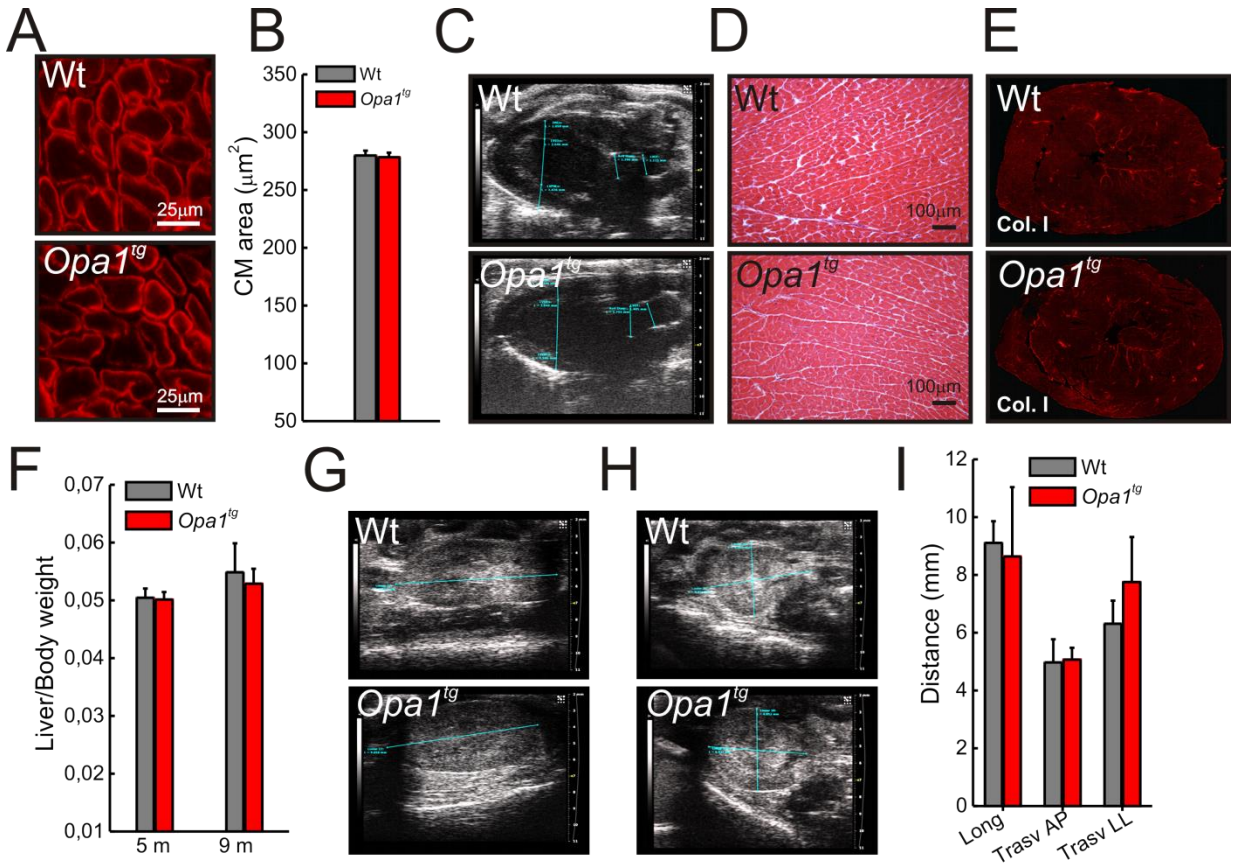
A
Wt
25µm
Opa1tg
25µm
B
CM area (µm2)
350
300
250
200
150
100
50
Wt
Opa1tg
C
Wt
Opa1tg
D
Wt
100µm
Opa1tg
100µm
E
Wt
Col. I
Opa1tg
Col. I
F
Liver/Body weight
0,07
0,06
0,05
0,04
0,03
0,02
0,01
Wt
Opa1tg
5 m
9 m
G
Wt
Opa1tg
H
Wt
Opa1tg
I
Distance (mm)
12
10
8
6
4
2
0
Wt
Opa1tg
Long
Trasv AP
Trasv LL

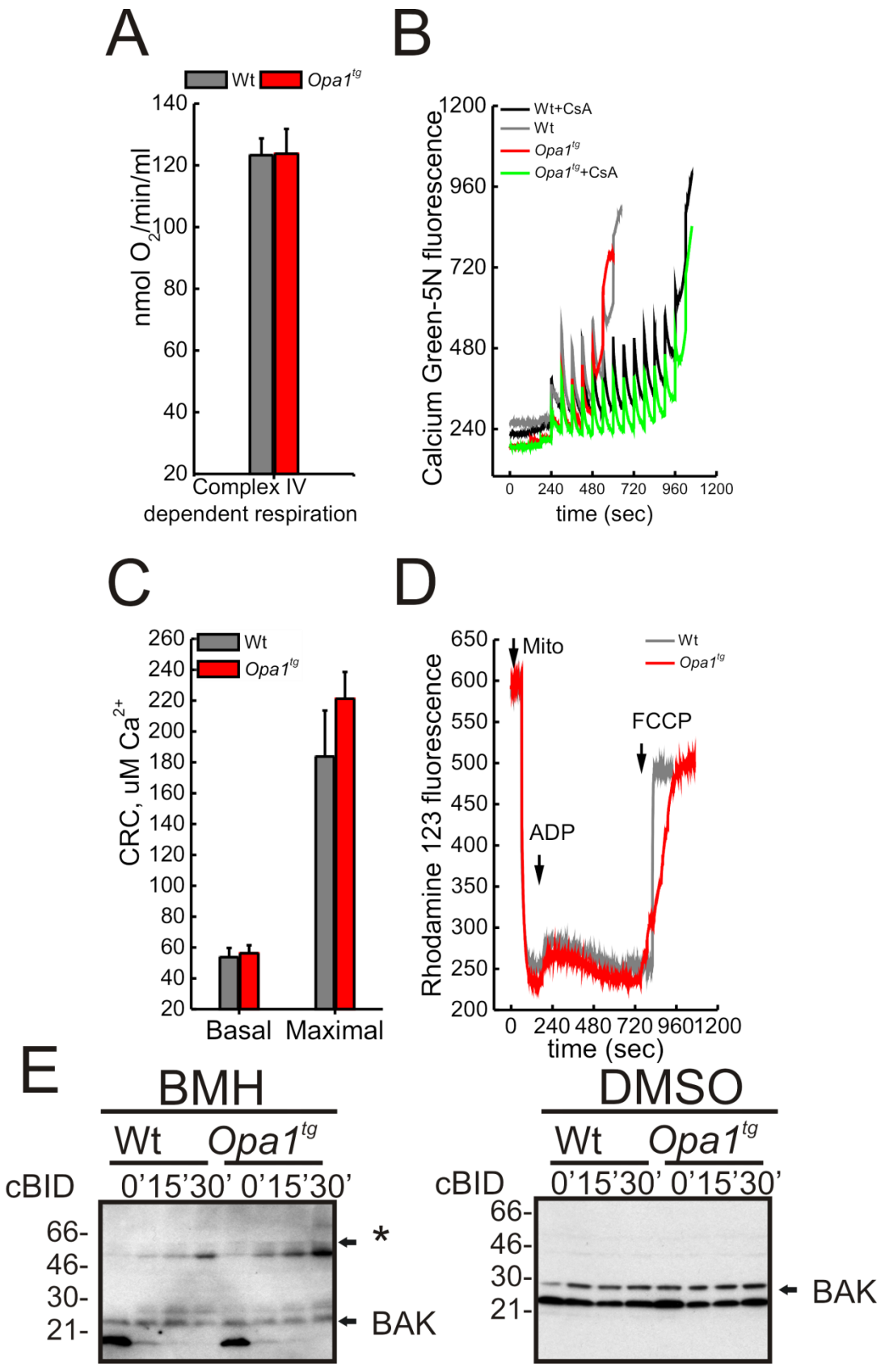
A
Wt
Opa1tg
nmol O2/min/ml
140
120
100
80
60
40
20
Complex IV
dependent respiration
B
Wt+CsA
Wt
Opa1tg
Opa1tg+CsA
Calcium Green-5N fluorescence
1200
960
720
480
240
0
240
480
720
960
1200
time (sec)
C
Wt
Opa1tg
CRC, uM Ca2+
260
240
220
200
180
160
140
120
100
80
60
40
20
Basal
Maximal
D
Mito
Wt
Opa1tg
FCCP
ADP
Rhodamine 123 fluorescence
650
600
550
500
450
400
350
300
250
200
0
240
480
720
960
1200
time (sec)
E
BMH
DMSO
Wt
Opa1tg
cBID
0'15'30'
0'15'30'
66-
46-
30-
21-
*
BAK

Figure 3S

5 Conclusions and perspectives

In this thesis we addressed the role of OPA1 overexpression in the tissue response to damage in vivo. We used a mouse model with a specific targeted insertion that resulted in OPA1 ubiquitous mild overexpression in a variety of tissues. Our data indicate that a slight increase of OPA1 is sufficient to improve the response to several death stimuli.

Increased levels of OPA1 can retrogradely inhibit the program of muscular atrophy induced by denervation due to the maintenance of functional mitochondria. In addition *Opa1*^{tg} mice were resistant to brain ischemia, cardiac ischemia/reperfusion and Fas mediated hepatocellular apoptosis. We biochemically elucidated the mechanism behind this protective effect of OPA1 overexpression. Increased OPA1 levels resulted in an augmented OPA1 oligomerization, which is known to correlate with the maintenance of cristae tightness and with the prevention of cytochrome c mobilization.

Fibroblasts derived from *Opa1*^{tg} mice have been used to dissect the role of cristae shape in mitochondrial bioenergetics. Acute ablation of *Opa1* resulted in aberrant cristae morphology, reduced RCS assembly and impaired complex I dependent respiration. On the other hand *Opa1*^{tg} fibroblasts display an increase RCS assembly, respiratory function and cell growth. *Opa1*^{tg} cells have been an useful tool to unveil how OPA1 regulates respiratory efficiency and we can predict that they will be useful also to address the molecular mechanism by which Opa1 overexpression protects for example from mitochondrial dysfunction. One tempting possibility is

that Opa1 and the so called permeability transition pore (PTP) crosstalk. The PTP is an IMM channel whose opening is associated with multiple forms of mitochondrial dysfunction and death, due to the collapse of the electrochemical gradient and to mitochondrial swelling. Interestingly, during mitochondrial cristae remodeling the PTP opens and it was recently discovered that dimers of the ATPase, that control cristae morphology, constitute the PTP. In a plausible scenario, Opa1 overexpression could interfere with ATPase dimerization or even better with the binding of the PTP activator cyclophilin D to the ATPase dimers. Elucidating this mechanism could be of great impact to deploy a two pronged strategy of mitochondrial preservation for example in heart ischemia, where PTP inhibitors are already in Phase II clinical trials.

Another interesting paradigm in which it is worth exploring whether Opa1 overexpression can be beneficial is mitochondrial disorders, a group of clinical entities associated with defects of OXPHOS, most often partial (i.e., caused by a partial, above threshold depletion in one respiratory chain complex). It would be tempting to speculate that OPA1 overexpression could help in the context of these diseases by enhancing RCS, which increase the efficiency of electron flow among complexes as well as individual complex stability. Since the mild overexpression of OPA1 is sufficient to ameliorate cristae morphology and consequently mitochondrial bioenergetics, we have already set out to investigate this possibility and we bred *Opa1*^{tg} mice with a mouse model of OXPHOS deficiency. A muscle specific COX15 knockout mouse recapitulates the clinical manifestation of several complex IV deficiency, displaying a severe atrophic phenotype, heavily reduced

running performance and dying before it reaches 6 months of age (Viscomi et al 2011). Interestingly, our preliminary results indicate that the mild overexpression of OPA1 is sufficient to ameliorate every aspects of this pathological phenotype. This model further supports the role of OPA1 in RCS stabilization and it open new therapeutic perspectives in the treatment of mitochondrial diseases characterized by impairment of mitochondrial bioenergetics.

Our studies allow to conclude that Opa1-dependent cristae remodeling and biogenesis may be exploited to treat not only primary mitochondrial disorders, but also sporadic pathological conditions that are widespread in an aging society such as heart ischemia, stroke and muscular atrophy.

Acin-Perez,R., Bayona-Bafaluy,M.P., Fernandez-Silva,P., Moreno-Loshuertos,R., Perez-Martos,A., Bruno,C., Moraes,C.T., and Enriquez,J.A. (2004). Respiratory complex III is required to maintain complex I in mammalian mitochondria. Mol Cell *13*, 805-815.

Acin-Perez,R., Fernandez-Silva,P., Peleato,M.L., Perez-Martos,A., and Enriquez,J.A. (2008). Respiratory active mitochondrial supercomplexes. Mol Cell *32*, 529-539.

Adachi,M., Suematsu,S., Kondo,T., Ogasawara,J., Tanaka,T., Yoshida,N., and Nagata,S. (1995). Targeted Mutation in the Fas Gene Causes Hyperplasia in Peripheral Lymphoid Organs and Liver. Nature Genetics *11*, 294-300.

Adhihetty,P.J., O'Leary,M.F.N., Chabi,B., Wicks,K.L., and Hood,D.A. (2007). Effect of denervation on mitochondrially mediated apoptosis in skeletal muscle. Journal of Applied Physiology *102*, 1143-1151.

Ahting,U., Thun,C., Hegerl,R., Typke,D., Nargang,F.E., Neupert,W., and Nussberger,S. (1999). The TOM core complex: The general protein import pore of the outer membrane of mitochondria. Journal of Cell Biology *147*, 959-968.

Akepati,V.R., Muller,E.C., Otto,A., Strauss,H.M., Portwich,M., and Alexander,C. (2008). Characterization of OPA1 isoforms isolated from mouse tissues. J. Neurochem. *106*, 372-383.

Al Rawi,S., Louvet-Vallee,S., Djeddi,A., Sachse,M., Culetto,E., Hajjar,C., Boyd,L., Legouis,R., and Galy,V. (2011). Postfertilization Autophagy of Sperm Organelles Prevents Paternal Mitochondrial DNA Transmission. Science *334*, 1144-1147.

Alexander,C., Votruba,M., Pesch,U.E., Thiselton,D.L., Mayer,S., Moore,A., Rodriguez,M., Kellner,U., Leo-Kottler,B., Auburger,G., Bhattacharya,S.S., and Wissinger,B. (2000). OPA1, encoding a dynamin-related GTPase, is mutated in autosomal dominant optic atrophy linked to chromosome 3q28. Nat. Genet. *26*, 211-215.

Amati-Bonneau,P., Valentino,M.L., Reynier,P., Gallardo,M.E., Bornstein,B., Boissiere,A., Campos,Y., Rivera,H., de la Aleja,J.G., Carroccia,R., Iommarini,L., Labauge,P., Figarella-Branger,D., Marcorelles,P., Furby,A., Beauvais,K., Letournel,F., Liguori,R., La Morgia,C., Montagna,P., Liguori,M., Zanna,C., Rugolo,M., Cossarizza,A., Wissinger,B., Verny,C., Schwarzenbacher,R., Martin,M.A., Arenas,J., Ayuso,C., Garesse,R., Lenaers,G., Bonneau,D., and Carelli,V. (2008). OPA1 mutations induce mitochondrial DNA instability and optic atrophy plus phenotypes. Brain *131*, 338-351.

Amutha,B., Gordon,D.M., Gu,Y., and Pain,D. (2004). A novel role of Mgm1p, a dynamin-related GTPase, in ATP synthase assembly and cristae formation/maintenance. Biochem J *381*, 19-23.

Antonicka,H., Mattman,A., Carlson,C.G., Glerum,D.M., Hoffbuhr,K.C., Leary,S.C., Kennaway,N.G., and Shoubridge,E.A. (2003). Mutations in COX15 produce a defect in the mitochondrial heme biosynthetic pathway, causing early-onset fatal hypertrophic cardiomyopathy. American Journal of Human Genetics *72*, 101-114.

Apostolova,N., Blas-Garcia,A., and Esplugues,J.V. (2011). Mitochondria Sentencing About Cellular Life and Death: A Matter of Oxidative Stress. Current Pharmaceutical Design *17*, 4047-4060.

Arselin,G., Vaillier,J., Salin,B., Schaeffer,J., Giraud,M.F., Dautant,A., Brethes,D., and Velours,J. (2004). The modulation in subunits e and g amounts of yeast ATP synthase modifies mitochondrial cristae morphology. Journal of Biological Chemistry *279*, 40392-40399.

Attardi,G. and Schatz,G. (1988). Biogenesis of mitochondria. Annu. Rev. Cell. Biol. *4*, 289-333.

Baldelli,S., Aquilano,K., and Ciriolo,M.R. (2013). Punctum on two different transcription factors regulated by PGC-1 alpha: Nuclear factor erythroid-derived 2-like 2 and nuclear respiratory factor 2. Biochimica et Biophysica Acta-General Subjects *1830*, 4137-4146.

Balsa,E., Marco,R., Pereles-Clemente,E., Szklarczyk,R., Calvo,E., Landazuri,M.O., and Enriquez,J.A. (2012). NDUFA4 Is a Subunit of Complex IV of the Mammalian Electron Transport Chain. Cell Metabolism *16*, 378-386.

Baradaran,R., Berrisford,J.M., Minhas,G.S., and Sazanov,L.A. (2013). Crystal structure of the entire respiratory complex I. Nature *494*, 443-448.

Baricault,L., Segui,B., Guegand,L., Olichon,A., Valette,A., Larminat,F., and Lenaers,G. (2007). OPA1 cleavage depends on decreased mitochondrial ATP level and bivalent metals. Exp. Cell Res. *313*, 3800-3808.

Belenguer,P. and Pellegrini,L. (2013). The dynamin GTPase OPA1: more than mitochondria? Biochim. Biophys. Acta *1833*, 176-183.

Bender,T. and Martinou,J.C. (2013). Where Killers Meet-Permeabilization of the Outer Mitochondrial Membrane during Apoptosis. Cold Spring Harbor Perspectives in Biology *5*.

Bernardi,P. and Azzone,G.F. (1981). Cytochrome c as an electron shuttle between the outer and inner mitochondrial membranes. J. Biol. Chem. *256*, 7187-7192.

Bernardi,P., Scorrano,L., Colonna,R., Petronilli,V., and Di Lisa F. (1999). Mitochondria and cell death. Mechanistic aspects and methodological issues. Eur. J. Biochem. *264*, 687-701.

Borutaite,V., Toleikis,A., and Brown,G.C. (2013). In the eye of the storm: mitochondrial damage during heart and brain ischaemia. Febs Journal *280*, 4999-5014.

Calvani,R., Joseph,A.M., Adhihetty,P.J., Miccheli,A., Bossola,M., Leeuwenburgh,C., Bernabei,R., and Marzetti,E. (2013). Mitochondrial pathways in sarcopenia of aging and disuse muscle atrophy. Biological Chemistry *394*, 393-414.

Campbell,C.T., Kolesar,J.E., and Kaufman,B.A. (2012). Mitochondrial transcription factor A regulates mitochondrial transcription initiation, DNA packaging, and genome copy number. Biochimica et Biophysica Acta-Gene Regulatory Mechanisms *1819*, 921-929.

Carreira,R.S., Lee,P., and Gottlieb,R.A. (2011). Mitochondrial Therapeutics for Cardioprotection. Current Pharmaceutical Design *17*, 2017-2035.

Chakraborty,J.B., Oakley,F., and Walsh,M.J. (2012). Mechanisms and biomarkers of apoptosis in liver disease and fibrosis. Int. J. Hepatol. *2012*, 648915.

Chang,D.T., Honick,A.S., and Reynolds,I.J. (2006). Mitochondrial trafficking to synapses in cultured primary cortical neurons. J. Neurosci. *26*, 7035-7045.

Chen,H. and Chan,D.C. (2005). Emerging functions of mammalian mitochondrial fusion and fission. Hum Mol Genet *14 Spec No. 2*.

Chen,H., Chomyn,A., and Chan,D.C. (2005a). Disruption of fusion results in mitochondrial heterogeneity and dysfunction. J. Biol. Chem. *280*, 26185-26192.

Chen,H., Detmer,S.A., Ewald,A.J., Griffin,E.E., Fraser,S.E., and Chan,D.C. (2003a). Mitofusins Mfn1 and Mfn2 coordinately regulate mitochondrial fusion and are essential for embryonic development. J. Cell Biol. *160*, 189-200.

Chen,H., Vermulst,M., Wang,Y.E., Chomyn,A., Prolla,T.A., McCaffery,J.M., and Chan,D.C. (2010). Mitochondrial fusion is required for mtDNA stability in skeletal muscle and tolerance of mtDNA mutations. Cell *141*, 280-289.

Chen,H.C., Chomyn,A., and Chan,D.C. (2005b). Disruption of fusion results in mitochondrial heterogeneity and dysfunction. Journal of Biological Chemistry *280*, 26185-26192.

Chen,L., Gong,Q.Z., Stice,J.P., and Knowlton,A.A. (2009). Mitochondrial OPA1, apoptosis, and heart failure. Cardiovascular Research *84*, 91-99.

Chen,Q., Vazquez,E.J., Moghaddas,S., Hoppel,C.L., and Lesnefsky,E.J. (2003b). Production of reactive oxygen species by mitochondria - Central role of complex III. Journal of Biological Chemistry *278*, 36027-36031.

Cheng,E.H., Wei,M.C., Weiler,S., Flavell,R.A., Mak,T.W., Lindsten,T., and Korsmeyer,S.J. (2001). Bcl-2, bcl-x(l) sequester bh3 domain-only molecules preventing bax- and bak-mediated mitochondrial apoptosis. Mol. Cell *8*, 705-711.

Cipolat,S., de Brito,O.M., Dal Zilio,B., and Scorrano,L. (2004). OPA1 requires mitofusin 1 to promote mitochondrial fusion. Proc. Natl. Acad. Sci. U. S. A *101*, 15927-15932.

Cipolat,S., Rudka,T., Hartmann,D., Costa,V., Serneels,L., Craessaerts,K., Metzger,K., Frezza,C., Annaert,W., D'Adamio,L., Derks,C., Dejaegere,T., Pellegrini,L., D'Hooge,R., Scorrano,L., and De Strooper,B. (2006). Mitochondrial Rhomboid PARL Regulates Cytochrome c Release during Apoptosis via OPA1-Dependent Cristae Remodeling. Cell *126*, 163-175.

Cipolat,S. and Scorrano,L. (2006). To fuse and to protect. A novel role for CED-9 in mitochondrial morphology reveals an ancient function. Cell Death. Differ.

Colombini,M. and Mannella,C.A. (2012). VDAC, The early days. Biochimica et Biophysica Acta-Biomembranes *1818*, 1438-1443.

Corrado,M., Scorrano,L., and Campello,S. (2012). Mitochondrial dynamics in cancer and neurodegenerative and neuroinflammatory diseases. Int. J. Cell Biol. *2012*, 729290.

Crompton,M. (1999). The mitochondrial permeability transition pore and its role in cell death. Biochemical Journal *341*, 233-249.

Crow,M.T., Mani,K., Nam,Y.J., and Kitsis,R.N. (2004). The mitochondrial death pathway and cardiac myocyte apoptosis. Circulation Research *95*, 957-970.

Davies,V.J., Hollins,A.J., Piechota,M.J., Yip,W., Davies,J.R., White,K.E., Nicols,P.P., Boulton,M.E., and Votruba,M. (2007). Opa1 deficiency in a mouse model of autosomal dominant optic atrophy impairs mitochondrial morphology, optic nerve structure and visual function. Hum. Mol. Genet. *16*, 1307-1318.

de Brito,O.M. and Scorrano,L. (2008). Mitofusin 2 tethers endoplasmic reticulum to mitochondria. Nature *456*, 605-610.

De Stefani,D., Raffaello,A., Teardo,E., Szabo,I., and Rizzuto,R. (2011). A forty-kilodalton protein of the inner membrane is the mitochondrial calcium uniporter. Nature *476*, 336-U104.

Delettre,C., Griffoin,J.M., Kaplan,J., Dollfus,H., Lorenz,B., Faivre,L., Lenaers,G., Belenguer,P., and Hamel,C.P. (2001). Mutation spectrum and splicing variants in the OPA1 gene. Hum. Genet. *109*, 584-591.

Delettre,C., Lenaers,G., Griffoin,J.M., Gigarel,N., Lorenzo,C., Belenguer,P., Pelloquin,L., Grosgeorge,J., Turc-Carel,C., Perret,E., Astarie-Dequeker,C., Lasquellec,L., Arnaud,B., Ducommun,B., Kaplan,J., and Hamel,C.P. (2000). Nuclear gene OPA1, encoding a mitochondrial dynamin-related protein, is mutated in dominant optic atrophy. Nat. Genet. *26*, 207-210.

Deng,H., Dodson,M.W., Huang,H., and Guo,M. (2008). The Parkinson's disease genes pink1 and parkin promote mitochondrial fission and/or inhibit fusion in Drosophila. Proc. Natl. Acad. Sci. U. S. A. *105*, 14503-14508.

Detmer,S.A. and Chan,D.C. (2007). Complementation between mouse Mfn1 and Mfn2 protects mitochondrial fusion defects caused by CMT2A disease mutations. J. Cell Biol. *176*, 405-414.

Di Lisa,F. and Bernardi,P. (2006). Mitochondria and ischemia-reperfusion injury of the heart: fixing a hole. Cardiovasc. Res. *70*, 191-199.

Di,L.F., Kaludercic,N., Carpi,A., Menabo,R., and Giorgio,M. (2009). Mitochondrial pathways for ROS formation and myocardial injury: the relevance of p66(Shc) and monoamine oxidase. Basic Res. Cardiol. *104*, 131-139.

Diaz,F., Fukui,H., Garcia,S., and Moraes,C.T. (2006). Cytochrome c oxidase is required for the assembly/stability of respiratory complex I in mouse fibroblasts. Molecular and Cellular Biology *26*, 4872-4881.

Dimmer,K.S. and Scorrano,L. (2006). (De)constructing mitochondria: what for? Physiology. (Bethesda.) *21*, 233-241.

Du,C., Fang,M., Li,Y., Li,L., and Wang,X. (2000). Smac, a mitochondrial protein that promotes cytochrome c-dependent caspase activation by eliminating IAP inhibition. Cell *102*, 33-42.

Duchen,M.R. (2000). Mitochondria and calcium: from cell signalling to cell death. J. Physiol. *529 Pt 1:57-68.*, 57-68.

Duvezin-Caubet,S., Jagasia,R., Wagener,J., Hofmann,S., Trifunovic,A., Hansson,A., Chomyn,A., Bauer,M.F., Attardi,G., Larsson,N.G., Neupert,W., and Reichert,A.S. (2006). Proteolytic processing of OPA1 links mitochondrial dysfunction to alterations in mitochondrial morphology. J. Biol. Chem. *281*, 37972-37979.

Duvezin-Caubet,S., Koppen,M., Wagener,J., Zick,M., Israel,L., Bernacchia,A., Jagasia,R., Rugarli,E.I., Imhof,A., Neupert,W., Langer,T., and Reichert,A.S. (2007). OPA1 processing reconstituted in yeast depends on the subunit composition of the m-AAA protease in mitochondria. Mol. Biol. Cell *18*, 3582-3590.

Ehses,S., Raschke,I., Mancuso,G., Bernacchia,A., Geimer,S., Tondera,D., Martinou,J.C., Westermann,B., Rugarli,E.I., and Langer,T. (2009). Regulation of OPA1 processing and mitochondrial fusion by m-AAA protease isoenzymes and OMA1. J Cell Biol *187*, 1023-1036.

Estaquier,J. and Arnoult,D. (2007). Inhibiting Drp1-mediated mitochondrial fission selectively prevents the release of cytochrome c during apoptosis. Cell Death. Differ. *14*, 1086-1094.

Eura,Y., Ishihara,N., Yokota,S., and Mihara,K. (2003). Two mitofusin proteins, mammalian homologues of FZO, with distinct functions are both required for mitochondrial fusion. J. Biochem. (Tokyo) *134*, 333-344.

Faubion,W.A. and Gores,G.J. (1999). Death receptors in liver biology and pathobiology. Hepatology *29*, 1-4.

Feldmann,G. (2006). [Liver apoptosis]. Gastroenterol. Clin. Biol. *30*, 533-545.

Frank,S., Gaume,B., Bergmann-Leitner,E.S., Leitner,W.W., Robert,E.G., Catez,F., Smith,C.L., and Youle,R.J. (2001). The role of dynamin-related protein 1, a mediator of mitochondrial fission, in apoptosis. Dev. Cell *1*, 515-525.

Frey,T.G. and Mannella,C.A. (2000). The internal structure of mitochondria. Trends. Biochem. Sci. *25*, 319-324.

Frezza,C., Cipolat,S., Martins,d.B., Micaroni,M., Beznoussenko,G.V., Rudka,T., Bartoli,D., Polishuck,R.S., Danial,N.N., De Strooper,B., and Scorrano,L. (2006). OPA1 Controls Apoptotic Cristae Remodeling Independently from Mitochondrial Fusion. Cell *126*, 177-189.

Gandre-Babbe,S. and van der Bliek,A.M. (2008). The novel tail-anchored membrane protein Mff controls mitochondrial and peroxisomal fission in mammalian cells. Mol. Biol. Cell *19*, 2402-2412.

Germain,M., Mathai,J.P., McBride,H.M., and Shore,G.C. (2005). Endoplasmic reticulum BIK initiates DRP1-regulated remodelling of mitochondrial cristae during apoptosis. EMBO J. *24*, 1546-1556.

Gilkerson,R.W., Selker,J.M., and Capaldi,R.A. (2003). The cristal membrane of mitochondria is the principal site of oxidative phosphorylation. FEBS Lett. *546*, 355-358.

Gomes,L.C., Benedetto,G.D., and Scorrano,L. (2011). During autophagy mitochondria elongate, are spared from degradation and sustain cell viability. Nat Cell Biol.

Griffin,E.E., Graumann,J., and Chan,D.C. (2005). The WD40 protein Caf4p is a component of the mitochondrial fission machinery and recruits Dnm1p to mitochondria. J Cell Biol *170*, 237-248.

Griparic,L., Kanazawa,T., and van der Bliek,A.M. (2007). Regulation of the mitochondrial dynamin-like protein Opa1 by proteolytic cleavage. J. Cell Biol *178*, 757-764.

Griparic,L. and van der Bliek,A.M. (2001). The many shapes of mitochondrial membranes. Traffic *2*, 235-244.

Griparic,L., van der Wel,N.N., Orozco,I.J., Peters,P.J., and van der Bliek,A.M. (2004). Loss of the intermembrane space protein Mgm1/OPA1 induces swelling and localized constrictions along the lengths of mitochondria. J. Biol. Chem. *279*, 18792-18798.

Guan,K., Farh,L., Marshall,T.K., and Deschenes,R.J. (1993). Normal mitochondrial structure and genome maintenance in yeast requires the dynamin-like product of the MGM1 gene. Curr Genet *24*, 141-148.

Guicciardi,M.E. and Gores,G.J. (2009). Life and death by death receptors. FASEB J. *23*, 1625-1637.

Guicciardi,M.E., Malhi,H., Mott,J.L., and Gores,G.J. (2013). Apoptosis and necrosis in the liver. Compr. Physiol *3*, 977-1010.

Guillery,O., Malka,F., Landes,T., Guillou,E., Blackstone,C., Lombes,A., Belenguer,P., Arnoult,D., and Rojo,M. (2008). Metalloprotease-mediated OPA1 processing is modulated by the mitochondrial membrane potential. Biol. Cell. *100*, 315-325.

Guzy,R.D. and Schumacker,P.T. (2006). Oxygen sensing by mitochondria at complex III: the paradox of increased reactive oxygen species during hypoxia. Experimental Physiology *91*, 807-819.

Hackenbrock,C.R., Chazotte,B., and Gupte,S.S. (1986). The Random Collision Model and A Critical-Assessment of Diffusion and Collision in Mitochondrial Electron-Transport. Journal of Bioenergetics and Biomembranes *18*, 331-368.

Hackenbrock,C.R., Schneider,H., Lemasters,J.J., and Hochli,M. (1980). Relationships between bilayer lipid, motional freedom of oxidoreductase components, and electron transfer in the mitochondrial inner membrane. Adv. Exp. Med. Biol. *132*, 245-263.

Hales,K.G. and Fuller,M.T. (1997). Developmentally regulated mitochondrial fusion mediated by a conserved, novel, predicted GTPase. Cell *90*, 121-129.

Hein,S., Arnon,E., Kostin,S., Schonburg,M., Elsasser,A., Polyakova,V., Bauer,E.P., Klovekorn,W.P., and Schaper,J. (2003). Progression from compensated hypertrophy to

failure in the pressure-overloaded human heart - Structural deterioration and compensatory mechanisms. Circulation *107*, 984-991.

Hermann,G.J., Thatcher,J.W., Mills,J.P., Hales,K.G., Fuller,M.T., Nunnari,J., and Shaw,J.M. (1998). Mitochondrial fusion in yeast requires the transmembrane GTPase Fzo1p. J. Cell Biol. *143*, 359-373.

Herrmann,J.M. and Neupert,W. (2000). Protein transport into mitochondria. Current Opinion in Microbiology *3*, 210-214.

Hinshaw,J.E. (1999). Dynamin spirals. Curr. Opin. Struct. Biol *9*, 260-267.

Hochhauser,E., Kivity,S., Offen,D., Maulik,N., Otani,H., Barhum,Y., Pannet,H., Shneyvays,V., Shainberg,A., Goldshtaub,V., Tobar,A., and Vidne,B.A. (2003). Bax ablation protects against myocardial ischemia-reperfusion injury in transgenic mice. American Journal of Physiology-Heart and Circulatory Physiology *284*, H2351-H2359.

Hollenbeck,P.J. and Saxton,W.M. (2005). The axonal transport of mitochondria. J. Cell Sci. *118*, 5411-5419.

Hoppeler,H. (1986). Exercise-Induced Ultrastructural-Changes in Skeletal-Muscle. International Journal of Sports Medicine *7*, 187-204.

Hoppins,S., Lackner,L., and Nunnari,J. (2007). The machines that divide and fuse mitochondria. Annu. Rev. Biochem. *76*, 751-780.

Hudson,G., Amati-Bonneau,P., Blakely,E.L., Stewart,J.D., He,L.P., Schaefer,A.M., Griffiths,P.G., Ahlqvist,K., Suomalainen,A., Reynier,P., McFarland,R., Turnbull,D.M., Chinnery,P.F., and Taylor,R.W. (2008). Mutation of OPA1 causes dominant optic atrophy with external ophthalmoplegia, ataxia, deafness and multiple mitochondrial DNA deletions: a novel disorder of mtDNA maintenance. Brain *131*, 329-337.

Iqbal,S., Ostojic,O., Singh,K., Joseph,A.M., and Hood,D.A. (2013). Expression of Mitochondrial Fission and Fusion Regulatory Proteins in Skeletal Muscle During Chronic Use and Disuse. Muscle & Nerve *48*, 963-970.

Ishihara,N., Fujita,Y., Oka,T., and Mihara,K. (2006). Regulation of mitochondrial morphology through proteolytic cleavage of OPA1. EMBO J. *25*, 2966-2977.

James,D.I., Parone,P.A., Mattenberger,Y., and Martinou,J.C. (2003). hFis1, a novel component of the mammalian mitochondrial fission machinery. J. Biol. Chem. *278*, 36373-36379.

Jones,B.A. and Fangman,W.L. (1992). Mitochondrial DNA maintenance in yeast requires a protein containing a region related to the GTP-binding domain of dynamin. Genes. Dev. *6*, 380-389.

Joseph,A.M., Adhihetty,P.J., Buford,T.W., Wohlgemuth,S.E., Lees,H.A., Nguyen,L.M.D., Aranda,J.M., Sandesara,B.D., Pahor,M., Manini,T.M., Marzetti,E., and Leeuwenburgh,C. (2012). The impact of aging on mitochondrial function and biogenesis pathways in skeletal muscle of sedentary high- and low-functioning elderly individuals. Aging Cell *11*, 801-809.

Jost,P.J., Grabow,S., Gray,D., McKenzie,M.D., Nachbur,U., Huang,D.C.S., Bouillet,P., Thomas,H.E., Borner,C., Silke,J., Strasser,A., and Kaufmann,T. (2009). XIAP discriminates between type I and type II FAS-induced apoptosis. Nature *460*, 1035-U128.

Karbowski,M., Arnoult,D., Chen,H., Chan,D.C., Smith,C.L., and Youle,R.J. (2004). Quantitation of mitochondrial dynamics by photolabeling of individual organelles shows that mitochondrial fusion is blocked during the Bax activation phase of apoptosis. J. Cell Biol. *164*, 493-499.

Kerr,J.F., Wyllie,A.H., and Currie,A.R. (1972). Apoptosis: a basic biological phenomenon with wide-ranging implications in tissue kinetics. Br. J. Cancer. *26*, 239-257.

Kijima,K., Numakura,C., Izumino,H., Umetsu,K., Nezu,A., Shiiki,T., Ogawa,M., Ishizaki,Y., Kitamura,T., Shozawa,Y., and Hayasaka,K. (2005). Mitochondrial GTPase mitofusin 2 mutation in Charcot-Marie-Tooth neuropathy type 2A. Hum. Genet. *116*, 23-27.

Kirkwood,S.P., Packer,L., and Brooks,G.A. (1987). Effects of Endurance Training on A Mitochondrial Reticulum in Limb Skeletal-Muscle. Archives of Biochemistry and Biophysics *255*, 80-88.

Kischkel,F.C., Hellbardt,S., Behrmann,I., Germer,M., Pawlita,M., Krammer,P.H., and Peter,M.E. (1995). Cytotoxicity-Dependent Apo-1 (Fas/Cd95)-Associated Proteins Form A Death-Inducing Signaling Complex (Disc) with the Receptor. Embo Journal *14*, 5579-5588.

Koirala,S., Bui,H.T., Schubert,H.L., Eckert,D.M., Hill,C.P., Kay,M.S., and Shaw,J.M. (2010). Molecular architecture of a dynamin adaptor: implications for assembly of mitochondrial fission complexes. Journal of Cell Biology *191*, 1127-1139.

Koshiba,T., Detmer,S.A., Kaiser,J.T., Chen,H., McCaffery,J.M., and Chan,D.C. (2004). Structural basis of mitochondrial tethering by mitofusin complexes. Science *305*, 858-862.

Kroemer,G., Galluzzi,L., Vandenabeele,P., Abrams,J., Alnemri,E.S., Baehrecke,E.H., Blagosklonny,M.V., El-Deiry,W.S., Golstein,P., Green,D.R., Hengartner,M., Knight,R.A., Kumar,S., Lipton,S.A., Malorni,W., Nunez,G., Peter,M.E., Tschopp,J., Yuan,J., Piacentini,M., Zhivotovsky,B., and Melino,G. (2009). Classification of cell death: recommendations of the Nomenclature Committee on Cell Death 2009. Cell Death and Differentiation *16*, 3-11.

Kroemer,G. and Zitvogel,L. (2007). Death, danger, and immunity: an infernal trio. Immunological Reviews *220*, 5-7.

Kubli,D.A., Quinsay,M.N., Huang,C.Q., Lee,Y., and Gustafsson,A.B. (2008). Bnip3 functions as a mitochondrial sensor of oxidative stress during myocardial ischemia and reperfusion. American Journal of Physiology-Heart and Circulatory Physiology *295*, H2025-H2031.

Labrousse,A.M., Zappaterra,M.D., Rube,D.A., and van der Bliek,A.M. (1999). C. elegans dynamin-related protein DRP-1 controls severing of the mitochondrial outer membrane. Mol. Cell *4*, 815-826.

Lacronique,V., Mignon,A., Fabre,M., Viollet,B., Rouquet,N., Molina,T., Porteu,A., Henrion,A., Bouscary,D., Varlet,P., Joulin,V., and Kahn,A. (1996). Bcl-2 protects from lethal hepatic apoptosis induced by an anti-Fas antibody in mice. Nature Medicine *2*, 80-86.

Lapuente-Brun,E., Moreno-Loshuertos,R., Acin-Perez,R., Latorre-Pellicer,A., Colas,C., Balsa,E., Perales-Clemente,E., Quiros,P.M., Calvo,E., Rodriguez-Hernandez,M.A., Navas,P., Cruz,R., Carracedo,A., Lopez-Otin,C., Perez-Martos,A., Fernandez-Silva,P., Fernandez-Vizarra,E., and Enriquez,J.A. (2013). Supercomplex Assembly Determines Electron Flux in the Mitochondrial Electron Transport Chain. Science *340*, 1567-1570.

Lavrik,I., Golks,A., and Krammer,P.H. (2005). Death receptor signaling. Journal of Cell Science *118*, 265-267.

Lawson,V.H., Graham,B.V., and Flanigan,K.M. (2005). Clinical and electrophysiologic features of CMT2A with mutations in the mitofusin 2 gene. Neurology. *65*, 197-204.

Lee,S., Jeong,S.Y., Lim,W.C., Kim,S., Park,Y.Y., Sun,X., Youle,R.J., and Cho,H. (2007). Mitochondrial fission and fusion mediators, hFis1 and OPA1, modulate cellular senescence. Journal of Biological Chemistry *282*, 22977-22983.

Lee,S.Y., Wenk,M.R., Kim,Y., Nairn,A.C., and De Camilli,P. (2004a). Regulation of synaptojanin 1 by cyclin-dependent kinase 5 at synapses. Proc Natl Acad Sci U S A *101*.

Lee,Y., Quinsay,M.N., Rikka,S., Huang,C.Q., and Gustafsson,A.B. (2009). The BH3-only Protein Bnip3 Mediates Mitochondrial Autophagy via Recruitment of the Ubiquitin Ligase Parkin. Circulation *120*, S901-S902.

Lee,Y.J., Jeong,S.Y., Karbowski,M., Smith,C.L., and Youle,R.J. (2004b). Roles of the mammalian mitochondrial fission and fusion mediators Fis1, Drp1, and Opa1 in apoptosis. Mol. Biol. Cell *15*, 5001-5011.

Legros,F., Lombes,A., Frachon,P., and Rojo,M. (2002). Mitochondrial fusion in human cells is efficient, requires the inner membrane potential, and is mediated by mitofusins. Mol Biol Cell *13*, 4343-4354.

Lesnefsky,E.J., Moghaddas,S., Tandler,B., Kerner,J., and Hoppel,C.L. (2001). Mitochondrial dysfunction in cardiac disease: Ischemia-reperfusion, aging, and heart failure. Journal of Molecular and Cellular Cardiology *33*, 1065-1089.

Li,L.Y., Luo,X., and Wang,X. (2001). Endonuclease G is an apoptotic DNase when released from mitochondria. Nature *412*, 95-99.

Liu,X., Weaver,D., Shirihai,O., and Hajnoczky,G. (2009). Mitochondrial 'kiss-and-run': interplay between mitochondrial motility and fusion-fission dynamics. EMBO J. *28*, 3074-3089.

Loson,O.C., Song,Z.Y., Chen,H.C., and Chan,D.C. (2013). Fis1, Mff, MiD49, and MiD51 mediate Drp1 recruitment in mitochondrial fission. Molecular Biology of the Cell *24*, 659-667.

Mannella,C.A., Marko,M., and Buttle,K. (1997). Reconsidering mitochondrial structure: New views of an old organelle. Trends in Biochemical Sciences *22*, 37-38.

Margulis,L. (1971). The origin of plant and animal cells. Am. Sci. *59*, 230-235.

McCarron,J.G., Wilson,C., Sandison,M.E., Olson,M.L., Girkin,J.M., Saunter,C., and Chalmers,S. (2013). From Structure to Function: Mitochondrial Morphology, Motion and Shaping in Vascular Smooth Muscle. Journal of Vascular Research *50*, 357-371.

Meeusen,S., DeVay,R., Block,J., Cassidy-Stone,A., Wayson,S., McCaffery,J.M., and Nunnari,J. (2006). Mitochondrial inner-membrane fusion and crista maintenance requires the dynamin-related GTPase Mgm1. Cell *127*, 383-395.

Meier,P., Finch,A., and Evan,G. (2000). Apoptosis in development. Nature. *407*, 796-801.

Merkwirth,C., Dargazanli,S., Tatsuta,T., Geimer,S., Lower,B., Wunderlich,F.T., von Kleist-Retzow,J.C., Waisman,A., Westermann,B., and Langer,T. (2008). Prohibitins control cell proliferation and apoptosis by regulating OPA1-dependent cristae morphogenesis in mitochondria. Genes Dev. *22*, 476-488.

Misaka,T., Miyashita,T., and Kubo,Y. (2002). Primary structure of a dynamin-related mouse mitochondrial GTPase and its distribution in brain, subcellular localization, and effect on mitochondrial morphology. J. Biol. Chem. *277*, 15834-15842.

Mootha,V.K., Wei,M.C., Buttle,K.F., Scorrano,L., Panoutsakopoulou,V., Mannella,C.A., and Korsmeyer,S.J. (2001). A reversible component of mitochondrial respiratory dysfunction in apoptosis can be rescued by exogenous cytochrome c. EMBO J. *20*, 661-671.

Muller,F.L., Song,W., Jang,Y.C., Liu,Y., Sabia,M., Richardson,A., and Van Remmen,H. (2007). Denervation-induced skeletal muscle atrophy is associated with increased mitochondrial ROS production. American Journal of Physiology-Regulatory Integrative and Comparative Physiology *293*, R1159-R1168.

Murphy,E. and Steenbergen,C. (2008). Mechanisms underlying acute protection from cardiac ischemia-reperfusion injury. Physiological Reviews *88*, 581-609.

Ogasawara,J., Watanabefukunaga,R., Adachi,M., Matsuzawa,A., Kasugai,T., Kitamura,Y., Itoh,N., Suda,T., and Nagata,S. (1993). Lethal Effect of the Anti-Fas Antibody in Mice. Nature *364*, 806-809.

Olesen,J., Kiilerich,K., and Pilegaard,H. (2010). PGC-1 alpha-mediated adaptations in skeletal muscle. Pflugers Archiv-European Journal of Physiology *460*, 153-162.

Olichon,A., Baricault,L., Gas,N., Guillou,E., Valette,A., Belenguer,P., and Lenaers,G. (2003). Loss of OPA1 perturbates the mitochondrial inner membrane structure and integrity, leading to cytochrome c release and apoptosis. J. Biol. Chem. *278*, 7743-7746.

Olichon,A., Elachouri,G., Baricault,L., Delettre,C., Belenguer,P., and Lenaers,G. (2007a). OPA1 alternate splicing uncouples an evolutionary conserved function in mitochondrial fusion from a vertebrate restricted function in apoptosis. Cell Death. Differ. *14*, 682-692.

Olichon,A., Emorine,L.J., Descoins,E., Pelloquin,L., Brichese,L., Gas,N., Guillou,E., Delettre,C., Valette,A., Hamel,C.P., Ducommun,B., Lenaers,G., and Belenguer,P. (2002).

The human dynamin-related protein OPA1 is anchored to the mitochondrial inner membrane facing the inter-membrane space. FEBS Lett. *523*, 171-176.

Olichon,A., Landes,T., rnaune-Pelloquin,L., Emorine,L.J., Mils,V., Guichet,A., Delettre,C., Hamel,C., mati-Bonneau,P., Bonneau,D., Reynier,P., Lenaers,G., and Belenguer,P. (2007b). Effects of OPA1 mutations on mitochondrial morphology and apoptosis: relevance to ADOA pathogenesis. J. Cell Physiol *211*, 423-430.

Ong,S.B. and Gustafsson,A.B. (2012). New roles for mitochondria in cell death in the reperfused myocardium. Cardiovasc. Res. *94*, 190-196.

Ong,S.B., Subrayan,S., Lim,S.Y., Yellon,D.M., Davidson,S.M., and Hausenloy,D.J. (2010). Inhibiting Mitochondrial Fission Protects the Heart Against Ischemia/Reperfusion Injury. Circulation *121*, 2012-U107.

Otera,H., Wang,C., Cleland,M.M., Setoguchi,K., Yokota,S., Youle,R.J., and Mihara,K. (2010). Mff is an essential factor for mitochondrial recruitment of Drp1 during mitochondrial fission in mammalian cells. J Cell Biol. *191*, 1141-1158.

Padrao,A.I., Ferreira,R.M.P., Vitorino,R., Alves,R.M.P., Neuparth,M.J., Duarte,J.A., and Amado,F. (2011). OXPHOS susceptibility to oxidative modifications: The role of heart mitochondrial subcellular location. Biochimica et Biophysica Acta-Bioenergetics *1807*, 1106-1113.

Palade,G.E. (1952). The fine structure of mitochondria. Anat. Rec. *114*, 427-451.

Palmer,C.S., Elgass,K.D., Parton,R.G., Osellame,L.D., Stojanovski,D., and Ryan,M.T. (2013). Adaptor proteins MiD49 and MiD51 can act independently of Mff and Fis1 in Drp1 recruitment and are specific for mitochondrial fission. J. Biol. Chem. *288*, 27584-27593.

Palmer,J.W., Tandler,B., and Hoppel,C.L. (1985). Biochemical differences between subsarcolemmal and interfibrillar mitochondria from rat cardiac muscle: effects of procedural manipulations. Arch. Biochem. Biophys. *236*, 691-702.

Papanicolaou,K.N., Khairallah,R.J., Ngoh,G.A., Chikando,A., Luptak,I., O'Shea,K.M., Riley,D.D., Lugus,J.J., Colucci,W.S., Lederer,W.J., Stanley,W.C., and Walsh,K. (2011). Mitofusin-2 Maintains Mitochondrial Structure and Contributes to Stress-Induced Permeability Transition in Cardiac Myocytes. Molecular and Cellular Biology *31*, 1309-1328.

Parsons,M.J. and Green,D.R. (2011). Death Receptors and Mitochondria: Life Depends on the Liver. Hepatology *54*, 13-15.

Pasdois,P., Parker,J.E., Griffiths,E.J., and Halestrap,A.P. (2011). The role of oxidized cytochrome c in regulating mitochondrial reactive oxygen species production and its perturbation in ischaemia. Biochemical Journal *436*, 493-505.

Paumard,P., Vaillier,J., Coulary,B., Schaeffer,J., Soubannier,V., Mueller,D.M., Brethes,D., di Rago,J.P., and Velours,J. (2002). The ATP synthase is involved in generating mitochondrial cristae morphology. EMBO J. *21*, 221-230.

Pecina,P., Houstkova,H., Hansikova,H., Zeman,J., and Houstek,J. (2004). Genetic defects of cytochrome C oxidase assembly. Physiological Research *53*, S213-S223.

Pelloquin,L., Belenguer,P., Menon,Y., Gas,N., and Ducommun,B. (1999). Fission yeast Msp1 is a mitochondrial dynamin-related protein. J. Cell Sci. *112*.

Perkins,G., Bossy-Wetzel,E., and Ellisman,M.H. (2009). New insights into mitochondrial structure during cell death. Exp. Neurol. *218*, 183-192.

Perkins,G., Renken,C., Martone,M.E., Young,S.J., Ellisman,M., and Frey,T. (1997). Electron tomography of neuronal mitochondria: three-dimensional structure and organization of cristae and membrane contacts. J. Struct. Biol. *119*, 260-272.

Perotti,M.E., Anderson,W.A., and Swift,H. (1983). Quantitative cytochemistry of the diaminobenzidine cytochrome oxidase reaction product in mitochondria of cardiac muscle and pancreas. J. Histochem. Cytochem. *31*, 351-365.

Picard,M., Hepple,R.T., and Burelle,Y. (2012). Mitochondrial functional specialization in glycolytic and oxidative muscle fibers: tailoring the organelle for optimal function. American Journal of Physiology-Cell Physiology *302*, C629-C641.

Powers,S.K., Kavazis,A.N., and McClung,J.M. (2007). Oxidative stress and disuse muscle atrophy. Journal of Applied Physiology *102*, 2389-2397.

Praefcke,G.J. and McMahon,H.T. (2004). The dynamin superfamily: universal membrane tubulation and fission molecules? Nat Rev Mol Cell Biol *5*, 133-147.

Ren,D.C., Tu,H.C., Kim,H., Wang,G.X., Bean,G.R., Takeuchi,O., Jeffers,J.R., Zambetti,G.P., Hsieh,J.J.D., and Cheng,E.H.Y. (2010). BID, BIM, and PUMA Are Essential for Activation of the BAX- and BAK-Dependent Cell Death Program. Science *330*, 1390-1393.

Riva,A., Tandler,B., Lesnefsky,E.J., Conti,G., Loffredo,F., Vazquez,E., and Hoppel,C.L. (2006). Structure of cristae in cardiac mitochondria of aged rat. Mechanisms of Ageing and Development *127*, 917-921.

Rizzuto,R., Bernardi,P., and Pozzan,T. (2000). Mitochondria as all-round players of the calcium game. Journal of Physiology-London *529*, 37-47.

Rodriguez,I., Matsuura,K., Khatib,K., Reed,J.C., Nagata,S., and Vassalli,P. (1996). A bcl-2 transgene expressed in hepatocytes protects mice from fulminant liver destruction but not from rapid death induced by anti-Fas antibody injection. Journal of Experimental Medicine *183*, 1031-1036.

Rojo,M., Legros,F., Chateau,D., and Lombes,A. (2002). Membrane topology and mitochondrial targeting of mitofusins, ubiquitous mammalian homologs of the transmembrane GTPase Fzo. J. Cell Sci. *115*, 1663-1674.

Romanello,V., Guadagnin,E., Gomes,L., Roder,I., Sandri,C., Petersen,Y., Milan,G., Masiero,E., Del,P.P., Foretz,M., Scorrano,L., Rudolf,R., and Sandri,M. (2010). Mitochondrial fission and remodelling contributes to muscle atrophy. EMBO J *29*, 1774-1785.

Romanello,V. and Sandri,M. (2010). Mitochondrial Biogenesis and Fragmentation as Regulators of Muscle Protein Degradation. Current Hypertension Reports *12*, 433-439.

Rouzier,C., Bannwarth,S., Chaussenot,A., Chevrollier,A., Verschueren,A., Bonello-Palot,N., Fragaki,K., Cano,A., Pouget,J., Pellissier,J.F., Procaccio,V., Chabrol,B., and

Paquis-Flucklinger,V. (2012). The MFN2 gene is responsible for mitochondrial DNA instability and optic atrophy 'plus' phenotype. Brain *135*, 23-34.

Saelens,X., Festjens,N., Vande Walle,L., van Gurp,M., van Loo,G., and Vandenabeele,P. (2004). Toxic proteins released from mitochondria in cell death. Oncogene *23*, 2861-2874.

Sandri,M. (2008). Signaling in muscle atrophy and hypertrophy. Physiology *23*, 160-170.

Sandri,M., Lin,J.D., Handschin,C., Yang,W.L., Arany,Z.P., Lecker,S.H., Goldberg,A.L., and Spiegelman,B.M. (2006). PGC-1 alpha a protects skeletal muscle from atrophy by suppressing Fox03 action and atrophy-specific gene transcription. Proceedings of the National Academy of Sciences of the United States of America *103*, 16260-16265.

Santel,A., Frank,S., Gaume,B., Herrler,M., Youle,R.J., and Fuller,M.T. (2003). Mitofusin-1 protein is a generally expressed mediator of mitochondrial fusion in mammalian cells. J. Cell Sci. *116*, 2763-2774.

Santel,A. and Fuller,M.T. (2001). Control of mitochondrial morphology by a human mitofusin. J. Cell Sci. *114*, 867-874.

Sato,M. and Sato,K. (2011). Degradation of Paternal Mitochondria by Fertilization-Triggered Autophagy in C. elegans Embryos. Science *334*, 1141-1144.

Satoh,M., Hamamoto,T., Seo,N., Kagawa,Y., and Endo,H. (2003). Differential sublocalization of the dynamin-related protein OPA1 isoforms in mitochondria. Biochem. Biophys. Res. Commun. *300*, 482-493.

Saxton,W.M. and Hollenbeck,P.J. (2012). The axonal transport of mitochondria. Journal of Cell Science *125*, 2095-2104.

Scaffidi,C., Fulda,S., Srinivasan,A., Friesen,C., Li,F., Tomaselli,K.J., Debatin,K.M., Krammer,P.H., and Peter,M.E. (1998). Two CD95 (APO-1/Fas) signaling pathways. EMBO J. *17*, 1675-1687.

Scaffidi,C., Schmitz,I., Zha,J., Korsmeyer,S.J., Krammer,P.H., and Peter,M.E. (1999). Differential modulation of apoptosis sensitivity in CD95 type I and type II cells. J. Biol. Chem. *274*, 22532-22538.

Schagger,H. and Pfeiffer,K. (2000). Supercomplexes in the respiratory chains of yeast and mammalian mitochondria. Embo Journal *19*, 1777-1783.

Schiaffino,S., Dyar,K.A., Ciciliot,S., Blaauw,B., and Sandri,M. (2013). Mechanisms regulating skeletal muscle growth and atrophy. Febs Journal *280*, 4294-4314.

Scorrano,L. (2013). Keeping mitochondria in shape: a matter of life and death. European Journal of Clinical Investigation *43*, 886-893.

Scorrano,L., Ashiya,M., Buttle,K., Weiler,S., Oakes,S.A., Mannella,C.A., and Korsmeyer,S.J. (2002). A Distinct Pathway Remodels Mitochondrial Cristae and Mobilizes Cytochrome c during Apoptosis. Dev. Cell *2*, 55-67.

Scorrano,L. and Korsmeyer,S.J. (2003). Mechanisms of cytochrome c release by proapoptotic BCL-2 family members. Biochemical and Biophysical Research Communications *304*, 437-444.

Servais,S., Couturier,K., Koubi,H., Rouanet,J.L., Desplanches,D., Sornay-Mayet,M.H., Sempore,B., Lavoie,J.M., and Favier,R. (2003). Effect of voluntary exercise on H2O2 release by subsarcolemmal and intermyofibrillar mitochondria. Free Radical Biology and Medicine *35*, 24-32.

Sesaki,H., Southard,S.M., Yaffe,M.P., and Jensen,R.E. (2003). Mgm1p, a dynamin-related GTPase, is essential for fusion of the mitochondrial outer membrane. Mol. Biol. Cell *14*, 2342-2356.

Shenouda,S.M., Widlansky,M.E., Chen,K., Xu,G.Q., Holbrook,M., Tabit,C.E., Hamburg,N.M., Frame,A.A., Caiano,T.L., Kluge,M.A., Duess,M.A., Levit,A., Kim,B., Hartman,M.L., Joseph,L., Shirihai,O.S., and Vita,J.A. (2011). Altered Mitochondrial Dynamics Contributes to Endothelial Dysfunction in Diabetes Mellitus. Circulation *124*, 444-U251.

Shutt,T., Geoffrion,M., Milne,R., and McBride,H.M. (2012). The intracellular redox state is a core determinant of mitochondrial fusion. Embo Reports *13*, 909-915.

Sjostrand,F.S. (1953). Electron microscopy of mitochondria and cytoplasmic double membranes. Nature *171*, 30-32.

Smirnova,E., Griparic,L., Shurland,D.L., and van der Bliek,A.M. (2001). Dynamin-related protein Drp1 is required for mitochondrial division in mammalian cells. Mol. Biol. Cell *12*, 2245-2256.

Song,Z., Chen,H., Fiket,M., Alexander,C., and Chan,D.C. (2007). OPA1 processing controls mitochondrial fusion and is regulated by mRNA splicing, membrane potential, and Yme1L. J. Cell Biol *178*, 749-755.

Song,Z.Y., Ghochani,M., McCaffery,J.M., Frey,T.G., and Chan,D.C. (2009). Mitofusins and OPA1 Mediate Sequential Steps in Mitochondrial Membrane Fusion. Molecular Biology of the Cell *20*, 3525-3532.

Suen,D.F., Norris,K.L., and Youle,R.J. (2008). Mitochondrial dynamics and apoptosis. Genes Dev. *22*, 1577-1590.

Sugioka,R., Shimizu,S., and Tsujimoto,Y. (2004). Fzo1, a protein involved in mitochondrial fusion, inhibits apoptosis. J. Biol. Chem. *279*, 52726-52734.

Sun,M.G., Williams,J., Munoz-Pinedo,C., Perkins,G.A., Brown,J.M., Ellisman,M.H., Green,D.R., and Frey,T.G. (2007). Correlated three-dimensional light and electron microscopy reveals transformation of mitochondria during apoptosis. Nat. Cell Biol. *9*, 1057-1065.

Susin,S.A., Lorenzo,H.K., Zamzami,N., Marzo,I., Snow,B.E., Brothers,G.M., Mangion,J., Jacotot,E., Costantini,P., Loeffler,M., Larochette,N., Goodlett,D.R., Aebersold,R., Siderovski,D.P., Penninger,J.M., and Kroemer,G. (1999). Molecular characterization of mitochondrial apoptosis-inducing factor. Nature *397*, 441-446.

Suzuki,M., Jeong,S.Y., Karbowski,M., Youle,R.J., and Tjandra,N. (2003). The solution structure of human mitochondria fission protein Fis1 reveals a novel TPR-like helix bundle. J. Mol. Biol. *334*, 445-458.

Tieu,Q. and Nunnari,J. (2000). Mdv1p is a WD repeat protein that interacts with the dynamin-related GTPase, Dnm1p, to trigger mitochondrial division. Molecular Biology of the Cell *11*, 219A-220A.

Tompkins,A.J., Burwell,L.S., Digerness,S.B., Zaragoza,C., Holman,W.L., and Brookes,P.S. (2006). Mitochondrial dysfunction in cardiac ischemia-reperfusion injury: ROS from complex I, without inhibition. Biochimica et Biophysica Acta-Molecular Basis of Disease *1762*, 223-231.

Tondera,D., Grandemange,S., Jourdain,A., Karbowski,M., Mattenberger,Y., Herzig,S., Da Cruz,S., Clerc,P., Raschke,I., Merkwirth,C., Ehses,S., Krause,F., Chan,D.C., Alexander,C., Bauer,C., Youle,R., Langer,T., and Martinou,J.C. (2009). SLP-2 is required for stress-induced mitochondrial hyperfusion. EMBO. J. *28*, 1589-1600.

Tritos,N.A., Mastaitis,J.W., Kokkotoua,E.G., Puigserver,P., Spiegelman,B.M., and Maratos-Flier,E. (2003). Characterization of the peroxisome proliferator activated receptor coactivator 1 alpha (PGC 1 alpha) expression in the murine brain. Brain Research *961*, 255-260.

Tucker,E.J., Wanschers,B.F., Szklarczyk,R., Mountford,H.S., Wijeyeratne,X.W., van den Brand,M.A., Leenders,A.M., Rodenburg,R.J., Reljic,B., Compton,A.G., Frazier,A.E., Bruno,D.L., Christodoulou,J., Endo,H., Ryan,M.T., Nijtmans,L.G., Huynen,M.A., and Thorburn,D.R. (2013). Mutations in the UQCC1-Interacting Protein, UQCC2, Cause Human Complex III Deficiency Associated with Perturbed Cytochrome b Protein Expression. PLoS Genet. *9*, e1004034.

Twig,G., Elorza,A., Molina,A.J., Mohamed,H., Wikstrom,J.D., Walzer,G., Stiles,L., Haigh,S.E., Katz,S., Las,G., Alroy,J., Wu,M., Py,B.F., Yuan,J., Deeney,J.T., Corkey,B.E., and Shirihai,O.S. (2008). Fission and selective fusion govern mitochondrial segregation and elimination by autophagy. EMBO J. *27*, 433-446.

Vafai,S.B. and Mootha,V.K. (2012). Mitochondrial disorders as windows into an ancient organelle. Nature *491*, 374-383.

Verhagen,A.M., Ekert,P.G., Pakusch,M., Silke,J., Connolly,L.M., Reid,G.E., Moritz,R.L., Simpson,R.J., and Vaux,D.L. (2000). Identification of DIABLO, a mammalian protein that promotes apoptosis by binding to and antagonizing IAP proteins. Cell *102*, 43-53.

Viscomi,C., Bottani,E., Civiletto,G., Cerutti,R., Moggio,M., Fagiolari,G., Schon,E.A., Lamperti,C., and Zeviani,M. (2011). In Vivo Correction of COX Deficiency by Activation of the AMPK/PGC-1 alpha Axis. Cell Metabolism *14*, 80-90.

Vogel,F., Bornhovd,C., Neupert,W., and Reichert,A.S. (2006). Dynamic subcompartmentalization of the mitochondrial inner membrane. J. Cell Biol. *175*, 237-247.

Wasilewski,M. and Scorrano,L. (2009). The changing shape of mitochondrial apoptosis. Trends Endocrinol. Metab *20*, 287-294.

Wei,M.C., Lindsten,T., Mootha,V.K., Weiler,S., Gross,A., Ashiya,M., Thompson,C.B., and Korsmeyer,S.J. (2000). tBID, a membrane-targeted death ligand, oligomerizes BAK to release cytochrome c. Genes Dev. *14*, 2060-2071.

Wei,M.C., Zong,W.X., Cheng,E.H., Lindsten,T., Panoutsakopoulou,V., Ross,A.J., Roth,K.A., MacGregor,G.R., Thompson,C.B., and Korsmeyer,S.J. (2001). Proapoptotic BAX and BAK: a requisite gateway to mitochondrial dysfunction and death. Science *292*, 727-730.

Wells,R.C., Picton,L.K., Williams,S.C.P., Tan,F.J., and Hill,R.B. (2007). Direct binding of the dynamin-like GTPase, dnm1, to mitochondrial dynamics protein fis1 is negatively regulated by the fis1 n-terminal arm. Journal of Biological Chemistry *282*, 33769-33775.

Wenz,T. (2009). PGC-1 alpha Activation as a Therapeutic Approach in Mitochondrial Disease. Iubmb Life *61*, 1051-1062.

Wojtczak,L., Zaluska,H., Wroniszewska,A., and Wojtczak,A.B. (1972). Assay for the intactness of the outer membrane in isolated mitochondria. Acta Biochim. Pol. *19*, 227-234.

Wong,E.D., Wagner,J.A., Gorsich,S.W., McCaffery,J.M., Shaw,J.M., and Nunnari,J. (2000). The dynamin-related GTPase, Mgm1p, is an intermembrane space protein required for maintenance of fusion competent mitochondria. J. Cell Biol. *151*, 341-352.

Wu,J.J., Quijano,C., Chen,E., Liu,H.J., Cao,L., Fergusson,M.M., Rovira,I.I., Gutkind,S., Daniels,M.P., Komatsu,M., and Finkel,T. (2009). Mitochondrial dysfunction and oxidative stress mediate the physiological impairment induced by the disruption of autophagy. Aging-Us *1*, 425-437.

Yamaguchi,R., Lartigue,L., Perkins,G., Scott,R.T., Dixit,A., Kushnareva,Y., Kuwana,T., Ellisman,M.H., and Newmeyer,D.D. (2008). Opa1-mediated cristae opening is Bax/Bak and BH3 dependent, required for apoptosis, and independent of Bak oligomerization. Mol. Cell *31*, 557-569.

Yin,X.M., Wang,K., Gross,A., Zhao,Y., Zinkel,S., Klocke,B., Roth,K.A., and Korsmeyer,S.J. (1999). Bid-deficient mice are resistant to Fas-induced hepatocellular apoptosis. Nature *400*, 886-891.

Yoon,Y., Krueger,E.W., Oswald,B.J., and McNiven,M.A. (2003). The mitochondrial protein hFis1 regulates mitochondrial fission in mammalian cells through an interaction with the dynamin-like protein DLP1. Mol. Cell Biol. *23*, 5409-5420.

Youle,R.J. and van der Bliek,A.M. (2012). Mitochondrial Fission, Fusion, and Stress. Science *337*, 1062-1065.

Yu,T., Robotham,J.L., and Yoon,Y. (2006). Increased production of reactive oxygen species in hyperglycemic conditions requires dynamic change of mitochondrial morphology. Proc. Natl. Acad. Sci. U. S. A *103*, 2653-2658.

Zanna,C., Ghelli,A., Porcelli,A.M., Karbowski,M., Youle,R.J., Schimpf,S., Wissinger,B., Pinti,M., Cossarizza,A., Vidoni,S., Valentino,M.L., Rugolo,M., and Carelli,V. (2008). OPA1

mutations associated with dominant optic atrophy impair oxidative phosphorylation and mitochondrial fusion. Brain *131*, 352-367.

Zhu,P.P., Patterson,A., Stadler,J., Seeburg,D.P., Sheng,M., and Blackstone,C. (2004). Intra- and intermolecular domain interactions of the C-terminal GTPase effector domain of the multimeric dynamin-like GTPase Drp1. J. Biol. Chem. *279*, 35967-35974.

Zoratti,M. and Szabo,I. (1995). The mitochondrial permeability transition. Biochim. Biophys. Acta *1241*, 139-176.

Zou,H., Henzel,W.J., Liu,X., Lutschg,A., and Wang,X. (1997). Apaf-1, a human protein homologous to C. elegans CED-4, participates in cytochrome c-dependent activation of caspase-3. Cell *90*, 405-413.

Zuchner,S., Mersiyanova,I.V., Muglia,M., Bissar-Tadmouri,N., Rochelle,J., Dadali,E.L., Zappia,M., Nelis,E., Patitucci,A., Senderek,J., Parman,Y., Evgrafov,O., Jonghe,P.D., Takahashi,Y., Tsuji,S., Pericak-Vance,M.A., Quattrone,A., Battologlu,E., Polyakov,A.V., Timmerman,V., Schroder,J.M., and Vance,J.M. (2004). Mutations in the mitochondrial GTPase mitofusin 2 cause Charcot-Marie-Tooth neuropathy type 2A. Nat. Genet. *36*, 449-451.

Jackson CB, Nuoffer JM, Hahn D, Prokisch H, Haberberger B, Gautschi M, Häberli A, Gallati S, Schaller A. Mutations in SDHD lead to autosomal recessive encephalomyopathy and isolated mitochondrial complex II deficiency J Med Genet. 2013

Li XY, Yang YL Mitochondrial disorders associated with mitochondrial respiratory chain complex V deficiency. Zhongguo Dang Dai Er Ke Za Zhi. 2013 Jul;15(7):596-600.

Lockshin,R.A. and Williams,C.M. (1965). Programmed cell death. V. Cytolytic enzymes in relation to the breakdown of the intersegmental muscles of silkmoths. J. Insect Physiol *11*, 831-844.